EFFECTS OF NICKEL & COPPER PARTICLE SIZE ON P/M STEELS

EFFECTS OF NICKEL & COPPER PARTICLE SIZE ON THE PROPERTIES OF POWDER METAL STEELS

By

TAJ SINGH, B.A.SC.

A Thesis

Submitted to the School of Graduate Studies

in Partial Fulfillment of the Requirements

for the Degree

Master of Applied Science

McMaster University

MASTER OF APPLIED SCIENCE (2005)
(Materials Engineering)

McMaster Univeristy
Hamilton, Ontario

TITLE: Effects of Nickel and Copper Particle Size on the Properties of Powder Metal Steels

AUTHOR: Taj Singh, B.A.Sc. (University of Toronto)

SUPERVISOR: Professor D.S. Wilkinson

NUMBER OF PAGES: xi, 121

ABSTRACT

Powder Metallurgy (P/M) offers a very efficient method to produce high volume, high throughput steel parts. The two most important property issues affecting P/M steels are: (1) possessing high mechanical properties despite having inherent internal porosity; (2) maintaining very tight dimensional tolerances during processing (sintering). Researchers are continually looking at ways to improve these two properties while keeping costs down. As in wrought and cast steels, in most applications P/M steels are alloyed; in P/M processing, alloys are typically added to Fe + C powder mixes as elemental powders. The entire mix of Fe + C + elemental alloying additives are then consolidated under high pressure and sintered at high temperatures to strengthen the compact. The current work deals mainly with the the most commonly used alloying additives in P/M steels, Ni and Cu.

While it is well-known that Ni and Cu do indeed improve the mechanical performance of steels and do affect the dimensional change of P/M parts in specific ways, for over 50 years the same standard Ni and Cu powders have been used in the industry. With new breakthroughs in the production of extra-fine metal powders (~ 1-2 um) P/M researchers now must examine the effect of particle size of alloying additions on the performance of sintered steels. Prior to the current work, significant documented work investigating the effect of particle size of Ni and Cu on the performance of P/M steels was very limited.

The current work examined:

(1) Ni powder particle size effects in P/M Ni steels;
(2) Ni powder particle size effects in P/M Ni-Cu steels;
(3) Ni and Cu powder particle size effects in P/M Ni-Cu-Mo steels.

Specific focus was on determining the effects of particle sizes on the dimensional control and mechanical peformance of P/M steels. With both Ni and Cu, the finer the powder addition the better the dimensional control and mechanical performance of the steels. In steels containing both Ni and Cu, finer Ni also improved the distribution and diffusion of Cu. This suggested that there was a significant interaction between Ni and Cu during sintering which could be tailored to improve properties. The effect of changing Ni particle size on overall steel properties was significantly greater than the effect of changing Cu particle size.

Mechanistic analyses via optical microscopy, SEM-EDX and E-SEM investigation, dilatometry, and differential thermal analysis were carried out to explain the results. Mathematical models were also developed to show the effect of Ni and Cu particle size on diffusion into the Fe matrix during sintering.

ACKNOWLEDGEMENTS

I would like to express my sincere gratitude to my advisors, Dr. David Wilkinson, Professor in the Materials Science & Engineering (MSE) Department at McMaster University and Mr. Tom Stephenson, Technology Development Manager at Inco Special Products. Their encouraging attitude and technical expertise was critical to my intellectual growth and development. Furthermore, I would like to thank them both for their advice on matters outside of my thesis work, which has been beneficial to my life now and will continue to be so in the future.

I would like to acknowledge Inco Technical Services Ltd. (ITSL) for supplying the materials for my work and for the financial support of the project. ITSL is considered one of the best industrial research facilities in Canada and I am very proud that I am part of this team. The workplace is dynamic and challenging and I cannot say enough how grateful I am to Inco for all of their support. A special thanks to my supervisors Scott Campbell, Quan Yang and Sam Marcuson for their understanding and supportive attitudes. In addition, Bill Nowosiadly deserves recognition for his great support and assistance in the microscopy work. At McMaster University, I would like to thank Jim Garrett in the MSE Materials Characterization facility and Klaus Schulzes at the Life Sciences Electron Microscopy facility for their assistance during the project.

I am indebted to my parents and family. Their love and support constantly inspires me. I can say without a doubt that my successes would not be possible without them.

I would like to extend an extra special thanks to my loving wife Sharon for all her support of my dreams. This project could not have been completed successfully without her support.

TABLE OF CONTENTS

LIST OF FIGURES

LIST OF TABLES

1 BACKGROUND

1.1 Introduction

1.1.1 The Powder Metallurgy process

"Powder metallurgy" (P/M) refers to a variety of metal processing techniques, in which a metal in a powder form is consolidated to a specific shape and sintered for strength. The result is a component of "near-net shape" that requires little or no machining. The most attractive benefit of making metallic components via P/M is that the cost of manufacturing can be significantly less expensive compared to wrought and cast processes, especially in large volumes. One drawback to P/M is that the inherent porosity located within the material limits the mechanical performance of a component. The mechanical performance of a P/M component is a function of density. It is generally well-accepted that when porosity is less than 5%, P/M parts possess mechanical properties similar to wrought and cast parts [1]. However, as density is increased so too does the cost of P/M parts (requiring more specialized compaction or sintering procedures). Thus, in general, the P/M process is used for large volume parts for applications that require medium-to-high strength (5-10% porosity).

1.1.2 The P/M industry

The manufacture of metallic components by compaction and sintering powders is a large industry that, producing a variety of shapes from a extensive assortment of materials. Of these materials, steels are the most prevalent metals. Most P/M parts are in the range of

200 g- 2 kg. The shapes range from simple cylindrical bearings to very complex structures such as hollow golf-club heads and helical seat gears [2]. Due to expensive tooling costs, most P/M manufacture is targeted at structures made at high rates (measured typically in parts per year), such as for automobiles, lawnmowers, home appliances, business machines, computers, and other electromechanical structures [2]. Some P/M components, such as tantalum capacitors, bronze bearings and molybdenum heat sinks are produced at rates as high as 40 million parts per day. More typical to ferrous P/M are production rates of a few million parts per year (average part mass of ~ 1 kg). Almost 75% of P/M parts made are for the automotive industry [2]. The main alloying classes of steel are shown in Table 1.1, with specific mention of their use in P/M applications [2].

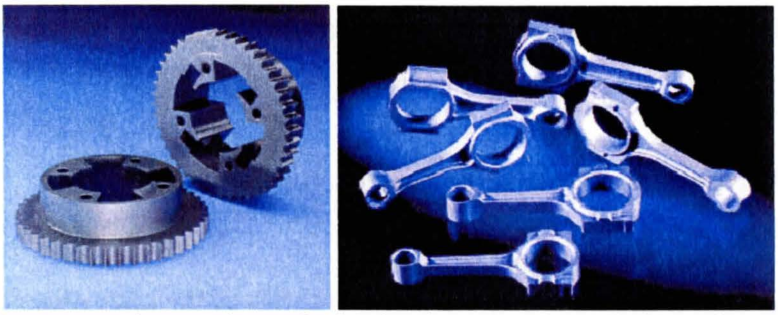

Figure 1-1. In automotive engines, fuel injection sprockets (left) and connecting rods (right) are made via the P/M process.

Table 1.1. Main alloying classes of steels & their use in P/M [2].

Alloy Class	Alloying Level	Key Uses	Use in P/M
Iron	None	Magnets	Somewhat
Plain carbon steel	≤0.8% carbon	Moderate strength, general purpose	Somewhat
Low-alloy steel	≤5%, some carbon	High strength	Very large
Stainless steel	≥12% chromium	Corrosion resistance	Moderate, growing
Tool steel	30–50%, >0.4% carbon, includes carbide forming metals	Wear resistance, tooling, cutting, drilling, machining	Limited
Cast iron	High carbon levels	Large structures, castings, automobiles engines	Not used
High-heat alloy	≤25%, high chromium and aluminium contents	High heat, jet engines, furnaces, heating elements	Very limited
Special alloy	≤50%	Special applications, electronics, glass seals, filters	Limited
Silicon alloy	≤8% silicon	Electrical transformers	Limited
Magnetic alloy	≤50% nickel, many special compositions	Magnetic components	Moderate, growing

1.1.3 Important material properties / characterization methods for P/M parts

1.1.3.1 Microstructure characterization

Since microstructure dictates properties, analysis of the microstructure lays the groundwork for characterizing a P/M product. Polished cross-sections of a sintered material provide information on the grain and pore structures. Quantitative measurements of the feature sizes are possible from 2-D images. Microstructure is revealed by polishing and etching the material, with subtle differences in etching between phases leading to 2-D images that reveal the grain, pore, and phase relations in the material. Because P/M steels are typically used in load-bearing applications, in general, the greater the amount of harder, stronger phases (e.g. martensite, bainite), the better. In some applications that require very high toughness, the goal is to obtain higher levels of retained austenite through the use of "austenite-stabilizing" alloying elements such as nickel or increasing the amount of carbon in the steel [3].

1.1.3.2 Mechanical properties

Most P/M steels are used for mechanical / structural applications so mechanical properties are one of the most important sets of properties for these materials. The most important types of static mechanical properties are uniaxial tensile strength, hardness, transverse rupture strength (3-pt bending strength, a commonly used strength value for low-ductility materials). Fatigue and impact toughness are important dynamic mechanical properties. The tensile strengths of different 4Ni P/M steels (as-sintered) with varying carbon contents are shown in Figure 1-2; note the dual effect of carbon level and density on tensile strength.

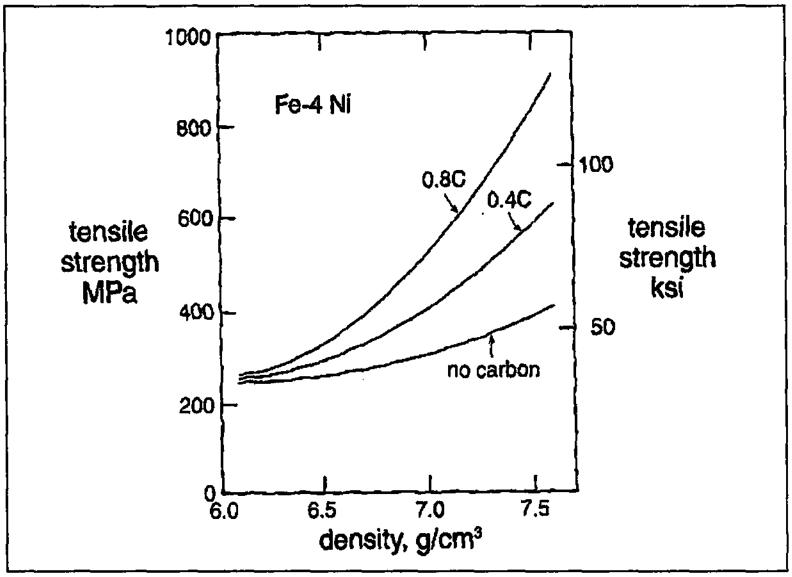

Figure 1-2. Tensile strength of 4Ni steels as a function of part density & carbon level [2].

1.1.3.3 Dimensional change properties

A major concern associated with ferrous sintering is sustaining predictable dimensional changes. The diffusional events associated with sintering, combined with thermal expansion and phase transformation events cause dimensions to vary over a wide range [2]. If the green body is not uniform in initial structure, then shrinkage will cause warpage and final dimensions will be not be repeatable and predictable [2]. Usually, as density levels are increased there is a loss of product dimensional uniformity. Repressing or machining after sintering is frequently used to correct these problems

Dimensional control in sintering represents a significant barrier to the expanded use of P/M. Many steel component applications could use P/M processing if the tolerance range could be decreased, especially in automotive transmissions and other moving mechanical systems [3]. Dimensions can vary over a significant range due to the diffusion, thermal expansion and phase transformation events that occur during sintering. A gear that is slightly out of round causes noise and wears faster than does one that is symmetric. However, even slight tolerance improvements, resulting in more predictable final dimensions, could immediately open the door for P/M into mainstream processing [2]. In P/M steels, size changes of a part occurs at two stages: (1) (prior to the sintering step) after the compact is ejected from the die, there is a small expansion of the part; this is on the order of 0.05-0.20% (of the original part size). This is mainly a function of the iron powder and does not differ between samples with the same base Fe powder; (2) during sintering, depending on the alloy content, the carbon level and the sintering conditions (time, temperature, etc.), the compact typically swells or shrinks from 0.0-2.0%.

The standard test piece for measuring dimensional change of P/M steel parts is a 25.4 mm (l) x 12.7 mm" (w) x 6.3 mm (h) rectangular bar. The percentage difference between the length of the die size (length of bar within the die) and the length of the bar after sintering is taken as the value of dimensional change. Additionally a value of dimensional precision is often stated; it is the standard deviation of dimensional change from part to part within a lot of a certain number of samples (typically 10). For most applications dimensional precision is even more important than the absolute dimensional change; if a part can repeatedly give a specific dimensional change, this value can be specified into the part-making operation, i.e. the die can be made slightly larger / smaller than the actual application size [3].

1.1.3.4 Dilatometry

Dilatometry is a useful means for monitoring dimensional change during sintering. Dilation meters continuously measure the size of a component in a furnace during sintering. The measurement is performed by contacting the compact with an external measuring transducer that uses electrical, magnetic, or optical signals to determine the instantaneous dimensions. As the test material shrinks or expands, the probe motion sends a signal to the computer along with temperature measurements from the thermocouple [2]. A dilatometry plot of expansion vs. time of two Fe-Cu alloys as they are heated up from room temperature and sintered is shown in Figure 1-3. The compacts expand from thermal expansion during heating, shrink as a result of the ferrite-to-austenite transformation and expand due to the dissolution of copper into the iron when copper melts. The amount of dimensional change is substantially different between the two compacts.

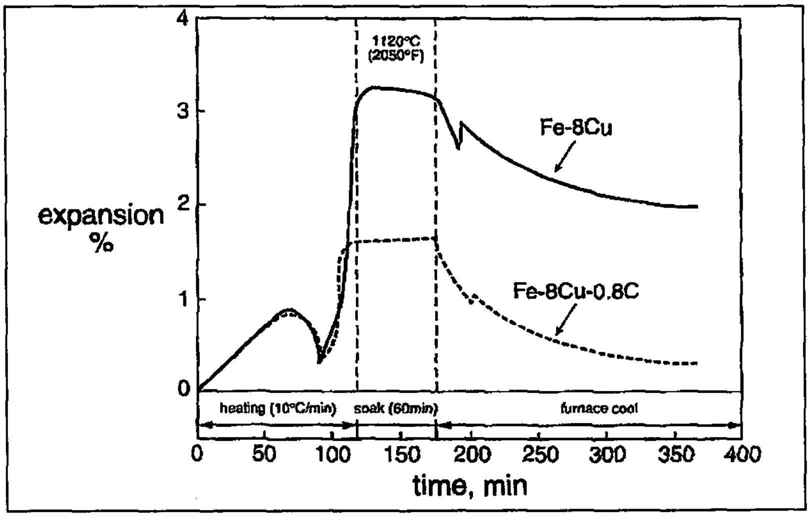

Figure 1-3. A dilatometry plot (expansion vs. time) of Fe-8Cu & Fe-8Cu-0.8C alloys [5].

1.1.4 P/M powders

As illustrated schematically in Figure 1-4, There are three different kinds of powders used in the ferrous P/M industry: (1) admixed elemental powders, (2) prealloyed powders and (3) partially alloyed powders. Most powder mixes used in industry are admixed, e.g. elemental Fe, Ni, Cu powders combined with powdered graphite carbon and a powdered lubricant).

In some cases prealloyed powders are used. Prealloyed powders give excellent uniformity in the final steel but have a major drawback in that they are harder (due to solid solution strengthening) and require higher compaction pressures to give an acceptable part density. Fe-Mo and Fe-Cr are the two most common prealloyed powders. Molybdenum is prealloyed to Fe powder, for example, because its diffusion at industrial sintering conditions is extremely slow; chromium is prealloyed to Fe because it oxidizes readily in elemental form during sintering.

Powders are sometimes partially alloyed (bonded) to Fe, either thermally (diffusion-bonding / diffusion-alloyed) or with polymers to improve the uniformity of the elements during sintering and / or reduce the dusting tendencies of very fine powders by adhering them to large Fe particles. Ni, Cu, Mo and C are the elements most often bonded to Fe. Often, industrial powder mixes are combinations of the three kinds of powders.

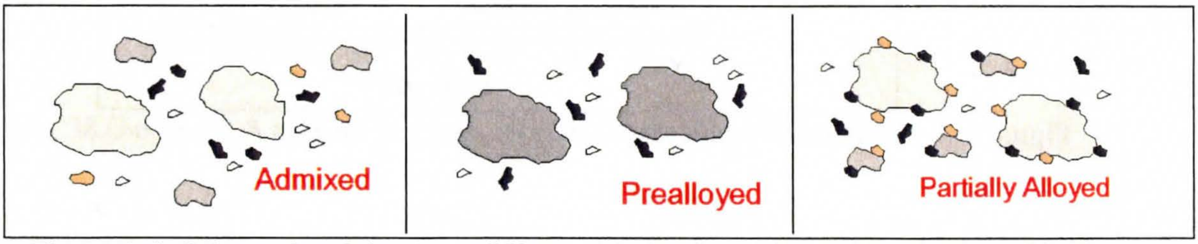

Figure 1-4. Schematic of the three different kinds of metal powder mixes used in ferrous P/M.

1.1.5 The Press & Sinter P/M process

The most common method of producing P/M components utilizes "pressed and sintered" (PS) processing. This method involves three major steps: (1) mixing of metal powders, graphite and lubricant; (2) pressing or compacting the powder mixture, typically uniaxially, under high pressure at room temperature; and (3) sintering the powder compact at elevated temperatures (typically 1100-1300°C for ferrous parts). The result is a near-net shape component that requires little to no finishing operations.

P/M-PS alloy steels exhibit high strengths, enabling these alloys to replace prior used wrought and cast alloys in low performance applications. However, increasing demand for high performance components, such as connecting rods and transmission components in automobiles, requires P/M components with improved mechanical properties if the powder-processed components are to replace the alloys that are typically used for these applications [4].

1.1.6 Other P/M processing techniques

For a P/M component to be considered for a high performance application porosity must be reduced to a minimum, i.e. density must be maximized. Many avenues to reduce porosity have been explored, such as a hydropulsor, warm-compaction, and high temperature sintering [5]. A hydropulsor is relatively new technology that utilizes high compaction velocities to compact the powder; high densities are attained by the transfer of energy from the tooling to the powder. Warm compaction involves the use of a heated die which softens the powder and thus increases compressibility. High temperature sintering involves sintering at temperatures above the standard sintering temperature of 1120 °C, increasing diffusion mechanisms to further densify the compact and improve the diffusion of admixed elemental alloying additions. One of the more prominent methods to reduce porosity is known as "double-press double-sintering" (DPDS), which decreases porosity from approximately 10 to 5 percent in comparison conventional PS processing of ferrous based materials [4]. The green compact is pressed into a green body, heated to temperature that is 50-75% of the sintering temperature for several minutes, repressed and then fully sintered at the appropriate temperature.

To keep costs to a minimum, 85% of all P/M parts are still produced in the conventional (PS) method [2].

1.1.7 Heat-Treatment

Depending on the severity of the application, P/M parts can be heat-treated to improve their strength, hardness, and high cycle fatigue strength. Heat-treating techniques of P/M parts generally follow those of wrought and cast metals. The most popular form of heat treatment is heating to the austenitic phase and quenching in oil or water to form martensite. In most cases, the material is tempered for a short time to regain some ductility and reduce brittleness [3]. Accelerated cooling of sample directly following sintering can produced an effect similar to heat-treating without the additional steps of reheating, quenching and cleaning, etc. required.

1.1.8 Alloying in P/M components

Other alternatives have been explored to increase the mechanical performance of P/M components. The use of alloy additions to steel has shown excellent promise in improving strength, ductility, and fatigue strength in P/M materials. Copper, nickel and molybdenum have been the primary alloying additions used to date [5]. The use of alloy additions such as manganese and chromium has been limited because sintering technology constraints have made these additions to P/M materials difficult [6]. However, advances in P/M processing have made alloys with such elements more viable.

The addition of other metals to a base iron matrix is an integral part in developing P/M alloys. As with wrought and cast steels, the effect of elemental additions can result in major changes in the properties of a specimen. Furthermore, the addition of several elements has a varying effect on the properties of an alloy, as interactions among alloy additions may occur [5]. The effect of various alloying elements on the strength of P/M steels is shown in Figure 1-5.

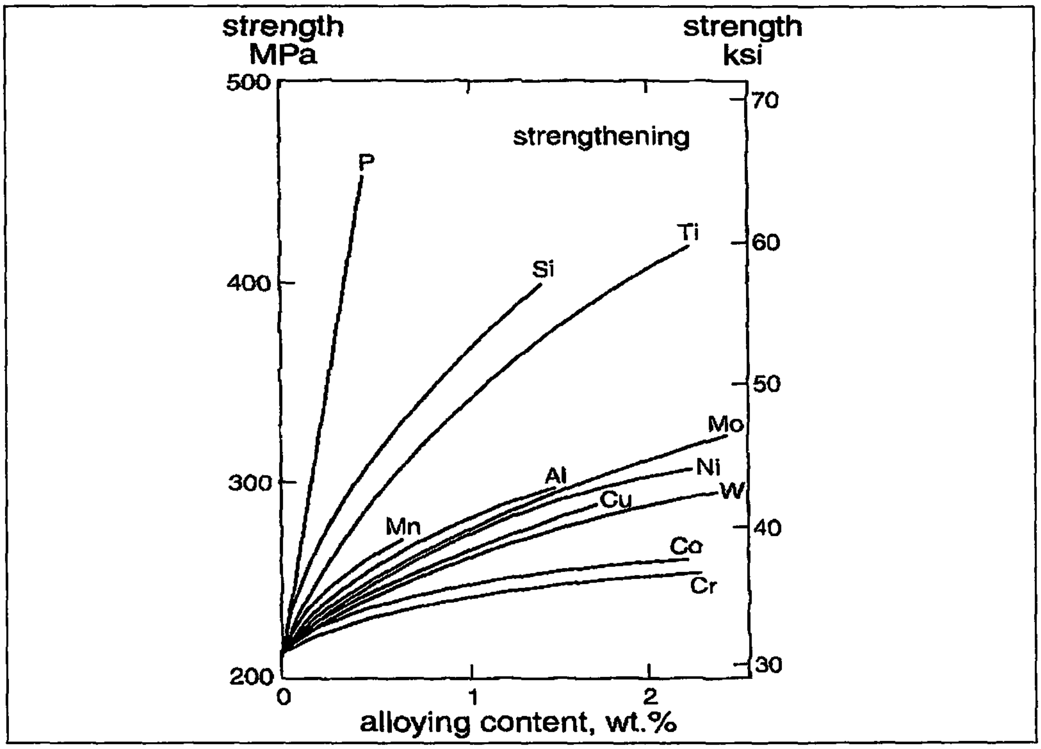

Figure 1-5. Strength vs. amount of alloying addition for bcc-Fe [2].

1.1.8.1 Copper

Copper was one of the earliest additions made to iron based powders and is typically added in ranges of 1 to 3 wt%. James reports that copper was found to increase strength and apparent hardness when pre-alloyed with iron based powders [7]. Copper strengthens the steel matrix primarily via preciptation hardening as well as by solid solution strengthening. Copper additions in admixed powders are most beneficial when heat-treating is not an option, as they tend to exhibit good as-sintered properties; copper alloyed components show relatively high hardness regardless of heat treatment. Motooka et al. determined that specimens with copper additions possessed the highest as-sintered tensile strength and hardness due to Cu-induced precipitate hardening [8].

Copper alloyed components show no increase in properties when heat-treated, presenting a major drawback for "ultra-high strength" parts. Furthermore, if heat-treated, copper additions with other elements have shown to decrease tensile strength, toughness, and fatigue properties [9,10,11].

1.1.8.2 Nickel

The use of nickel as an elemental addition to iron-based alloys is widely known. Nickel additions enhance strength by forming solid solutions with the matrix iron. Nickel is an austenite stabilizer in iron, changing the austenite-ferrite transformation characteristics by lowering both the upper and lower critical temperatures and reducing the eutectoid carbon level. The result is the ability to heat-treat at lower temperatures with less carbon needed for strengthening. Furthermore, nickel acts as a grain refiner, which also improves mechanical properties. In general, nickel additions in the range of 0.5 to 8 wt% show an increase in tensile, toughness, hardness, and fatigue properties [4, 7]. However, increasing the amount of nickel above approximately 4% results in a decrease in compressibility of powders, causing a reduction in green density that may adversely affect mechanical properties [12]. Overall, addition of nickel over 8% will reduce mechanical properties. Heat-treating parts with the optimum amount of nickel can greatly increase tensile and toughness properties through the formation of regions of strong martensite and ductile retained austenite [11].

1.1.8.3 Molybdenum

Molybdenum is a less popular addition to Fe-based P/M parts; because of its very slow diffusivity into iron at conventional sintering temperatures (~ 1100°C) it is primarily pre-alloyed to the matrix iron powder. Molybdenum additions can drastically increase tensile strength, toughness, and hardness, largely in part of solid solution strengthening [13]. Furthermore, molybdenum alloys respond well to heat-treatment, by increasing the hardenability of the compact [11]. The comparatively large size of the molybdenum atom limits its diffusion rate and retards formation of pearlite (Mo is relatively insoluble in the cementite), such that martensite is more easily attainable on cooling. Generally molybdenum is added in a range of 0.5 to 1.5 wt% with best properties being seen at 1.5 wt% [13]. The drawback of molybdenum is the expense, which is significantly high in comparison to aforementioned additions.

1.1.8.4 Manganese

Manganese in the amounts of 0.3-2 wt% has been used extensively in steels both to form sulfur/phosphorus-rich precipitates, reducing the tendency of sulfur to embrittle the steel, and to increase the hardenability of the steel for reasons similar to Mo. Manganese can thus strengthen steel upon heat-treatment, but it reduces ductility and toughness. Rarely is manganese the sole addition in an alloy steel, instead added with several other alloy additions [10].

1.1.8.5 Chromium

The addition of chromium to steel is well known for producing stainless steel, where it is added in excess of 12 wt%. The use of chromium is lesser amounts is less documented in P/M steels. The additions of chromium in amounts of 1 wt% or less have shown to increase the hardenability, hardness, and tensile strength of the alloy through solution strengthening [10].

1.1.9 Summary: Alloy effects in P/M steels

The major effects of the alloy additions described above are summarized in Table 1.2. Generally, each of these additions increase strength and hardness. Ni and Mo additions are the most advantageous additions, as they typically increase toughness and fatigue properties as well. Mn and Cr additions can adversely effect ductility, which could embrittle the alloy, and Cu additions increase properties only in the as-sintered condition.

Table 1.2. Summary of effects of alloying elements in P/M steels.

Alloy addition	**Major effects**
Copper	Increases strength and hardness (as-sintered only) Possibly decreases strength, hardness, and ductility (heat-treated)
Nickel	Increases strength, hardness, toughness, and fatigue strength (both as-sintered and heat treated) Increases hardenability
Molybdenum	Tensile strength and fatigue endurance limit increases when Ni content is increased from 1.75- 4% (as-sintered)
Manganese	Increases hardenability Reduces ductility and toughness
Chromimum	Increases strength and hardness (as-sintered and heat-treated) Increases hardenability Decreases ductility (as-sintered and heat-treated)

1.2 Ni Steels, Cu Steels & Ni-Cu Steels

Cu and Ni both strengthen and harden P/M steels in similar ways, forming a solid solution with Fe. The more an alloying element can dissolve in Fe, the tougher the ferrite becomes (strength without a loss of ductility). Ni can dissolve in Fe to a greater extent than Cu. Both Ni and Cu act as austenite stabilizers in Fe, changing the austenite-ferrite transformation characteristics by lowering both the upper and lower critical temperatures and reducing the eutectoid carbon level. The result is the ability to heat-treat at lower temperatures with less carbon needed for strengthening [8].

Typical mechanical properties of 0.5% C plain (F-005), 2%Cu (FC-0205) and 2%Ni (FN-0205) steels in the as-sintered and heat-treated (HT) conditions are shown in Table 1.3. In the as-sintered condition, both Ni and Cu are quite potent at hardening and strengthening. Cu seems to give slightly higher hardness values while the increased ductility of Ni results in higher dynamic properties (e.g. toughness, impact energy). In the heat-treated condition, the strengthening effect of Cu is insignificant, and its effect can even become deleterious if the heat-treated steel has been alloyed with other elements [2,3]. Studies show that Cu can combine readily with some elemental additions (e.g. Mo) and form intermetallic precipitates which lower the effect of the solid solution strengthening and act as fracture initiation sites [3]. Thus, Cu is not recommended for use in the heat-treated condition. Conversely, Ni is even more effective in the heat-treated condition than it is in the as-sintered condition. Many studies have shown that heat-treating parts with the optimum amount of nickel can greatly enhance tensile and toughness properties through the formation of regions of strong martensite and ductile retained austenite [4,5].

Table 1.3. Typical mechanical properties of 2Cu and 2Ni P/M steels with 0.5C [14].

	Density (g/cc)	Tensile Strength (MPa)	Ductility (%)	Unnotched Charpy Impact Energy (J)	Transverse Rupture Strength (MPa)	Hardness
F-0005	6.9	260	1.5	7	520	55 HRB
FC-0205	7.1	410	<1.0	10	790	72 HRB
FN-0205	7.2	410	4	28	860	69 HRB
F-0005 HT	7.0	480	<0.5	5	970	25 HRC
FC-0205 HT	7.0	690	<0.5	7	930	36 HRC
FN-0205 HT	7.1	1000	<0.5	8	1310	33 HRC

The most commonly used (standard) powder particle sizes for admixed Ni and Cu are approximately 10 μm and 50 μm, respectively. Since the standard Cu is much coarser than the standard Ni powder, Cu carries a lower cost, and this is one of the reasons it is used more than Ni in the industry. However, at similar particle sizes, Ni and Cu are approximately the same price. Much of the reason that coarser additions of Cu can be made is due to the fact that Cu melts at conventional sintering temperatures [16]. The transient liquid phase sintering enabled by Cu allows for improved sintering kinetics, microstructure uniformity and pore rounding. However, Cu has one very undesirable drawback in that it swells steels during sintering, causing a loss of density and poor dimensional control. Investigators have reported that, in steels with Cu contents higher than 2.5%, compacts tend to grow so much that the dimensional tolerances are "uncontrollable" [16]. Figure 1-6 shows a schematic of the swelling that can be caused by the liquid phase sintering of Cu in P/M steels.

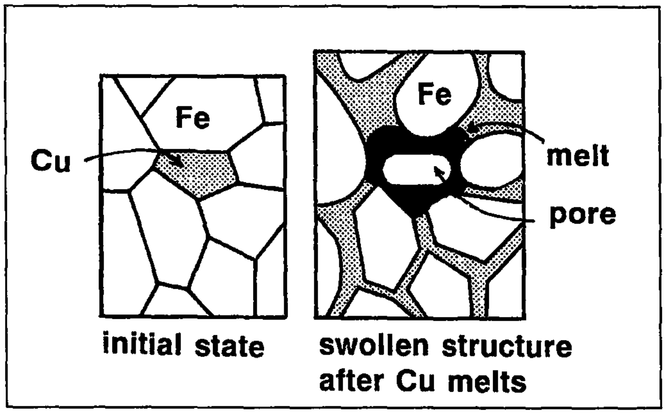

Figure 1-6. Schematic showing how Cu can swell P/M steel structure during sintering [5].

In the as-sintered condition, adding some Ni to Cu steels has approximately the same effect on mechanical properties as increasing the Cu content. The main reason for substituting some Cu with Ni in steel parts is the substantial reduction in dimensional swelling during sintering. Engström et al. compared the dimensional change, tensile strength and elongation of 2Cu, 4Cu and 2.5Cu/2.5Ni/0.6C steels sintered to 7.0 g/cm^3 [16]. They found that increasing the Cu content from 2 to 4 % caused dimensional swelling to double with a noticeable reduction in tensile strength and ductility. In comparing the 4Cu and 2.5Cu/2.5Ni steel, the Ni-containing steel showed significantly less swelling and an improvement in ductility.

Although it is known that Cu causes swelling and Ni causes shrinkage in sintered steels, the interactions of the two elements are not so straight-forward. Many part producers report results that do not seem to follow this simple behaviour and the interactions between Ni and Cu during sintering are not well understood. In Ni steels, Ni diffuses relatively slowly, some going into solid solution with Fe and some essentially remaining stationary, leaving behind Ni-rich areas (NRAs). As Ni enters the Fe lattice it leaves behind pores that are subsequently closed off during sintering, resulting in densification. In Cu steels, liquid Cu either penetrates between Fe particles or enters the Fe lattice to form a solid solution. The solidification of liquid Cu between particles often results in substantial growth of the part [15].

When Ni and Cu are combined in sintered steels, their interactions with Fe may (or may not) change. Understanding the Ni-Cu interaction would allow the end-user to control their behaviour in sintered parts. For instance, if Ni and Cu do indeed associate with one another, increasing the uniformity of Ni could simultaneously lead to an increased uniformity of Cu. Improved homogeneity of the alloying elements in the part would subsequently allow for more consistent part properties. Stephenson et al, using SEM-EDS elemental mapping, showed that finer Ni powder (~ 1 μm) distributes more uniformly than standard Ni powder (8 μm) during sintering of steel compacts [7].

1.3 Ni-Cu-Mo Steels

Tengzelius conducted a study comparing two pressed and sintered alloys of copper, nickel, and molybdenum with elemental carbon [9]. The first part of this investigation assessed the effect of a 1% Cu addition on a 6% Ni- 0.85% Mo alloy; both sintered densities and tensile strengths were measured. The experiment was then repeated, except the Mo content was changed to 1.5%. Table 1.4 is a summary of the conditions for the study. At 0.85% molybdenum, the alloy without copper showed better sinter density (7.43 to 7.38 g/cm^3) and similar tensile strength (1380 MPa) compared to the copper-containing alloy. At 1.5% molybdenum, alloys without copper showed higher density (7.42 to 7.35 g/cm^3) and tensile strength (1400 to 1270 MPa) compared to those with copper. Without copper, the alloys with 1.5% molybdenum exhibited higher strength compared to 0.85% molybdenum alloys, while the contrary was true with copper containing alloys.

Table 1.4. Tengzelius study conditions [9].

Steel	Composition (wt%), bal. Fe				Study conditions	
	Ni	Cu	Mo	C	Method	PS
1	6	0	0.85	0.5	Compaction pressure	690 MPa
2	6	1	0.85	0.5	Sintering temp	1290°C
3	6	0	1.5	0.5	Sintering time	45 mins.
4	6	1	1.5	0.5	Sintering atmosphere	$10H_2$-N_2

Motooka et al compared Cu/Ni/Mo alloys with Ni/Mo alloys [8]. Table 1.5 is a summary of the conditions for the study, where four different alloys were investigated. The results of their study revealed that the Cu/Ni/Mo alloy possessed the highest hardness (98 HRB) and tensile strength (876 MPa) in the as-sintered condition. When heat-treated, the Cu-containing alloy showed little improvement in tensile strength. The alloy with the highest "heat-treated" tensile strength was the 2Ni/1Mo/0.5C steel at 1946 MPa. The highest impact values were achieved in the as-sintered condition. The alloy containing (2%)/ Mo (1%)/C (0.5%) showed the highest toughness in both as-sintered (119 J) and heat-treated condition (70 J).

Table 1.5. Motooka et al study conditions [8].

Steel	Composition (wt%), bal. Fe				Study conditions	
	Ni	Cu	Mo	C	Method	DPDS, DPDS + HT
1	6	0	0.85	0.5	Compaction pressure	/
2	6	1	0.85	0.5	Sintering temp	800°C, 1300°C
3	6	0	1.5	0.5	Sintering time	30, 90 mins.
4	6	1	1.5	0.5	Sintering atmosphere	$10H_2$-N_2
					Heat-treating	870°C, 60 min air oil quenched to T_{room} 200°C temper, 90 mins.

A study conducted by Tracey, see Table 1.6 for conditions, revealed that increasing Ni concentration from 1.75 to 4% increases tensile strength and fatigue properties for an alloy containing Cu/Mo/C [12]. UTS increased from 610 MPa to 750 when 1.75% Ni was increased to 4%. Similarly, the fatigue endurance limit increased by 70 MPa to 300 MPa when the Ni content was shifted to 4% from 1.75%. Tracey concluded that the nickel-rich areas found (with higher wt% Ni) in the microstructure inhibited fatigue crack growth, but gave no indication as to why the tensile strength results varied.

Table 1.6. Tracey study conditions [12].

Steel	Composition (wt%), bal. Fe				Study conditions	
	Ni	Cu	Mo	C	Method	SP-S
1	1.75	1.5	0.5	0.5	Compaction pressure	600 MPa
2	4	1.5	0.5	0.5	Sintering temp	1120°C
					Sintering time	30 mins.
					Sintering atmosphere	$5H_2$-N_2

Yano et al composed a study comparing Ni/Mo/Cu steels; Table 1.7 is a summary of the conditions for the study [6]. Comparisons of high density attained after double-press double-sintering reveal that density slightly decreases after 2 % Ni additions (7.42 to 7.39 g/cm^3) and 1 percent Mo additions (7.42 to 7.39 g/cm^3). Comparisons were also made between steels of Ni/Mo and Cu/Ni/Mo. The study revealed that single-pressing, single-sintering, carburizing and tempering shows comparable characteristics. The copper added alloy has a slightly lower tensile strength (1380 to 1500 MPa), toughness (20 to 21 J), and fatigue (410 to 460 MPa). When double-pressing double-sintering, the Ni/Mo characteristics far exceed those of the Cu added powder, with larger increases in tensile strength (1920 to 1720 MPa) and toughness (53 to 39 J) and moderate increases in fatigue properties (390 to 350 MPa).

Table 1.7. Yano et al study conditions [6].

Steel	Composition (wt%), bal. Fe				Study conditions	
	Ni	Cu	Mo	C	Method	DPDS, DPDS + HT
1	2	-	1	0.6	Compaction pressure	/
2	4	1.5	0.5	0.6	Sintering temp	850°C, 1250°C
					Sintering time	30, 30 mins.
					Sintering atmosphere	$75H_2$-N_2
					Heat-treating	870oC, 60 min Ar oil quenched to T_{room} 180°C temper, 60 mins.

The properties of Ni-Cu-Mo and Cu-Mo steels sintered to 7.1 g/cm^3 have been investigated in a study by Engstrom [16]; a summary of the conditions is shown in Table 1.8. The addition of 4%Ni to a 2Cu/1.5Mo/0.5C steel reduced the dimensional change by approximately 200%. Hardness also increased and both the tensile strength and impact energy increased by approximately 50%. In comparing a 1.75Ni/1.5Cu/0.5Mo/ 0.6C steel to a 4Ni/1.5Cu/0.5Mo/0.5C steel, the steel with higher Ni showed much less swelling and noticeable improvements in tensile strength, impact energy and hardness.

Table 1.8. Engstrom et al. study conditions [16].

Steel	Composition (wt%), bal. Fe				Study conditions	
	Ni	Cu	Mo	C	Method	PS
1	0	2	1.5	0.5	Compaction pressure	590 MPa
2	4	2	1.5	0.5	Sintering temp	1120°C
3	1.75	1.5	0.5	0.6	Sintering time	30 mins.
4	4	1.5	0.5	0.6	Sintering atmosphere	$5H_2$-N_2

1.3.1 Summary: Ni-Cu-Mo Steels

Table 1.9 summarizes the main results of the studies that investigated Fe-based Cu/Ni/Mo/C alloys. In general, there exists some disparities exist with the effects of copper in the as-sintered condition. Tengzelius [9] and Causton [18] report a negative Cu effect on strength and no significant effect on other properties, while Motooka et al [8] and Morioka [10] report Cu additions increase strength and hardness. Motooka, Morioka, and Yano report that Cu additions decrease strength, hardness, toughness, and fatigue strength when heat-treatment occurs. General trends in the effects of Ni and Mo are more easily recognized. In both the as-sintered and heat-treated conditions, increasing Ni content (to at least 4%) and increasing Mo content (to at least 1.5%) results in an increase in tensile strength, hardness, and fatigue strength. Toughness increased with both Ni and Mo additions in the heat-treated condition, but toughness was reported to decrease with Mo additions in the as-sintered condition.

Table 1.9. Summary previous studies of Ni-Cu-Mo steels.

Study	Main findings
Tengzelius [9]	Cu addition (1%) has insignificant effect on strength at low Mo content, deleterious effect at high Mo content (as-sintered)
	Increasing Mo content from 0.85 to 1.5% increases strength (as-sintered)
Motooka et al [8]	Cu containing alloy (1.5%) exhibited highest strength in as-sintered condition; lower strength in heat-treated condition compared to non-Cu containing alloys
	Increasing Ni content (0.5- 2%) and Mo content (0.5- 1%) increases strength and toughness (heat-treated)
Tracey [12]	Tensile strength and fatigue endurance limit increases when Ni content is increased from 1.75- 4% (as-sintered)
Yano et al [6]	Increasing Ni content (>2%) and Mo content (>1%) decreases density
	For P&S, Cu additions (1.5%) decrease tensile and fatigue strength with comparable toughness (heat-treated)
	For DPDS, Cu additions (1.5%) further decrease tensile strength and toughness, with a moderate decrease in fatigue strength (heat-treated)
Engstrom [16]	Ni additions drastically reduce the amount of swelling of in Cu-Mo steels while also improving mechanical properties
	Ni (4%) added to 2Cu-1.5Mo-0.5C steel reduced dimensional swelling by ~ 200% while also improving UTS, and impact energy by 50%

1.4 Nickel particle size effects in P/M steels

The earliest significant work published dealing with the effect of Ni particle size on the mechanical properties of P/M steels was done by Stephenson et al [17] in 2002. The study compared the mechanical properties of 2Ni/0.8C P/M steels with additions of standard (8 μm d_{50} discrete), fine (2-3 μm d_{50} filamentary) and ultra-fine (0.5-1 μm d_{50} filamentary) Ni powders. The steels were tested in both the as-sintered (AS) and heat-treated conditions (HT). As well, fatigue endurance tests, via rotating beam fatigue testing, were carried out on the heat-treated steels.

In the as-sintered condition, the steel with fine Ni powder possessed the highest static mechanical properties. A summary of this data is shown in Table 1.10. UTS, failure strain, impact energy (IE) were all highest in this steel. It was hypothesized that fine Ni powder possessed a greater diffusion into the Fe matrix over standard Ni powder; the mechanical property improvement was correlated to the greater diffusion of Ni into the iron matrix resulting from the finer Ni particle size. The standard and extra-fine powders had approximately similar levels of mechanical properties. Physical properties of the extra-fine blend were limited by agglomeration of the extra-fine Ni powder. The authors suggested that the scaling law (of improved mechanical properties with finer Ni particle size) could continue if a discrete, non-agglomerated Ni powder of extra fine size (1-2 μm) was used. In the heat-treated condition, the mechanical properties of the three steels were similar but the highest fatigue endurance limit measured was for the steel containing extra-fine Ni powder. Fatigue life curves of the three steels are shown in Figure 1-7. The authors suggested that the fatigue samples of steels with extra-fine Ni powder most likely possessed less agglomeration than the tensile samples of the same steel and thus it was able to follow the proposed scaling law.

Table 1.10. Summary of results from Stephenson et al study [17].

Composition	Ni powder	UTS (MPa)	Strain (%)	IE (J)	HRB (AS) / HRC (HT)	Sintered Density (g/cc)
2Ni-0.8C-Fe (AS)	Standard (8 μm)	432	0.8	10.4	79	7.02
	Fine (2.5 μm)	452	1.2	12	81	7.02
	X-fine (0.75 μm)	446	1	8.75	80	7.03
2Ni-0.8C-Fe (HT)	Standard (8 μm)	838	-	6.3	34.5	6.88
	Fine (2.5 μm)	828	-	5.5	33.7	6.92
	X-fine (0.75 μm)	813	-	4.9	34	6.92

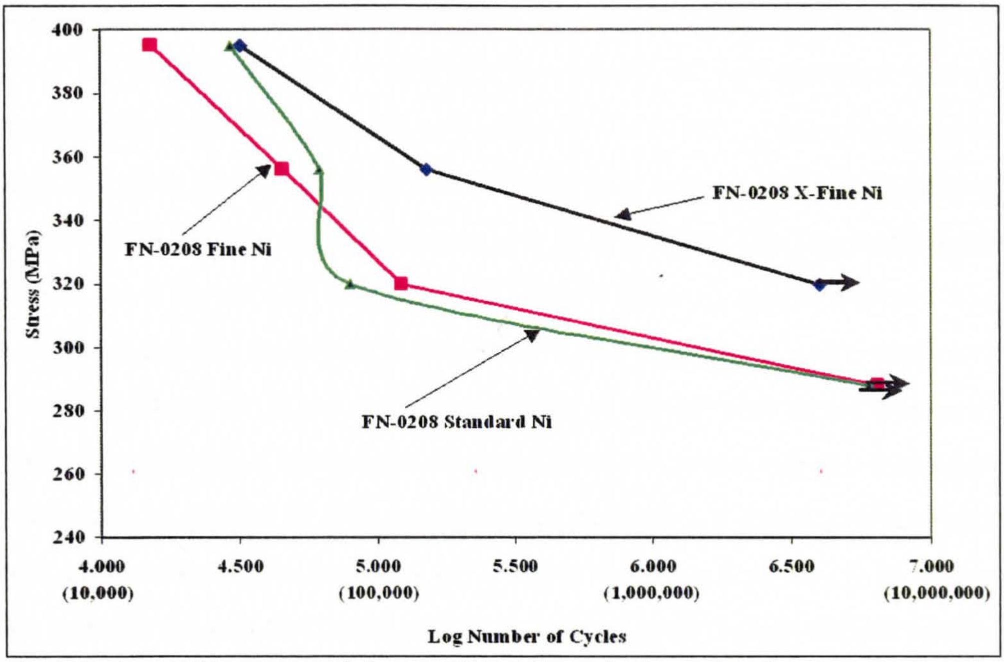

Figure 1-7. Fatigue life curves of three 2Ni/0.8C steels from Stephenson et al study [17].

Ni powder morphology / size strongly affected the microstructure of the sintered nickel steels. Discrete powders are obviously favoured over filamentary powders as they are not as susceptible to agglomeration to form large Ni "chunks" which can be very difficult to diffuse during P/M sintering. Relatively large (50 to 100 μm) Ni-rich areas were found for standard grade Ni powder, which persisted after heat treatment. Ni distribution became more homogeneous with finer Ni powder grade. For the extra-fine Ni powder blend, the large Ni-rich areas were no longer visible in the microstructure, however relatively narrow Ni-rich bands were found around the perimeter of most pores. The absence of large Ni-rich regions was found not to be detrimental to the fatigue properties. On the contrary, the improved distribution of Ni to the perimeter of most of the pores appeared to enhance the endurance limit significantly.

1.5 Objective of Current Work

The current work will investigate the particle size effects of Ni and Cu (the most commonly used alloying additives) on the properties of several well-known, frequently-used P/M steel compositions. The work is subdivided into three studies. The first study looks at properties of 4Ni/0.5C steels with 2 different particle sizes of *discrete* Ni powder: 8 µm d_{50} and 1.5 µm d_{50}. Previous work in the field has only looked at steels with extra-fine *filamentary* Ni powders which were found to agglomerate and negate the effects of fine particle size.

2Ni/2Cu steels is the focus of the second study. Ni-Cu steels are a frequently-used combination in the P/M industry because of their ability to strengthen steels while remaining relatively dimensionally stable during sintering. The characteristic of dimensionally stability is very important for this alloy system as it is frequently used in applications that require tight tolerances. The study investigates the effect of Ni particle size on the dimensional change and mechanical properties of these steels and if / how Ni particle size affects its interaction with Cu during sintering. 2Ni/2Cu steels at 0.5C and 0.8C are investigated to understand if / how carbon level may affect the dimensional change and / or Ni-Cu interactions in this system. Mechanistic analyses are carried out via SEM-EDS linescans and dilatometry.

The third study is an extension of the second into a more complex, more high-performance steel system – 2Ni/2Cu/0.8Mo/0.7C. The system is similar to steel of the second study except for the fact that steel now contains an additional element, Mo. The effect of Ni particle size *and Cu particle size* (40 µm to 2 µm) on the dimensional change and mechanical properties of this steel will be investigated. Interactions between Ni, Cu, Mo and the base Fe-C will be studied via metallography, dilatometry and differential thermal analysis.

2 EXPERIMENTAL

2.1 P/M Procedure

For each steel blend, the powders (base Fe, alloying powders, carbon and lubricant) were placed in a mixing container and mixed for 30 mins in a Turbula T2F multi-axis mixer (with a motion similar to a paint can mixer), shown in Figure 2-1. Each blend was ~ 300 g of total powder. After the blend was mixed, powders were compacted into test pieces. Appropriate masses of powder were poured into a die and compacted uniaxially at 550 MPa to a target density of 7.0 g/cm^3 (which is 90% of full density of steel, or 10 % porosity) A schematic of the compaction process is shown in Figure 2-2 [2]. Samples were placed in a laboratory tube furnace at 1120°C for 30 min. in a 95/5 N_2/H_2 atmosphere and sintered. The cooling rate was approximately 0.5°C/s.

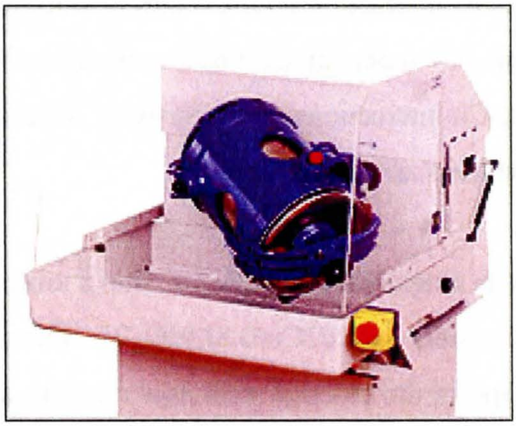

Figure 2-1. Turbula T2F Multi-axis powder mixer.

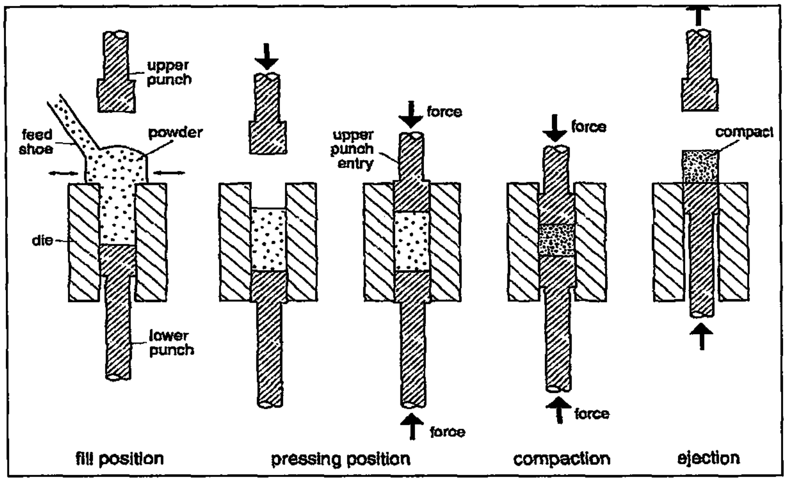

Figure 2-2. Schematic of the P/M compaction process [2].

2.2 Materials

2.2.1 Fe powders

2.2.1.1 Plain Fe powder

QMP (Quebec Metal Powders®) AT1001 water atomized Fe was used as the base powder in all of the steels in Study 1 and Study 2. A SEM micrograph of the powder is shown in Figure 2-3 and particle size, chemical and physical properties are summarized in Table 2.1. Fe powders for use in P/M steels can be quite large; they can remain relatively stationary and do not have to diffuse into other components as alloying additives need to do.

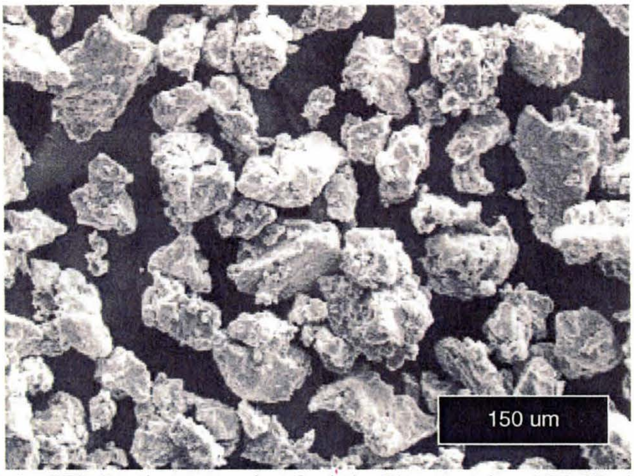

Figure 2-3. SEM micrograph of plain Fe powder (QMP AT1001).

Table 2.1. Particle properties of plain Fe powder [19].

Malvern Laser Diffraction Particle Size (µm)			**Chemical Analysis (ppm)**			**Scott Bulk Density (g/cc)**
d10	d50	d90	C	O	S	
55	75	110	300	8000	700	2.52

2.2.1.2 Prealloyed Fe-Mo powder

Hoeganes® 85HP Fe-0.85wt%Mo powder was used as the base Fe powder in Study 3. A Particle size, chemical and physical properties are summarized in Table 2.2. The particle morphology was very similar to that of AT1001 plain Fe powder.

Table 2.2. Particle properties of Fe-Mo powder [20].

Malvern Laser Diffraction Particle Size (µm)			**Chemical Analysis (ppm)**			**Scott Bulk Density (g/cc)**
d10	d50	d90	C	O	S	
60	80	120	200	7000	700	2.6

2.2.2 Carbon & Lubricant

Southwestern® powdered carbon graphite is the industry-standard for P/M steel parts. It has a very fine particle size of ~ 0.5 μm [21]. Lonza® Acrawax C was used as the powdered lubricant for increasing compressibility of the steel blends during compaction; it is also one of several industry-standard lubricants.

2.2.3 Ni powders

2.2.3.1 Standard (STD) Ni powder

INCO® Type 123 PM nickel powder consists of fine, high purity, discrete particles, developed and produced by carbonyl decomposition. The powder is uniform in size, with a typical variation of less than 1 μm in diameter. Its surface consists of spiky, needle-like structures which are known to improve packing and compressibility [22].

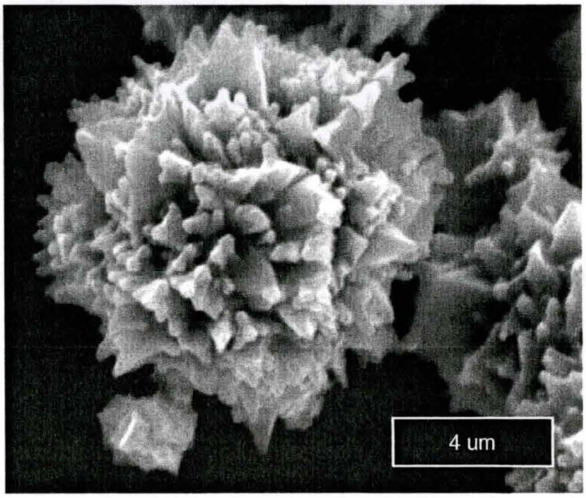

Figure 2-4. SEM micrograph of STD-Ni powder.

Table 2.3. Particle properties of STD-Ni powder [22].

Malvern Laser Diffraction Particle Size (µm)			Chemical Analysis (ppm)			Scott Bulk Density (g/cc)
d10	d50	d90	C	O	S	
4	8.5	20	600-1000	600-1000	1	1.6-2.6

2.2.3.2 *Extra-fine (XF) Ni powder*

INCO® Type 110 PM nickel powder is an extra fine, discrete, spherical particle developed and produced carbonyl decomposition. The powder is tightly sized in the 1 to 2 µm range and is the finest commercially available nickel powder for P/M applications [23].

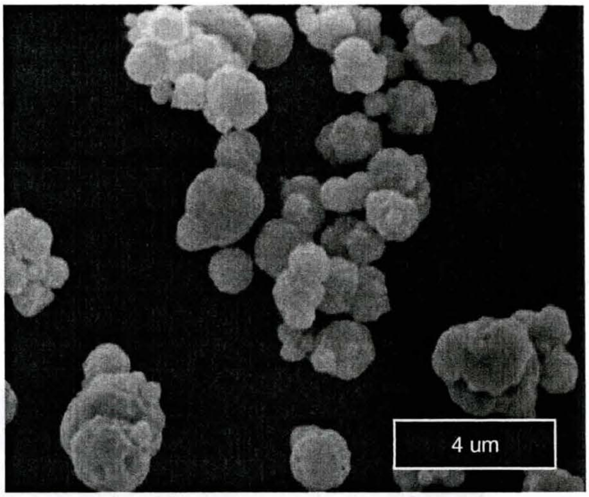

Figure 2-5. SEM micrograph of XF-Ni powder.

Table 2.4. Particle properties of XF-Ni powder [23].

Malvern Laser Diffraction Particle Size (µm)			Chemical Analysis (ppm)			Scott Bulk Density (g/cc)
d10	d50	d90	C	O	S	
0.5	1.5	4	30000	1500	3	1.0-2.0

2.2.4 Cu powders

2.2.4.1 Standard (STD) Cu powder

ACuPowder® Grade 165 Cu powder (STD-Cu) is produced by a water atomization process and is irregular in shape. An SEM micrograph of the powder is shown in Figure 2-6 and a table of chemical and physical properties is shown in Table 2.5.

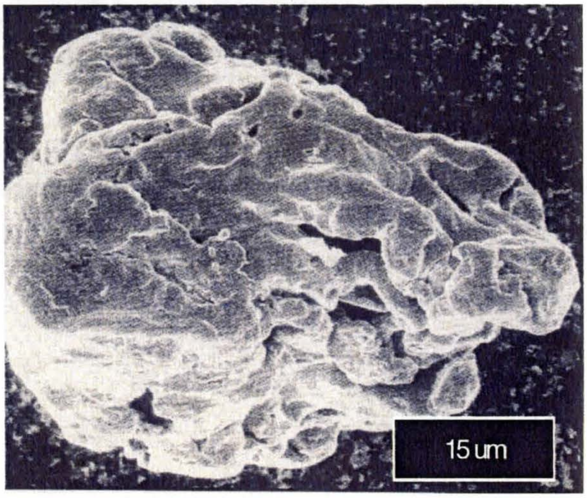

Figure 2-6. SEM micrograph of STD-Cu.

Table 2.5. Particle properties of STD-Cu powder [24].

Malvern Laser Diffraction Particle Size (µm)			**Chemical Analysis (ppm)**			**Scott Bulk Density (g/cc)**
d10	d50	d90	C	O	S	
25	50	100	800	1500	50	2.6-2.8

2.2.4.2 Extra-fine (XF) Cu powder

ACuPowder® Grade 2000 is produced by a gas atomization process and is spheroidal in shape. An SEM micrograph of the powder is shown in Figure 2-7 and a table of chemical and physical properties is shown in Table 2.6.

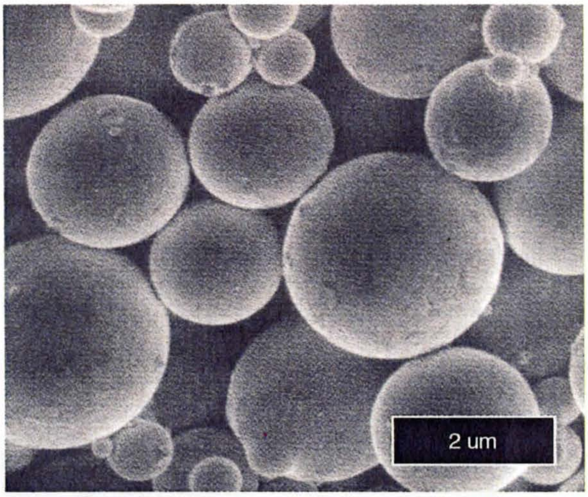

Figure 2-7. SEM micrograph of XF-Cu powder.

Table 2.6. Particle properties of XF-Cu powder [24].

Malvern Laser Diffraction Particle Size (μm)			**Chemical Analysis (ppm)**			**Scott Bulk Density (g/cc)**
d10	d50	d90	C	O	S	
1.5	3	5	800	1500	50	3.0

2.3 Sample preparation

2.3.1 Study 1 – Effect of Ni particle size on properties of 4Ni-0.5C steels

Samples of two 4Ni-0.5C steels (using plain Fe powder) were prepared and tested. The compositions of the two mixes are shown below.

Steel Name	**wt% composition**				
	STD-Ni	XF-Ni	C	Lubricant	Fe
STD-Ni steel	4		0.5	0.75	bal.
XF-Ni steel		4	0.5	0.75	bal.

2.3.2 Study 2 - Effect of Ni particle size on properties of 2Ni-2Cu steels with varying C contents

Samples of two 2Ni-2Cu-0.5C steels and 2Ni-2Cu-0.8C steels (using plain Fe powder) were prepared and tested. The compositions of the four mixes are shown below (In addition a 4STD-Ni steel, a 4XF-Ni steel and a 4STD-Cu steel were tested for comparison).

Steel Name	**wt% composition**					
	STD-Ni	XF-Ni	C	STD-Cu	Lubricant	Fe
STD-Ni/STD-Cu/0.5C steel	2		0.5	2	0.75	bal.
XF-Ni/STD-Cu/0.5Csteel		2	0.5	2	0.75	bal.
STD-Ni/STD-Cu/0.8Csteel	2		0.8	2	0.75	bal.
XF-Ni/STD-Cu/0.8Csteel		2	0.8	2	0.75	bal.

2.3.3 Study 3 - Effect of Ni particle size & Cu particle size on properties of high-performance 2Ni-2Cu-0.8Mo-0.7C steel

Samples of four 2Ni-2Cu-0.8Mo-0.7C steels and 2Ni-2Cu-0.8C steels (using prealloyed Fe-Mo powder) were prepared and tested. The compositions of the four mixes are shown below.

Steel Name	**wt%.composition**						
	STD-Ni	XF-Ni	C	STD-Cu	XF-Cu	Lubricant	Fe-0.85Mo
STD-Ni/STD-Cu steel	2		0.7	2		0.75	bal.
STD-Ni/XF-Cu steel	2		0.7		2	0.75	bal.
XF-Ni/STD-Cu steel		2	0.7	2		0.75	bal.
XF-Ni/XF-Cu steel		2	0.7		2	0.75	bal.

2.4 Characterization Methods

2.4.1 Microstructure

Cross-sections of steels were mounted, ground and polished as per conventional ASM P/M metallographic standards [25] to prepare metallographic samples (optical & SEM). Metallographic samples were etched for 5-10 secs in 5% nital solution. The optical microscope used was the Buehler XJ-15 model. The SEM used was a JEOL JSM 6400 (W filament) equipped with a EDAX EDS unit coupled with Genesis software package.

2.4.1.1 Phase analysis

Phases of steels were determined by applying a gridding software (ProTools® Imagegridder) to optical / SEM fields and taking the percentage area of phases. Approximate area % martensite, bainite, austenite and pearlite was determined. Three fields of each steel were viewed and a mean value of area % of each phase was determined.

2.4.1.2 SEM-EDX linescan analysis

EDX linescans of SEM micrographs at 100X magnification were taken; this corresponded to an approximate line length of 2500 μm. Conditions of the linescans were: field size 2.4 mm x 1.8 mm, 2-4 elements (Ni/Cu/Fe), 50 points, 50X magnification, 10 s dwell time, TC 50 μs, image size 1024 x 800 pixels. For each linescan, the line scanned was taken at exactly the centre of the micrograph in the vertical direction. Wt% values of Ni / Cu / Mo / Fe were taken depending on the bulk composition of the steel. Plots of wt% element vs. distance across field were generated.

2.4.2 Dimensional change properties

Dimensional change (from sintering) was tested as per MPIF Standard Test #44 [26]. The length dimension of standard bar size (~ 30 mm length x 12 mm wide x 6 mm thick) before (taken as die size length) and after sintering; the percentage difference is reported as % dimensional change (DC). A Fowler Checkmatic dimensional comparator, which has an accuracy to +/- 0.005 mm was used for DC measurements. In the current work, the mean value of 10 samples is taken as the %DC. As well, the standard deviation of dimensional change of the 10 samples is reported and is often known as dimensional precision.

2.4.3 Dilatometry

Dilatometry samples were 3 mm x 3 mm x 6 mm (thick). A SETARAM Setsys 16/18 TMA unit using Setsoft 2000 software was used for the testing and the schedule consisted of a 50°C/min ramp-up from room temperature to 1120°C, hold for 30 mins, and cool back down to room temperature at 60°C/min in a 5%H_2-N_2 atmosphere. The same unit was also used for Differential Thermal Analysis (DTA).

It is important to note that the *dimensional change values obtained from dilatometry studies are only taken as relative* and are used as an analytical tool rather than a standard test procedure. In the results of the current study, often dimensional change measurements will show that a steel experiences slight swelling but dilatometry seems to indicate slight shrinkage. The two reasons that dilatometry recordings are not taken as absolute values for dimensional change are:

(1) Dilatometry samples were 3 times thinner than UTS or TRS test bar pieces but were sintered at the same soak temperature (1120°C) for the same length of time (30

mins.). Thus, the amount of densification during soaking in the dilatometry samples will be exaggerated.

(2) For dilatometry samples, "original size" (100%) of the compact is considered as the size *just prior* to the sintering cycle and does not include the dimensional change that occurs during springback as the part exits the die. In a standard dimensional change test, original size is considered to be the size of the die, so the dimensional change value considers the contribution of both the part ejection and size change during sintering (see section 1.1.3.3) and is thus used as the industry standard.

2.4.4 Mechanical properties

2.4.4.1 Transverse rupture strength (TRS)

TRS (3-pt) is a bending strength test usually used for brittle materials and was measured as per MPIF Standard # 45 [23]. A schematic of the test is shown in Figure 2-8 . A rectangular sample is loaded vertically downwards and is held in place by three cylindrical contacts. The stress at which the sample ruptures is recorded and is typically 1.5-2 times that of the ultimate tensile strength.

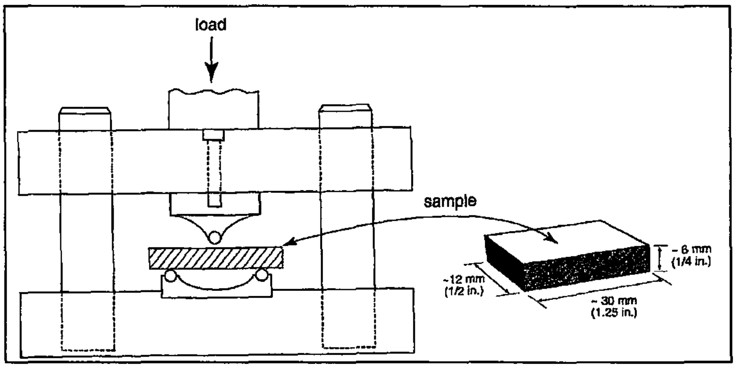

Figure 2-8. Schematic of TRS test for P/M steels [26].

2.4.4.2 Ultimate tensile strength (UTS)

UTS was measured as per MPIF Standard # 45 [26]. Elongation is also reported as obtained from the tensile test. Often in P/M, yield strength (YS) is not reported because the materials possess very little ductility (due to high C level and/or porosity) and thus have a YS that is approximately the same as UTS.

2.4.4.3 Hardness

Hardness was measured as per the Rockwell method is reported as either Rockwell A, B or C depending on the carbon level of the steel. Hardness was measured as per MPIF Standard # 46 [26].

3 RESULTS & DISCUSSION

3.1 Study 1 - Effect of Ni particle size on properties of 4Ni/0.5C steels

3.1.1 Microstructure

3.1.1.1 Phase Analysis

Both the STD-Ni steel and the XF-Ni steel had a pearlitic matrix with regions of bainite and martensite and retained austenite. XF-Ni steel had more bainte and martensite phases with less retained austenite. A breakdown of the phases of both steels as calculated by analysis of optical micrographs in ProTools Imagegridder is shown in Table 3.1. Optical micrographs of the STD-Ni and XF-Ni steels are shown in Figure 3-1 and Figure 3-2 respectively.

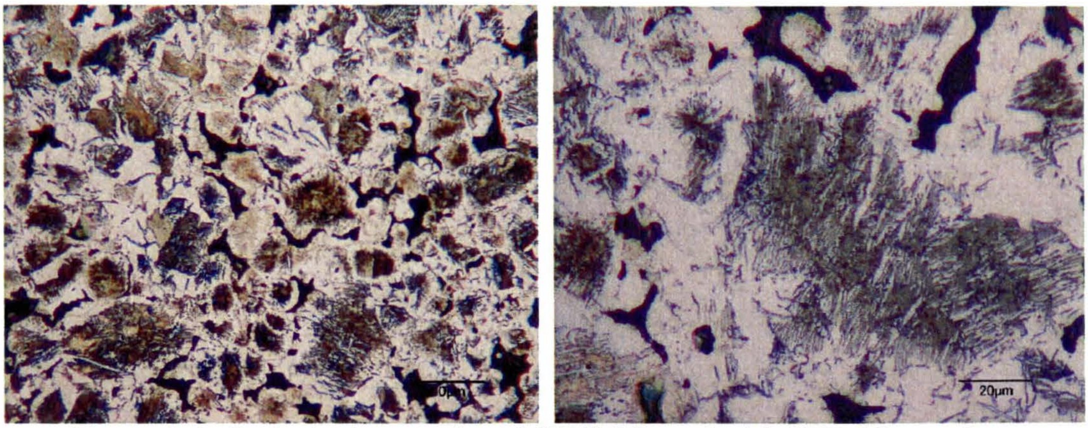

Figure 3-1. Optical micrographs of 4Ni/0.5C steel with STD-Ni powder.

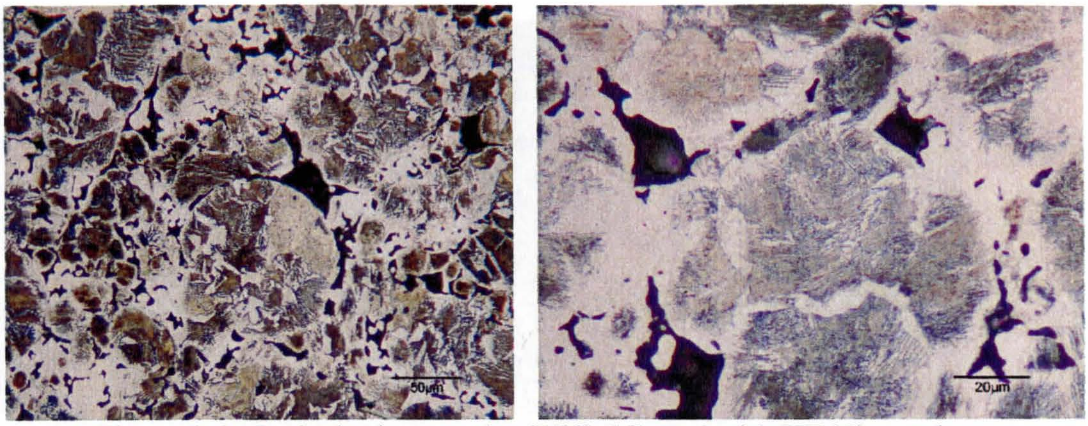

Figure 3-2. Optical micrographs 4Ni/0.5C steel with XF-Ni powder.

Table 3.1. Quantitative phase analysis of 4Ni/0.5C steels.

	Approximate area % phases +/- 5%			
	Martensite	*Bainite*	*Austenite*	*Pearlite*
STD-Ni steel	10	10	35	45
XF-Ni steel	25	15	30	30

3.1.1.2 SEM-EDX Linescan Analysis

Scanning electron microscope images of Ni-rich phases in a 4Ni/0.5C steel are shown in Figure 3-3, comparing steels made with STD and XF-Ni powder. Ni-rich phases are light in colour, with porosity represented by irregular black areas and the medium grey steel microstructure consisting mainly of pearlite and ferrite. Note that Ni-rich phases tend to be associated with porosity, a consequence of the slow diffusion of Ni and the location of Ni powder on the original surface of Fe particles. The light Ni-rich regions are seen to be larger and more prevalent in the STD Ni steel; they are also more intense in colour, indicating higher Ni content.

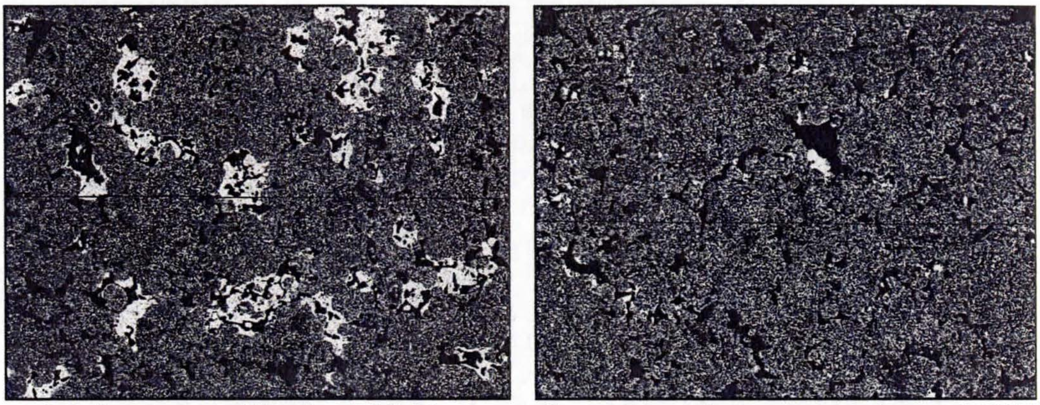

Figure 3-3. Low-magnification SEM images of representative cross-sections of 4Ni/0.5C steels with STD-Ni powder (left) and XF-Ni powder additions (right).

Representative Ni distribution cross-sectional linescans (2500 μm in length) of the STD-Ni and XF-Ni steel are shown in Figure 3-4 and Figure 3-5 respectively. While the STD-Ni steel shows an very unstable composition (wt%) of Ni across the line, the composition of Ni in the XF-Ni steel is relatively uniform and stable. This is a clear indication that the distribution of Ni within the XF-Ni steel is much more uniform than that in the STD-Ni steel.

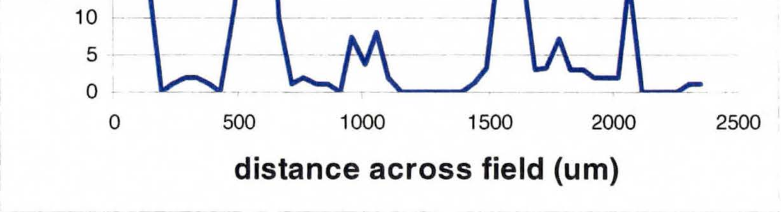

Figure 3-4. Representative linescan analysis of 2500 μm length in sample cross-section of 4Ni/0.5C steel with STD-Ni powder.

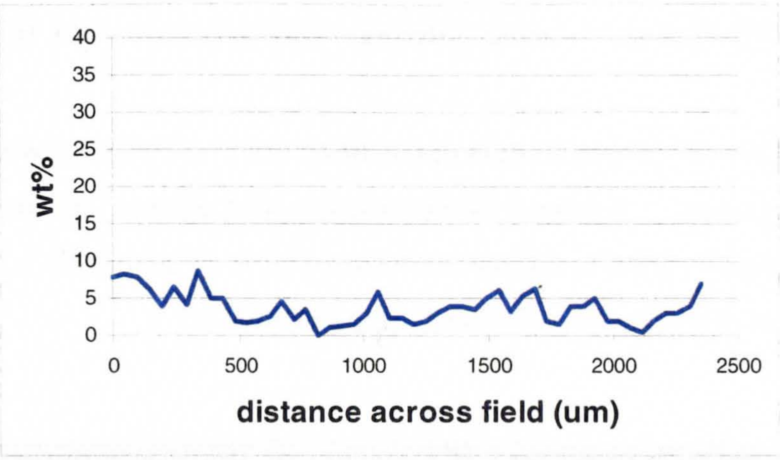

Figure 3-5. Representative linescan analysis of 2500 μm length in sample cross-section of 4Ni/0.5C steel with XF-Ni powder.

EDX image analysis was applied to SEM micrographs of sintered 4Ni/0.5C steels made with the two Ni powders used in the study. EDX maps of the two steels are shown in Figure 3-6. Ni-rich areas are represented by the green colour, with the Fe-C steel matrix in black. Differences between the two Ni powders are immediately obvious:

- Standard Ni leaves distinct Ni-rich areas (NRAs) with high wt% Ni combined with areas with little or no Ni in the steel matrix.
- Extra-fine Ni gives a Ni distribution that is almost complete uniform and has diffused throughout the entire steel matrix.

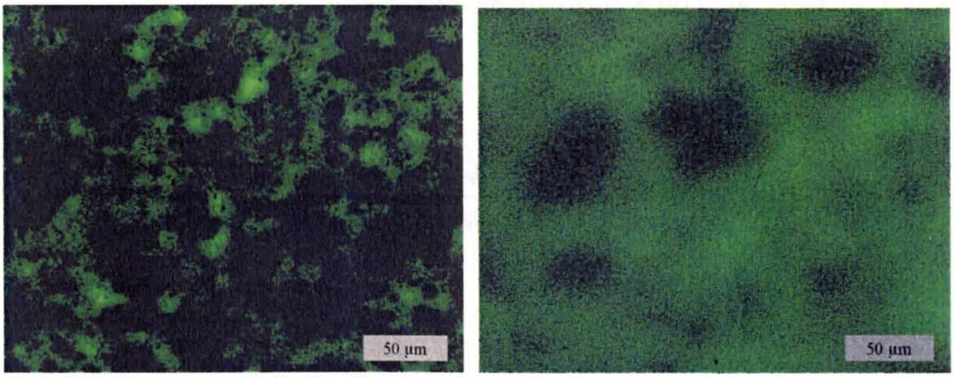

Figure 3-6. EDX maps of Ni distribution (green) of representative cross-sections of the four 4Ni/0.5C steels; STD-Ni (left) and XF-Ni (right).

3.1.1.3 Diffusion of Ni during sintering – Microstructure-NRA Method

In order have a better indication of the difference in diffusion between XF-Ni powder and STD-Ni powder, a technique (Microstructure-NRA Method) was developed to analyze SEM images in order to estimate diffusion. Figure 3-7 and Table 3.2 illustrate how the amount of diffusion was calculated using Equation 3.1.

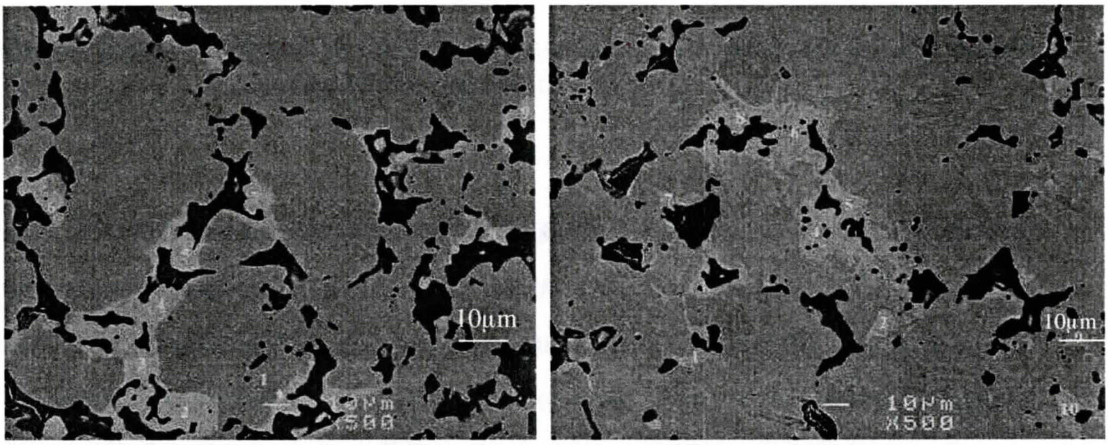

Figure 3-7. 4Ni/0.5C steel with STD-Ni (left) and XF-Ni (right). SEM images used for diffusion calculations. Note that the Ni-rich areas (NRAs) are numbered.

The equation used to calculate diffused Ni, where NRA is a Ni-rich area defined as any distinguishable area on a 500X SEM image, is:

$$\%\,diffused\ Ni = 100 - \left(\frac{\Sigma(NRAarea * \%Ni)}{\text{total metal area} * \%\ \text{total Ni added}} * 100\%\right) \ \ldots\ (\text{Eqn. } 3.1)$$

Table 3.2. Mean values for calculation of diffused nickel using the Microstructure-NRA method.

	A	B	C	D	E	F	G	H
	# of NRAs	%Ni	Area per NRA(um^{2})	Ni Area	Field	Porosity	Metal Area	Diffused Ni
				µm^2	mm^2	%	µm^2	%
XF	12	7.6	70	59	25000	11	22500	***91***
STD	10	16.1	350	560	25000	13	21750	***37***

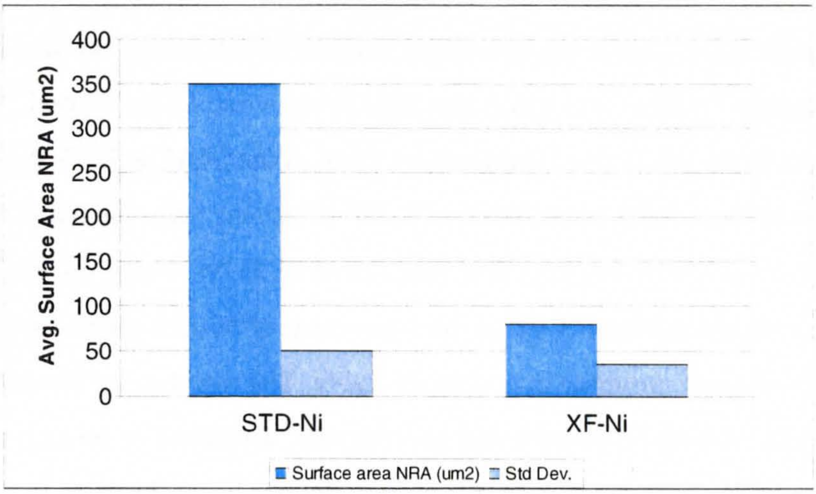

Figure 3-8. Mean size of Ni-rich areas (NRA) in different 4Ni/0.5C steels.

Surface area of Ni-rich areas in 4Ni/0.5C steels was determined by applying gridding software to SEM images taken at 200X magnification. Three cross-sections of each steel were measured and the mean values are reported. Mean surface areas of Ni-rich areas were from 70 and 350 µm^2 for steels made with XF-Ni and STD-Ni respectively. Standard deviation of the wt% Ni in the Ni-rich areas was more than two times higher in steels made with STD-Ni; this result coincides with the SEM-EDX linescan analysis done on the same samples.

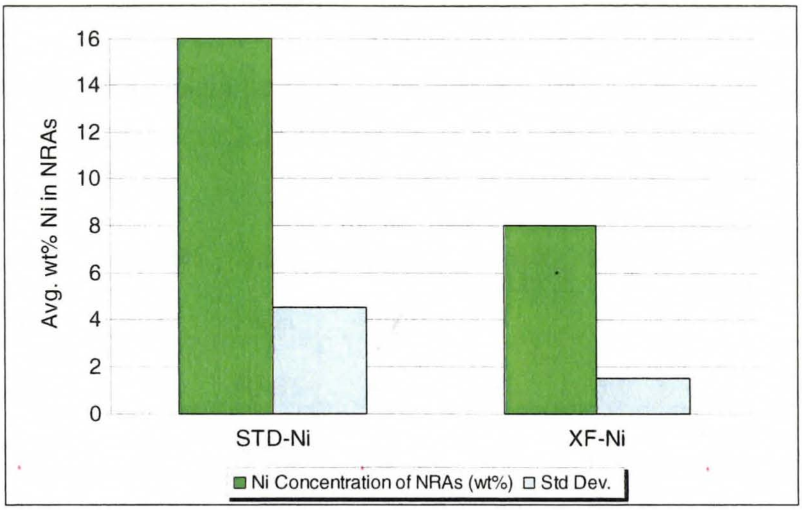

Figure 3-9. Average wt% Ni in NRAs for 4Ni/0.5C steels

Steels with XF-Ni had a slightly larger number of NRAs but the size and wt% Ni of these Ni-rich areas (NRAs) was much less than those in the STD-Ni steel. Average Ni content of NRAs in the steels was measured by EDX in the SEM at 500X magnification. Over an average of three fields each 200 x 125 um^2 in surface area, the mean wt % Ni was 7.6% in steels with XF-Ni and 16.1% in steels with STD-Ni. From the Fe-Ni binary phase diagram shown in Figure 3-10, as the Ni content of Ni-rich phases approaches values less than 5%, Ni-rich austenite is no longer stable. The structure of Ni-rich phases is therefore dependent on both Ni content and cooling rate. Evidence of Ni-rich martensite formation in as-sintered steels made with XF-Ni powder has been observed in other works by the author [15, 17].

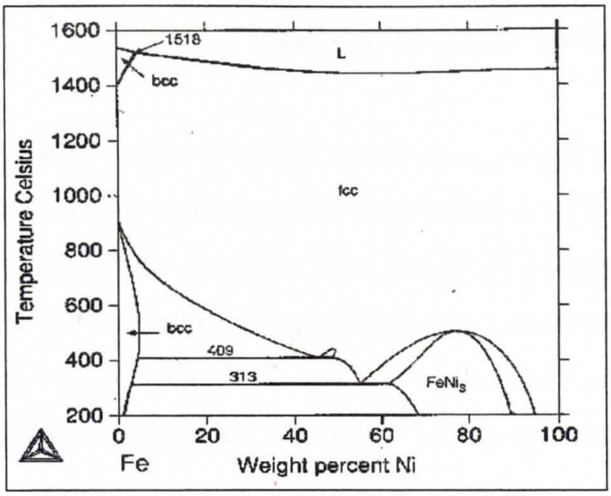

Figure 3-10. Fe-Ni phase diagram [27].

By combining the surface area and Ni content measurements (Microstructure-NRA method), a semi-quantitative method has been developed to estimate diffusion rates of the various Ni powders in P/M steels. Figure 3-11 plots the amount of Ni diffused in the steel (%) vs. the sintering time. The samples were sintered at 1120 °C for 5, 30 and 60 minutes. After conventional sintering for 30 minutes for example, approximately 90% of XF-Ni has diffused, whereas only approximately 40% of STD-Ni powder has diffused.

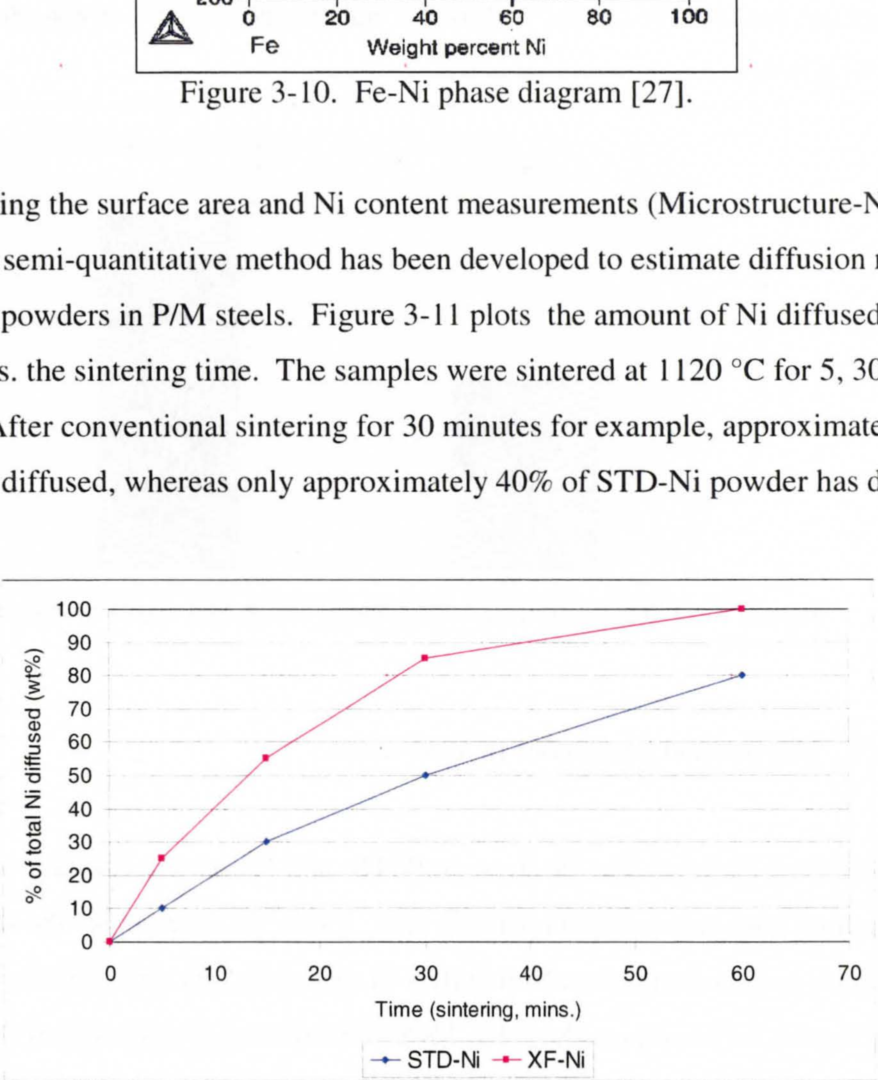

Figure 3-11. Ni diffusion vs. sintering time for 4/Ni-0.5/C steels as calculated using Microstructure-NRA Method. (Note reverse y-axis scales).

3.1.2 Dimensional change properties

It is well known that Ni steels shrink during sintering, leading to densification of P/M steel parts [6-8]. Ni is often added to Cu-steels to control swelling. The shrinkage of Ni steels is controlled by the extent of Ni diffusion into Fe during sintering [15]. Additional shrinkage can be obtained by higher sintering temperatures or longer sintering time and also by using finer Ni powder [15, 17]. In Figure 3-12, it is seen that not only the highest shrinkage, but also the lowest % dimensional change standard deviation is obtained with XF-Ni powder.

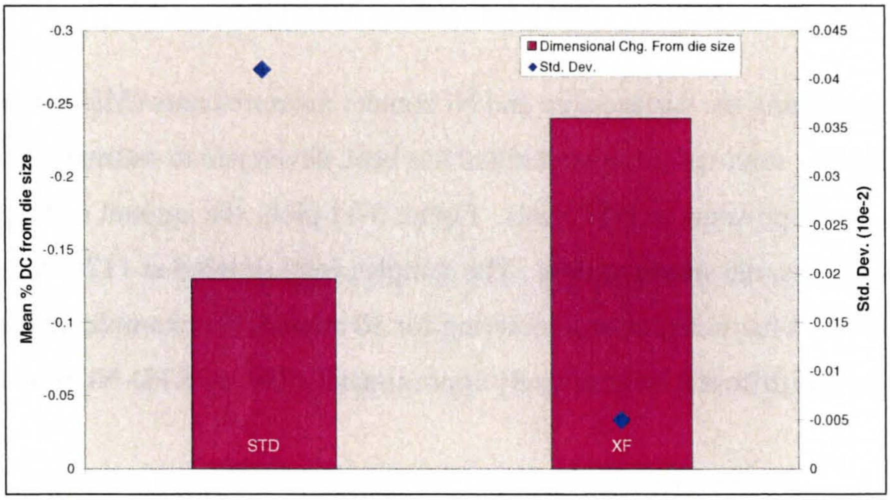

Figure 3-12. Mean dimensional change (% & Std. Dev) of 4Ni/0.5C steels.

3.1.3 Mechanical properties of P/M steels

As-sintered Ultimate Tensile strength (UTS) and Transverse Rupture strength (TRS) increased with decreasing Ni particle size. Table 3.3 summarizes the sintered properties of steels made with the two Ni powders in this study. As well, Figure 3-13, Figure 3-14, and Figure 3-15 compare the UTS, TRS and hardness respectively of the two steels. The XF-Ni powder gave UTS that was ~ 80 MPa larger, TRS ~ 50 MPa larger and hardness ~ 6 HRB more.

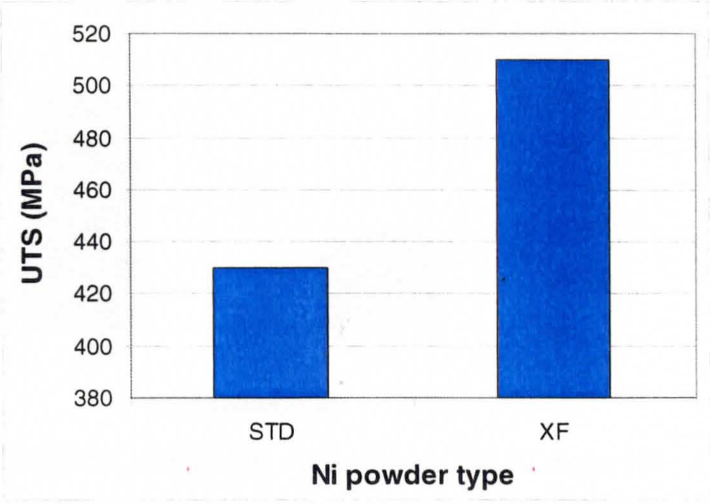

Figure 3-13. UTS values (+/- 20 MPa) of 4Ni/0.5C steels.

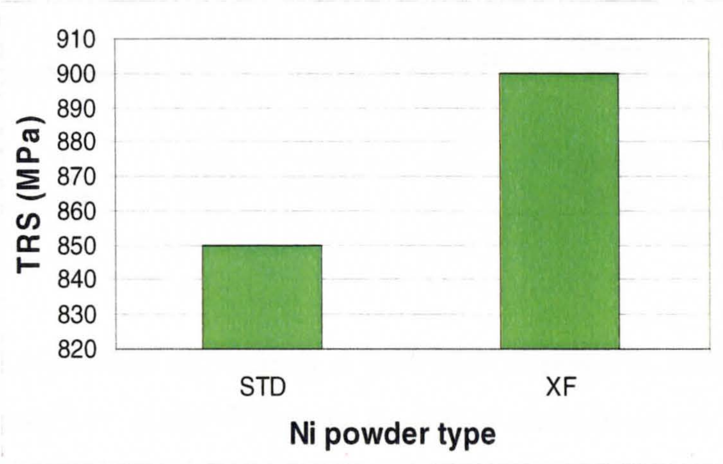

Figure 3-14. TRS values (+/- 20 MPa) of 4Ni/0.5C steels.

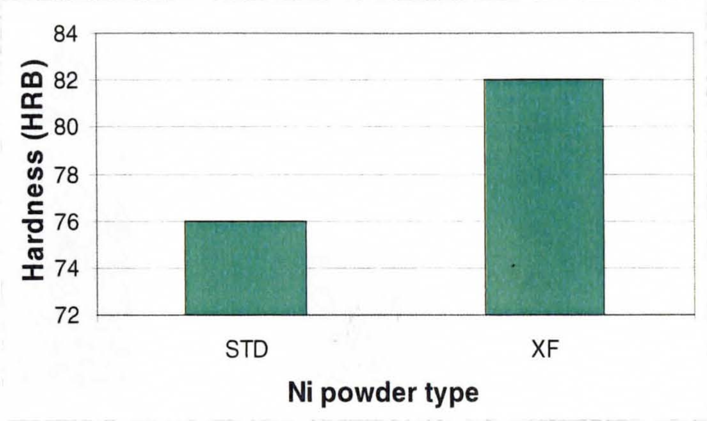

Figure 3-15. Hardness values (+/- 2HRB) of 4Ni/0.5C steels.

Table 3.3. Summary of Mechanical properties of 4Ni/0.5C steels.

Ni powder type	**Sintered Density (g/cc)**	**TRS (MPa)**	**UTS (MPa)**	**% Elongation**	**Apparent Hardness (HRB)**
STD-Ni	7.05	870	430	2.6	79
XF-Ni	7.1	990	520	2.6	84

The increased diffusion of Ni powder as particle size decreases can be measured in microindentation hardness profiles of sintered Ni steels. In Figure 3-16, microindentation hardness was measured along the sample length for as-sintered 4Ni/0.5C steels. Hardness was measured using the Vicker's scale with 500 g applied load. Average microindentation hardness of steels made with XF-Ni powder was 10-15% higher than that in steels with STD-Ni powder.

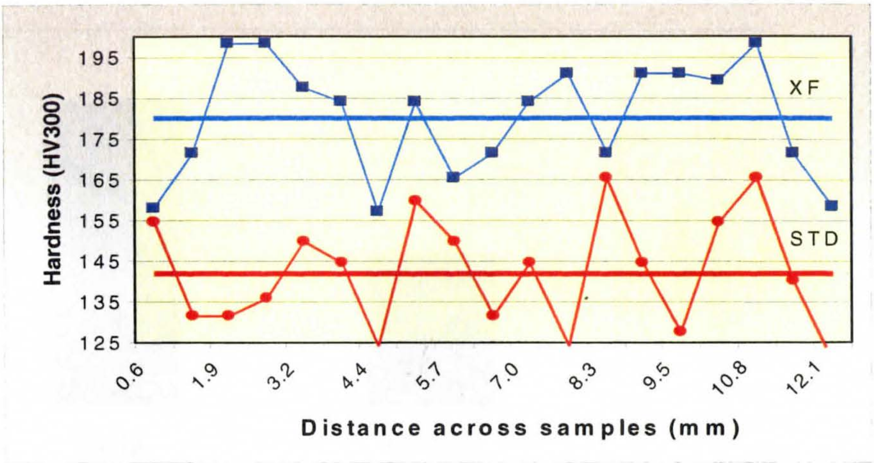

Figure 3-16. Microindentation hardness values of 4Ni/0.5C steels.

In addition to improved mechanical properties with XF-Ni powder vs. STD-Ni, optical micrographs showed increased martensite and bainite in steels with XF-Ni; these results suggested that the hardenability of the steels may be improved with XF-Ni powder. Hardenability analysis was carried out by the Jominy end quench method. Jominy bars of 4Ni-0.85Mo-0.5C steels with each Ni powder were austenitized and cooled at 3°C/s. The depth to which the hardness was at least HRA 65 was then measured. The results are shown in Figure 3.17. XF-Ni steel possessed a hardenability depth two times greater than that of STD-Ni steel. It appears as if the use of XF-Ni alters the phase transformations of the steel upon cooling such that more martensite and bainite are produced in the final structure. A model is proposed in section 3.1.4.2 which shows the phase transformation model.

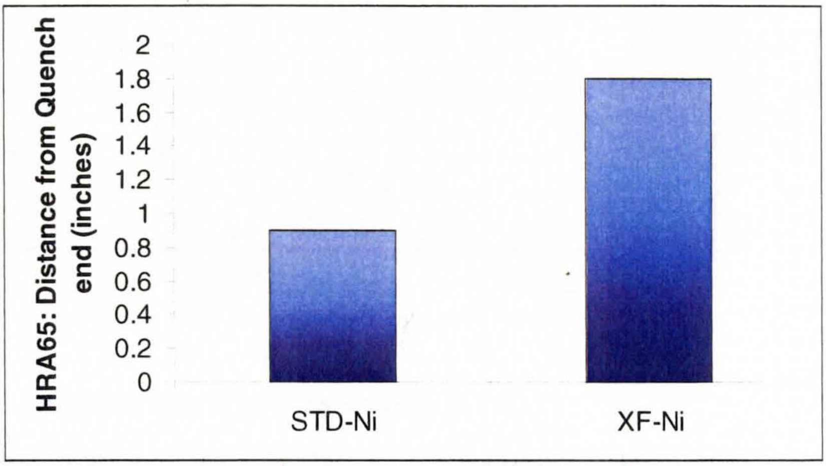

Figure 3-17. Jominy End Quench (Hardenability) depths of STD-Ni and XF-Ni steels (4Ni-0.85Mo-0.5C).

3.1.4 Dilatometry analysis

Figure 3-18 shows the dilatometry curve of the STD-Ni steel and XF-Ni steel, plotting dimensional change as a function of temperature during sintering (and cooling). Inflections in the curve can indicate the presence of mass transport and/or phase transformation events [2].

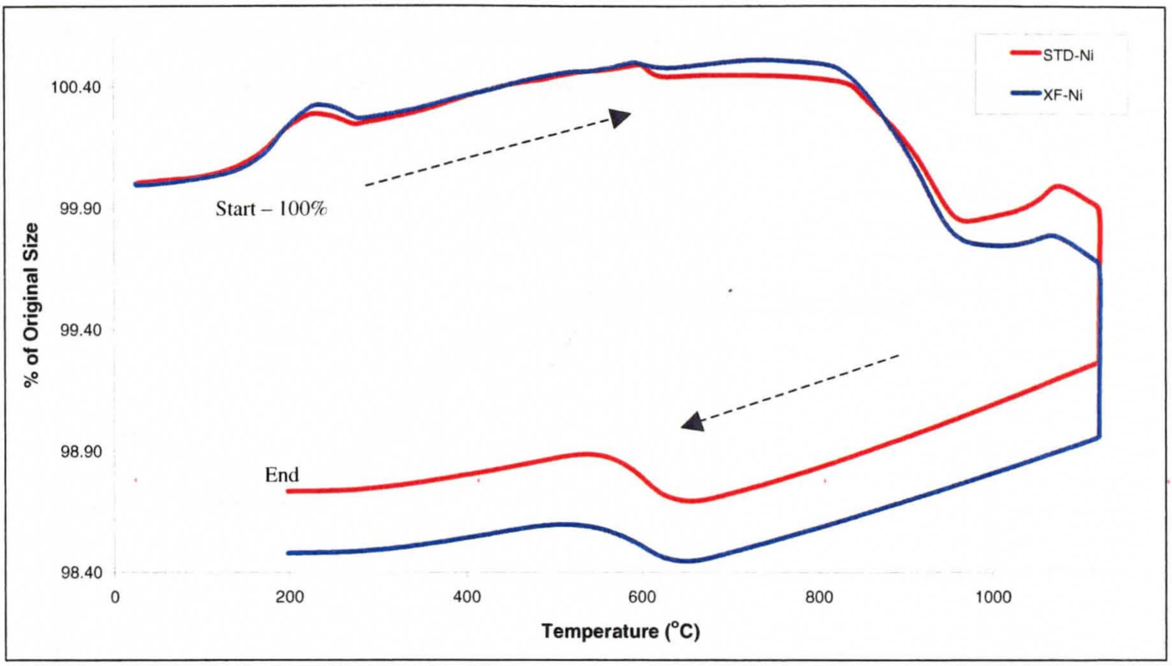

Figure 3-18. Full sintering cycle dilatometry curves of STD-Ni steel and XF-Ni steel.

3.1.4.1 Heating

The dilatometry curve for the heating (ramp-up + soak) of the two steels is shown in Figure 3-19. Up to about 650°C, specimens expand similarly as the temperature increases. The expansion rate, 1.5 x 10^{-3} %/°C corresponds to the thermal expansion coefficient of ferrite [28]. At about 750°C, the expansion rate decreases and the specimens begin shrinking in the temperature range of 800-950°C. This is the temperature range of the ferrite-austenite transformation [28]. At temperatures greater than 950°C, the diffusion of carbon into Fe is accelerated. The major difference in steels with STD-Ni vs. XF-Ni is that steels with STD-Ni begin to expand from 970-1070°C, as C diffuses into Fe, while steels with XF-Ni continue to slightly densify from 970-1020°C and then slightly expand from 1020-1070°C; The rate of expansion is notably less in steels with XF-Ni during this last expansion before reaching the sintering-soaking temperature. From 1070-1120°C, both steels begin to shrink and the overall expansion of the steel with XF-Ni is ~ 0.3% less even before soaking. During soaking at 1120°C (30 mins), the samples densify and show a significant amount of shrinking. The amount of shrinking during sintering is 0.6% for steels with STD-Ni and 0.9% for steels with XF-Ni.

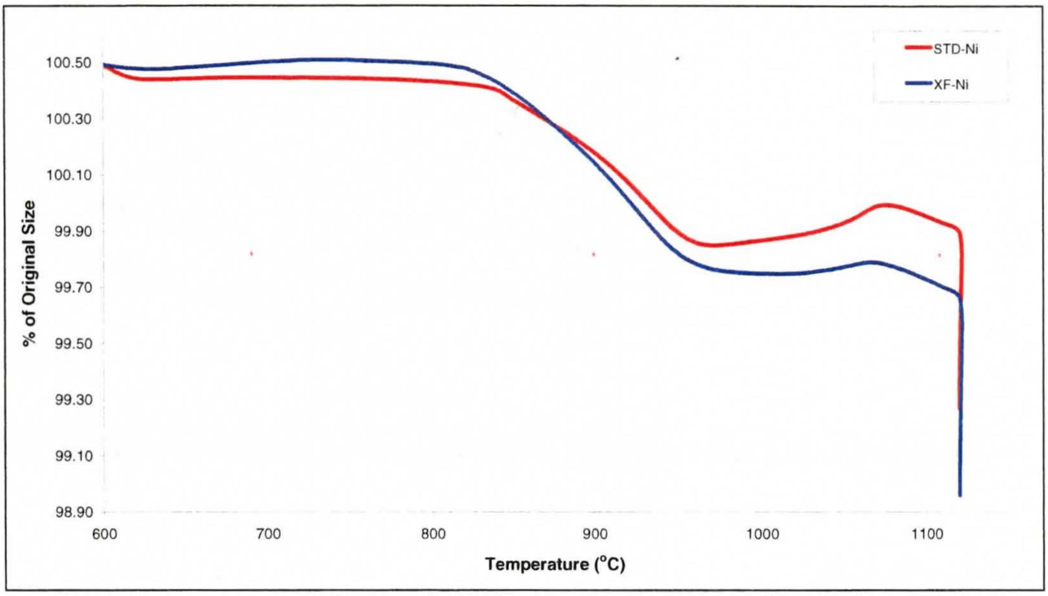

Figure 3-19. Ramp-up + soak sintering dilatometry curves of STD-Ni and XF-Ni steel.

3.1.4.2 Cooling

Figure 3-20 shows the dilatometry curves of the two Ni steels on cooling after sintering. The slopes of the cooling curves of the two Ni steels are very similar from 1120°C to 650°. At a temperature of ~ 650°C the steels undergo the austenite-ferrite transformation. The difference between the two steels is the temperature range of the austenite-ferrite transformation. While this range is approximately 100°C wide (650-550) for steels with STD-Ni, it is approximately 140°C wide (650-510) for steels with XF-Ni. The steels with STD-Ni begin this transformation slightly later at about 590°C and end slightly earlier at about 510°C. The difference in the size of the austenite-ferrite transformation range results in different microstructures begin produced. A larger austentite-ferrite range seems to result in more bainite and martensite being produced in the final microstructure as seen in steels with XF-Ni.

Since the phase transformation zone for XF-Ni is 40°C larger than that for STD-Ni, additional time for bainite and martensite transformation is possible. It is well known that higher Ni contents in steels shift the bainite/martensite (B-M) nose of the Fe-C diagram to the right [29]. Figure 3-21 shows the possible effect of having more Ni in solution with Fe on the phase transformations of steel during cooling. The green line represents a specific cooling curve of a steel and is constant for both steels. The blue dashed lines indicate the B & M lines if XF-Ni was used in the steel and the red lines are those for STD-Ni. With XF-Ni, the B-M nose is shifted to the right, which causes the transformation temperatures to be lowered; this corresponds with the dilatometry results of the current study. In Figure 3-21, the martensite-forming zone is represented by the length of time the cooling curve (green line) is below the dashed M line (nose). By shifting the B-M nose to the right, the amount of time that the cooling curve (green line) is under the M line is greater with XF-Ni. XF-Ni should thus result in a larger amount of martensite being formed in the final steel structure -- analysis of microstructural results support this hypothesis.

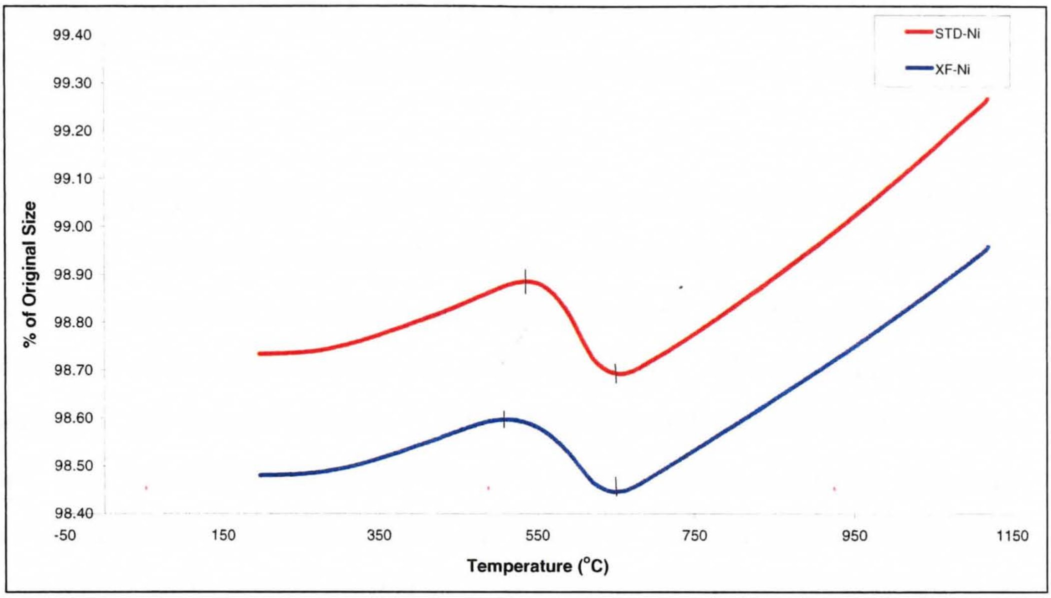

Figure 3-20. Post-sintering cool-down dilatometry curve of STD-Ni and XF-Ni steel.

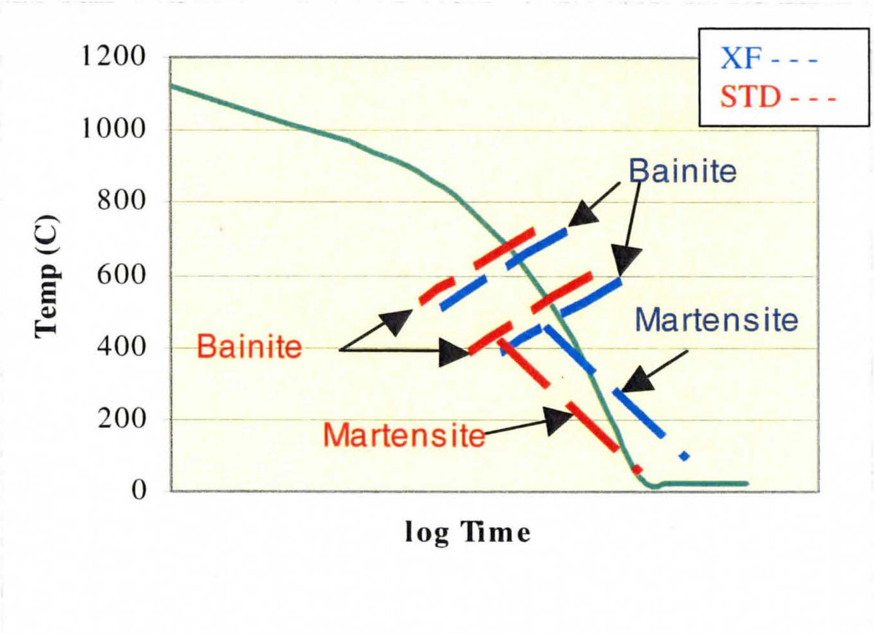

Figure 3-21. Possible effect of finer Ni particle size on phase transformation in steels. Schematic shows how cooling curve is able to be in the martensite-forming longer if phase-transformation zone is enlargened.

3.1.5 Mathematical modeling of Ni diffusion during sintering

The diffusion of Ni powder particles into the Fe matrix during sintering can be modeled using transient diffusion solution methods described in standard textbooks, such as that by Wilkinson [30] -- more specifically, the solution to Fick's Second Law Near Equilibrium (at intermediate times) considering a finite initial solute layer between two finite solvent slabs. Suppose that Ni is the solute layer, with thickness *2h* (STD-Ni = 8 μm, XF-Ni = 1.5 μm), sandwiched between two slabs of Fe, with thickness *2L* (80 μm), and is pressed together (as in compaction). This is shown in Figure 3-22.

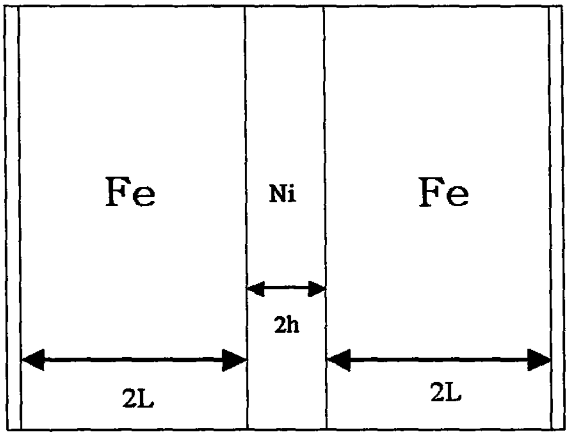

Figure 3-22. Diagram of *Fick's 2nd Law Near Equilibrium model* applied to Ni diffusion during sintering of P/M steels.

The temperature is now increased sufficiently so that significant diffusion can take place and the Ni atoms begin to diffuse into Fe. At the sintering temperature, Ni is completely soluble in bcc-Fe and thus the equation that defines this problem, consisting of a governing equation – Fick's Second Law – and initial and boundary conditions approximates to:

$$C(y,t) = \frac{C^*}{2}\left[erf\left(\frac{h-y}{2\sqrt{Dt}}\right) + erf\left(\frac{h+y}{2\sqrt{Dt}}\right)\right] \quad \ldots\text{(Eq. 3.2)}$$

Where y is the distance across the Fe particle, C* is the normalized wt% concentration of Ni on the Ni side (i.e. = 100%), D is the diffusion coefficient of Ni into Fe at the sintering temperature (1120°C) and t is the time at the sintering temperature. (Normally this equation involves a summation over *n* intervals but for the current approximation only the first iteration, *n*=0, was required). Diffusion profiles of C vs. y were constructed for the case of STD-Ni powder and XF-Ni powder sandwiched between Fe particles. The diffusion profiles of STD-Ni and XF-Ni diffusing across an Fe particle for various sintering times are shown in Figure 3-23 and Figure 3-24.

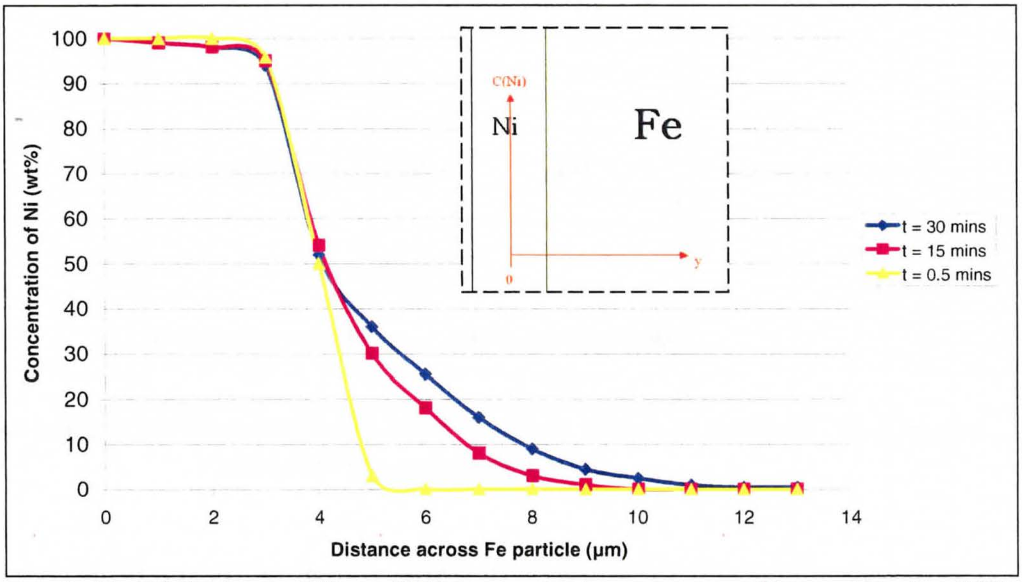

Figure 3-23. Diffusion profiles of Ni concentration across an Fe particle for STD-Ni using *Fick's 2nd Law Near Equilibrium model.*

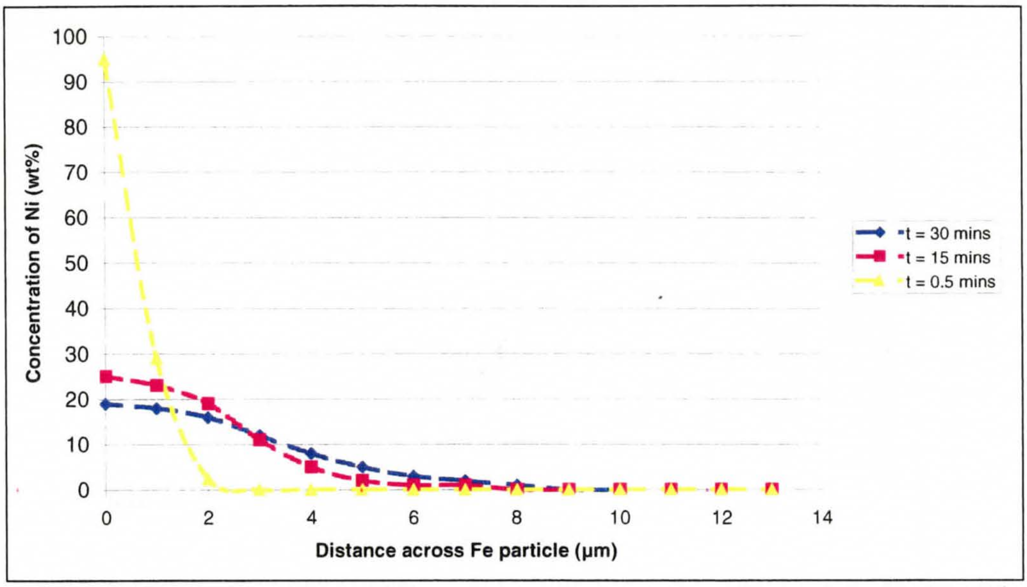

Figure 3-24. Diffusion profiles of Ni concentration across an Fe particle for XF-Ni using *Fick's 2nd Law Near Equilibrium model.*

Figure 3-25 compares the concentration of Ni at the middle of a Ni particle (y=0) as a function of sintering time. The dissolution of XF-Ni (decrease of wt% Ni at the middle of the Ni particle) is much faster than with the STD-Ni. If we use a concentration reduction to 20% nickel as a simple indicator of particle dissolution then the time required for the XF-Ni particles is about 25 minutes (i.e. within the normal sintering time period) whereas that for the STD-Ni is much longer, about 70 minutes. Moreover by the end of the sintering process (30 min) the Ni content at the centre of the STD-Ni particles is still over 90%

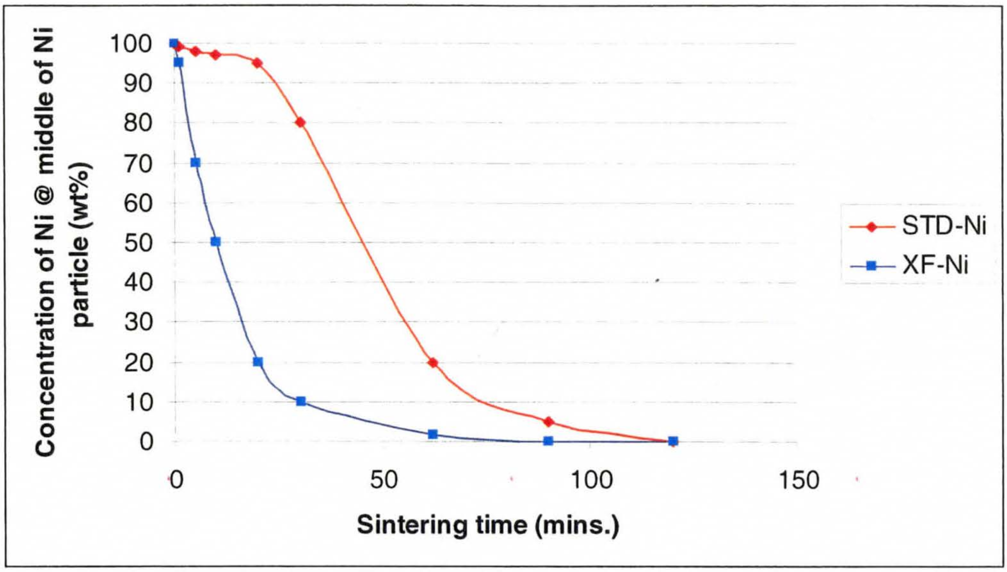

Figure 3-25. Comparison of time required for dissolution of single STD- and XF-Ni particle using *Fick's 2nd Law Near Equilibrium model.*

The most important and interesting results from the diffusion profiles are:

- In both cases Ni only diffuses approximately 10-12 μm into the Fe particle even after 30 mins at the sintering temperature.
- The diffusion profile of XF-Ni is much more uniform across the Fe particle
- At a distances less than 5 μm into the Fe particle, with STD-Ni the concentration of Ni is 20-100 wt% Ni; with XF-Ni, the concentration of Ni is 4-20 wt% Ni.
- The diffusion profiles support SEM micrographs which show large Ni-rich areas near pores in steels with STD-Ni and very little / no Ni-rich areas in steels with XF-Ni.
- The profiles show how the particle size of Ni powder affects the distribution of Ni within the steel matrix during sintering.

Figure 3-26 and Figure 3-27 show simple schematic 2-D diagrams of Ni dissolution of the two different Ni powders assuming a specific volume fraction before and after sintering respectively. XF-Ni, because of its fine size, almost completely coats the surface of the Fe powder; STD-Ni, with a much larger volume than XF-Ni, is found at few isolated regions on the Fe powder. Upon sintering, the XF-Ni gives a uniform "ring" of Ni steel area, while the STD-Ni powder leaves "trace stains" where it was originally located. Also note that the Ni-affected area is deeper into the Fe particle with XF-Ni than with STD-Ni (9 μm vs. 6 μm).

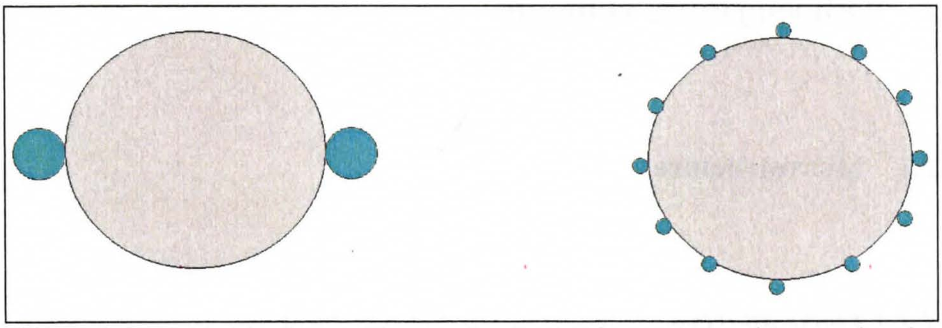

Figure 3-26. Schematic depicting Fe powder (grey) in contact with equal volumes of STD-Ni powder (left) and XF-Ni powder (right).

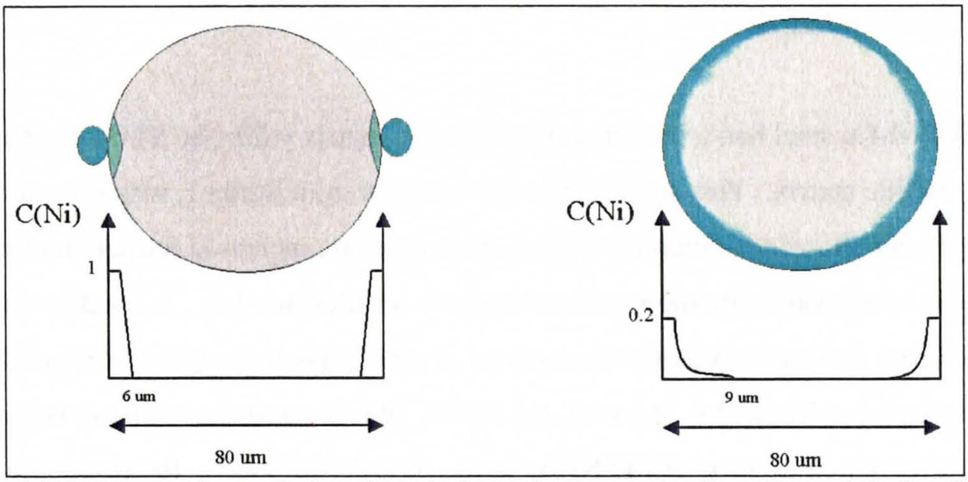

Figure 3-27. Schematic depicting dissolution of Ni powder into Fe particle for STD-Ni powder (left) and XF-Ni powder (right).

3.2 Study 2 – Effect of Ni particle size on properties of 2Ni/2Cu steels with varying C contents

3.2.1 Microstructure

3.2.1.1 Phase analysis

3.2.1.1.1 0.5 C steels

XF Ni-Cu steel had a predominantly bainitic matrix while the STD steel had a more pearlitic matrix. This result agrees with results from Study 1, which show that finer Ni powder allowed for increased levels of martensite, increased formation of harder phases and correspondingly higher microhardness profiles in steels. A breakdown of the phases of both steels as calculated by analysis of optical micrographs in ProTools Imagegridder is shown in Table 3.4. As well, the XF-Ni NRAs seemed to be more bainitic-martenstic as compared to the pearlitic NRAs in the STD Ni-Cu steels. Representative optical micrographs of cross-sectional microstructures are shown in Figure 3-28. In both samples, colonies of pearlite, ferrite, feathery textured bainite and widely dispersed (cream-coloured) Ni-rich areas (NRA) are evident. Cu (brownish-coloured) was often found bordering NRAs, indicating an interaction between Ni and Cu during sintering. Overall, the XF-Ni steel showed much better Ni distribution than the steel with STD-Ni.

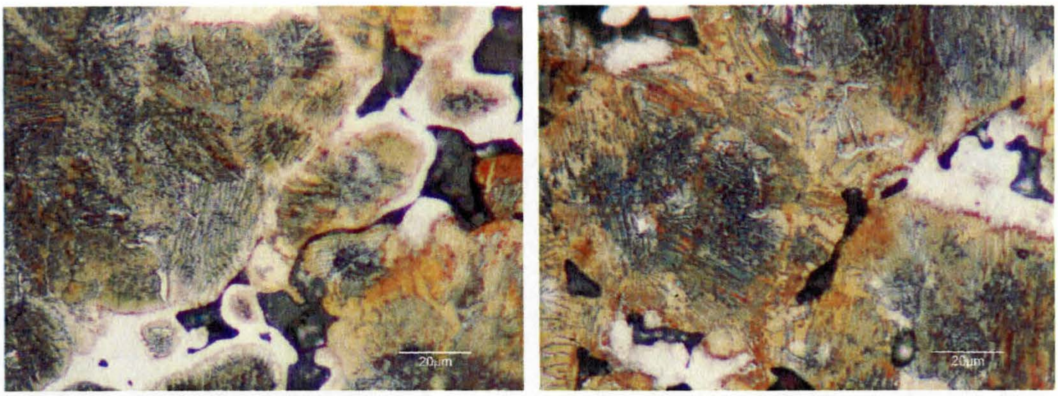

Figure 3-28. Optical micrographs of cross-sections of 2Ni/2Cu/0.5C steels with STD-Ni addition (left) and a XF-Ni addition (right).

Table 3.4. Quantitative phase analysis of 2Ni/2Cu/0.5C steels.

	Approximate area % phases +/- 5%			
	Martensite	*Bainite*	*Austenite*	*Pearlite*
STD-Ni/Cu/0.5C steel	25	15	30	30
XF-Ni/Cu/0.5C steel	35	25	20	20

3.2.1.1.20.8 C steels

The phases of both steels were very similar at the 0.8C level. The STD Ni steel has more of a pearlitic matrix, whereas the XF Ni steel has more of a bainitic (darker) matrix. The STD steel has hard phases of bainite-martensite and the XF seems to have hard phases of martensite. The effect of finer Ni size becomes somewhat masked by the higher C levels. The XF-Ni steel did however have more martensite than the steel with STD-Ni (as evidence by darker phases after etching). Also, it was seen that the NRAs were more martensitic with XF-Ni. This result corresponds well from results of Study 1 with Ni steels and with the results from the 0.5C Ni-Cu steels in the current study. The microstructures are shown in Figure 3-29. A breakdown of the phases of both steels as calculated by analysis of optical micrographs in ProTools Imagegridder is shown in Table 3.5. NRAs in the steel with XF-Ni are less austenitic because they contain a lower wt% Ni which matches hypotheses from observation of the Fe-Ni phase diagram.

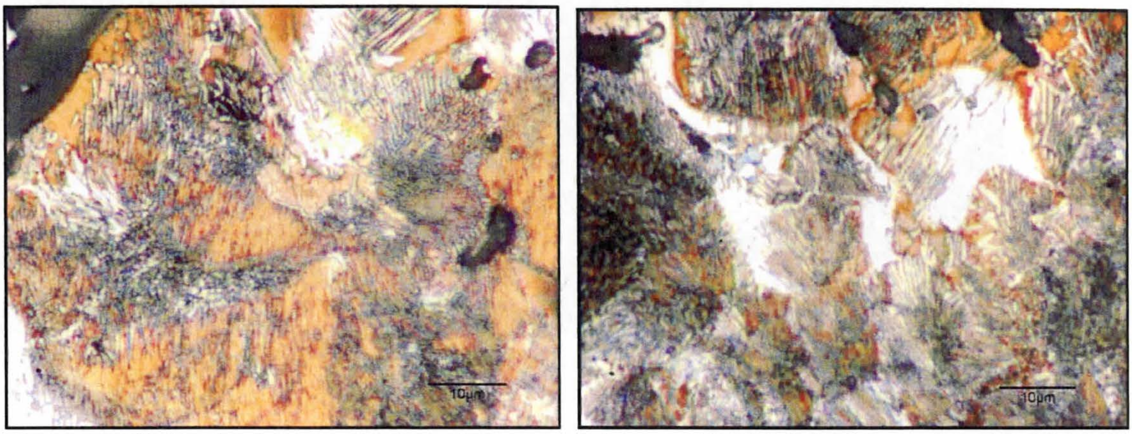

Figure 3-29. Optical micrographs of cross-sections of 2Ni/2Cu/0.8C steels with STD-Ni addition (left) and a XF-Ni addition (right).

Table 3.5. Quantitative phase analysis of 2Ni/2Cu/0.8C steels.

	Approximate area % phases +/- 5%			
	Martensite	*Bainite*	*Austenite*	*Pearlite*
STD-Ni/Cu/0.8C steel	35	35	30	-
XF-Ni/Cu/0.8C steel	55	25	20	-

3.2.1.2 SEM-EDX Linescan analysis

3.2.1.2.1 <u>0.5C steels</u>

The most significant difference in the microstructure was seen in the distributions of Ni and Cu in the samples. Representative low-magnification cross sections of each steel are shown in Figure 3-30. The whitish-coloured regions represent Ni-rich areas. These images clearly show how the number and size of NRAs is much smaller in steels with the XF Ni powder.

The corresponding linescan profiles of the two steels (Figure 3-31 and Figure 3-32 for STD-Ni/Cu and XF-Ni/Cu respectively) quantitatively show that Ni and Cu do indeed associate with each other in the sintered steel, as the wt % values of these alloying elements follow each other across the field. In comparing the two linescan profiles, the XF steel has a much more uniform Ni and Cu wt% distribution. Notice how the levels of Ni and Cu follow each other in both plots. Also note how the values of Ni and Cu fluctuate substantially across the field in the STD steel. This indicates a rather non-uniform alloy distribution. The fluctuation of Ni and Cu values is much reduced and the levels of Ni and Cu are much lower in the XF steel. This is a good indication of a uniform alloy distribution.

The uniformity of the alloying elements can also be depicted as a statistical distribution, as shown in Figure 3-33 and Figure 3-34 for steels with STD-Ni and XF-Ni respectively. The "ideal" wt % range of Ni and Cu was assumed to be greater than 0% (insufficient alloy concentration) and less than 4% (excessive alloy concentration). In the STD steels, the % of points in the non-ideal range for Ni and Cu is much larger; there is approximately two times more Ni and three times more Cu in the non-ideal range in the STD steels.

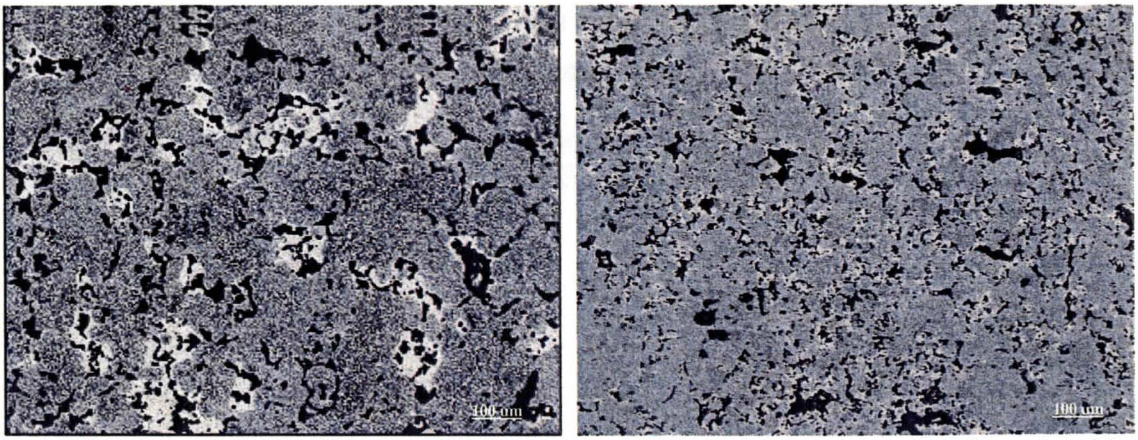

Figure 3-30. Low-magnification images of cross-sections of 2Ni/2Cu/0.5C steels with STD-Ni (left) and XF-Ni (right).

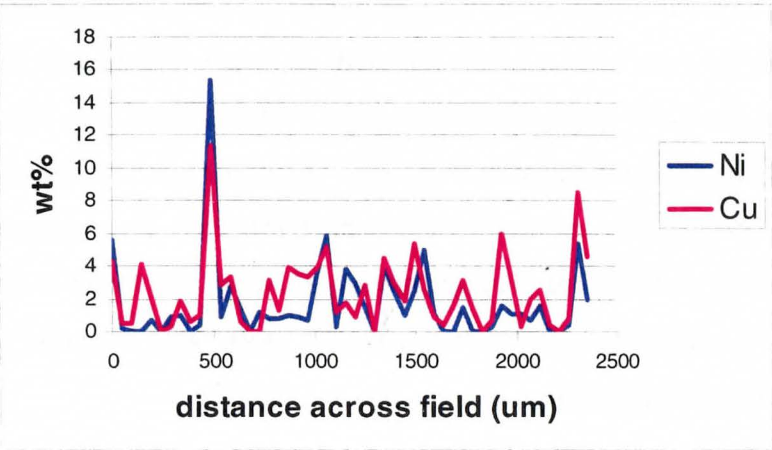

Figure 3-31. Linescan analysis of Ni and Cu wt% distribution across a representative field of 2Ni/2Cu/0.5C steel with STD-Ni.

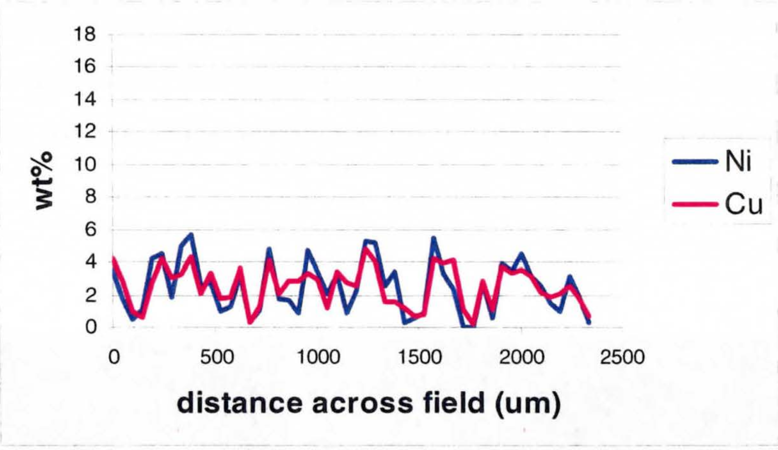

Figure 3-32. Linescan analysis of Ni and Cu wt% distribution across a representative field of 2Ni/2Cu/0.5C steel with XF-Ni.

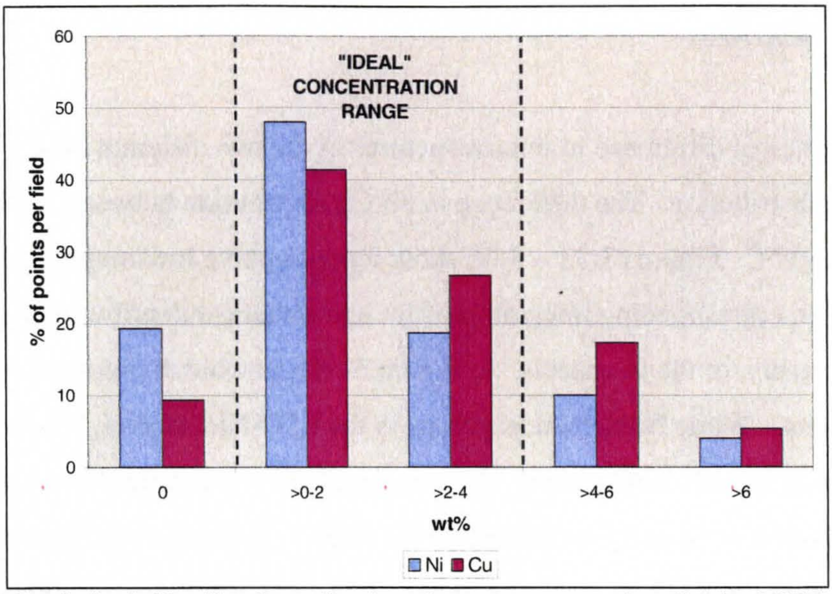

Figure 3-33. Statistical distribution of points in a representative field of STD-Ni/Cu/0.5C steel from linescan analyses.

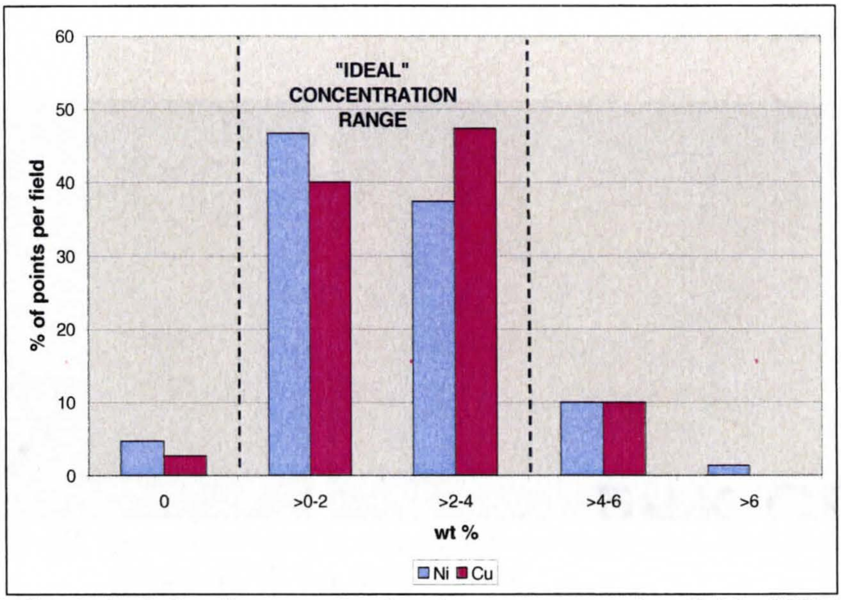

Figure 3-34. Statistical distribution of points in a representative field of XF-Ni/Cu/0.5C steel from linescan analyses.

3.2.1.2.2 0.8C steels

The principal difference in microstructures of the two different Ni-Cu steels was the Ni/Cu distribution. The difference in Ni/Cu distribution between the two steels was also seen at 0.5C. Figures 3-32 – 3-36 show representative low-magnification SEM cross-sections, corresponding linescan profiles and statistical distributions of the linescan respectively, of the two steels. In Figure 3-35, the whitish-coloured regions represent Ni-rich areas. While Ni-rich areas persist in the STD-Ni/Cu steel, NRAs are finer and less visible in the XF-Ni/Cu steel. The steels with XF-Ni powder have a much more uniform distribution of Ni and Cu throughout the field. In comparing Figure 3-36 and Figure 3-37, with the STD-Ni steel, the levels of Ni and Cu follow each other and the values of the alloying elements fluctuate from very low (0 %) to very high (> 18 %). In the linescan analysis of the XF-Ni steel , the Ni and Cu profiles are very uniform and follow each other as well.

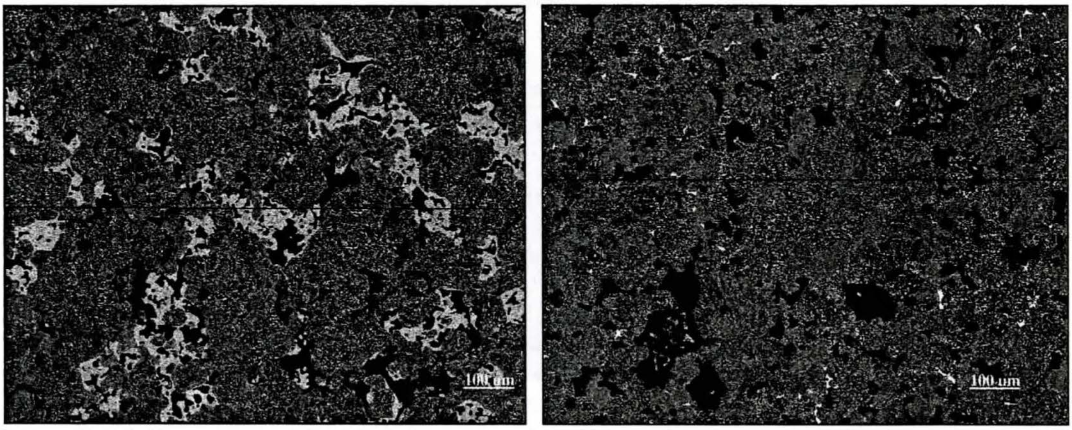

Figure 3-35. Low-magnification images of cross-sections of 2Ni/2Cu/0.8C steels with STD-Ni (left) and XF-Ni (right).

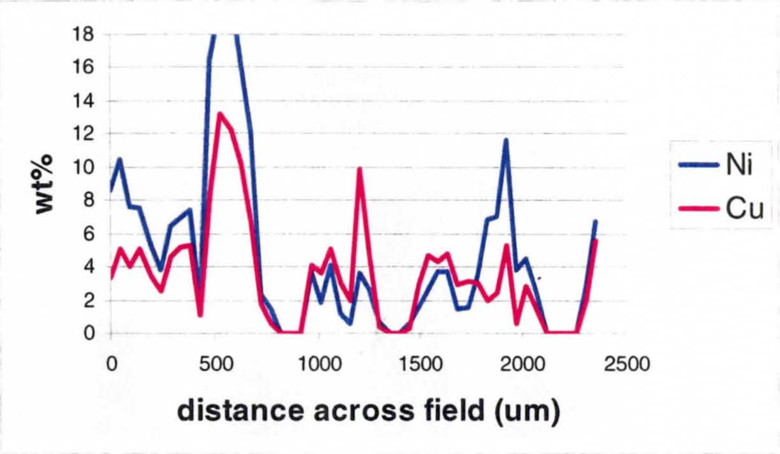

Figure 3-36. Linescan analysis of 2Ni/2Cu/0.8C steel with STD-Ni.

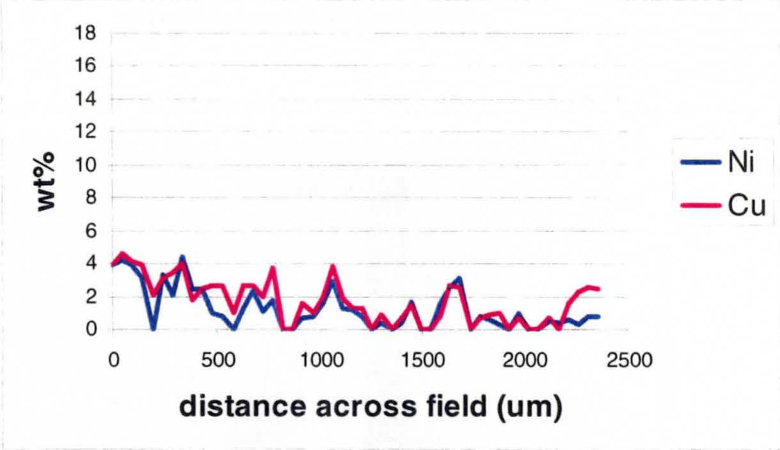

Figure 3-37. Linescan analysis of 2Ni/2Cu/0.8C steel with XF-Ni.

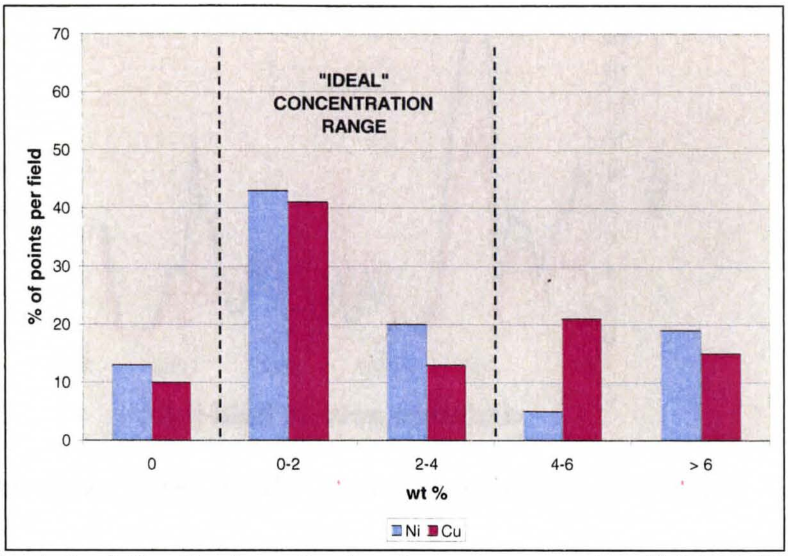

Figure 3-38. Statistical distribution of points in a representative field of STD-Ni/Cu/0.8C steel from linescan analyses.

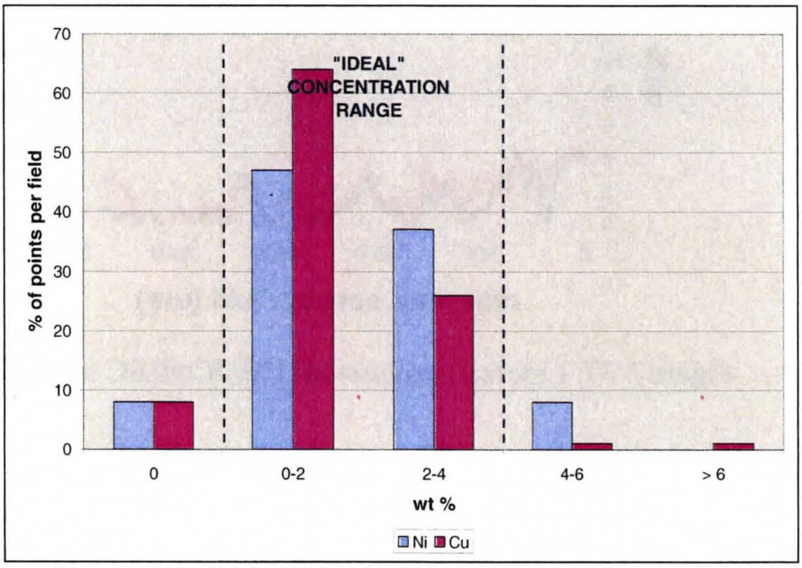

Figure 3-39. Statistical distribution of points in a representative field of XF-Ni/Cu/0.8C steel from linescan analyses.

3.2.1.3 Microstructural evolution during sintering

In order to measure the relative diffusion of Cu and Ni into the steel matrix during sintering, detailed quantitative SEM-EDX analysis was carried out on four different steels as a function of sintering temperature: (1) 2STD-Ni/Cu/0.5C steel, (2) 2XF-Ni/Cu/0.5C steel, (3) 4Cu/0.5C steel, and (4) 2XF-Ni/Cu/0.8C steel. Samples of each steel were sintered to 500°C, 800°C and 1120°C for 30 mins and the composition of the phases of each steel's microstructure was analysed. Three fields per steel were chosen for analysis. In each field, 5 EDX measurements were carried out to determine the wt% composition of the steel matrix and that of the Cu-rich phases. The mean values of 15 measurements per phase per steel are shown here (5 EDX measurements per phase x 3 fields per steel). The results of the EDX phase composition analyses at the three different temperatures are shown in Tables 3.6 – 3.8. Linescan Ni/Cu maps + SEM micrographs of the microstructure at 500X and 1000X for the three different temperatures are shown in Figs 3-37 – 3-40.

Results show that although slight Ni and Cu diffusion does occur at 500°C and 800°C, most of the diffusion takes place after 800°C, following the ferrite-to-austenite transformation. At 1120°C, approximately 70% of the total Cu added dissolved into the steel matrix in the 2STD-Ni/2Cu/0.5C steel. Cu-rich phases are usually very small areas (2-10 μm wide) typically encircling pores. With the same steel composition with XF-Ni, the diffusion of Cu into the matrix jumped to 95%. In addition, a stronger interaction between Ni and Cu was observed in the Cu-rich phase when XF-Ni was used, i.e. higher wt% Ni with Cu. In all steels containing Ni and Cu, Ni and Cu had a greater affinity for each other than with Fe, as indicated by higher Cu and Ni wt% values in Cu-Ni-Fe alloy regions. This supports results from linescan analyses and dimensional change measurements which showed increased Ni-Cu interaction between Ni and Cu and improved distribution of Cu and Ni in steels with finer Ni. The improved mechanical properties of steels with XF-Ni is most likely related to the improved diffusion of Cu in the steel matrix when using XF-Ni.

In comparing Ni-Cu steels with 0.5C vs. 0.8C, the diffusion of both Ni and Cu in the steel matrix decreases with higher C content and the interaction between Ni and Cu in Cu-rich regions increases. This is confirmed by linescan analyses / EDX mapping as well as dimensional change measurements.

Table 3.6. SEM-EDX compositional analysis of P/M steels sintered @ 500°C.

Steel	Phase	wt% Cu	wt% Ni	wt% Fe
4Cu/0.5C	*Matrix*	0.3	-	bal.
	Cu-rich phase	90.0	-	10.0
2STD-Ni/2Cu/0.5C	*Matrix*	0.2	0.1	bal.
	Cu-rich phase	85.0	10.0	5.0
2XF-Ni/2Cu/0.5C	*Matrix*	0.3	0.3	bal.
	Cu-rich phase	62.0	32.0	22.0
2XF-Ni/2Cu/0.8C	*Matrix*	0.3	0.3	bal.
	Cu-rich phase	58.0	38.0	4.0

Table 3.7. SEM-EDX compositional analysis of P/M steels sintered @ 800°C.

Steel	Phase	wt% Cu	wt% Ni	wt% Fe
4Cu/0.5C	*Matrix*	0.4	-	bal.
	Cu-rich phase	83.0	-	10.0
2STD-Ni/2Cu/0.5C	*Matrix*	0.4	0.2	bal.
	Cu-rich phase	78.0	10.0	5.0
2XF-Ni/2Cu/0.5C	*Matrix*	0.5	0.5	bal.
	Cu-rich phase	50.0	40.0	10.0
2XF-Ni/2Cu/0.8C	*Matrix*	0.3	0.3	bal.
	Cu-rich phase	50.0	45.0	5.0

Table 3.8. SEM-EDX compositional analysis of P/M steels sintered @ 1120°C.

Steel	Phase	wt% Cu	wt% Ni	wt% Fe
4Cu/0.5C	Matrix	2.5	-	bal.
	Cu-rich phase	65.0	-	35.0
2STD-Ni/2Cu/0.5C	Matrix	1.4	1.5	bal.
	Cu-rich phase	50.0	25.0	25.0
2XF-Ni/2Cu/0.5C	Matrix	1.9	2.0	bal.
	Cu-rich phase	40.0	38.0	22.0
2XF-Ni/2Cu/0.8C	Matrix	1.2	1.4	bal.
	Cu-rich phase	45.0	42.0	13.0

2STD-Ni/2Cu/0.5C steel

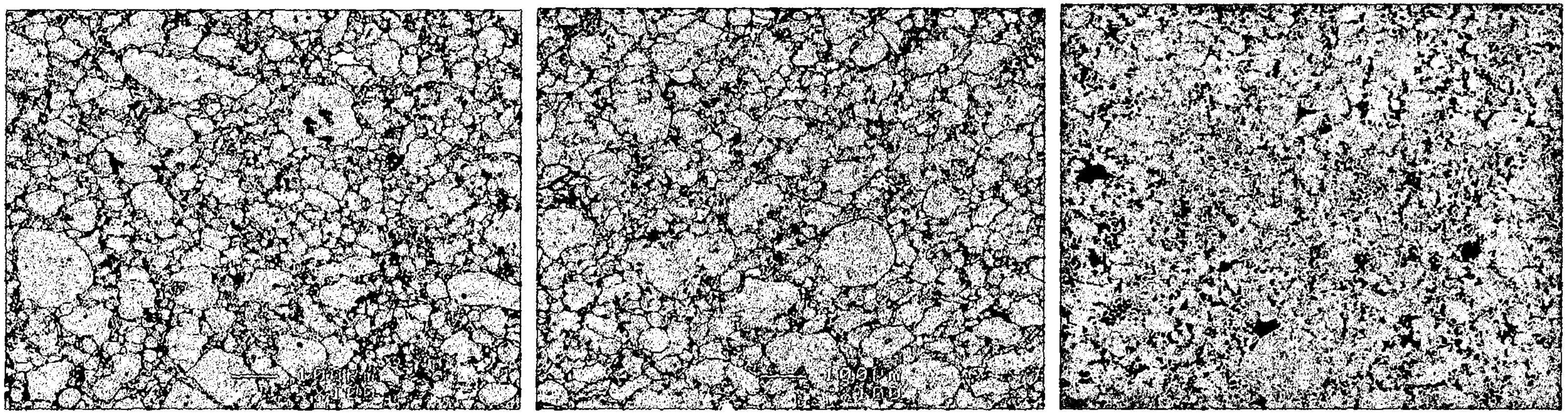

Fig. 3-37a. 100X SEM - 2STD-Ni/2Cu/0.5C steel sintered @ (from left to right) 500°C, 800°C, and 1120°C.

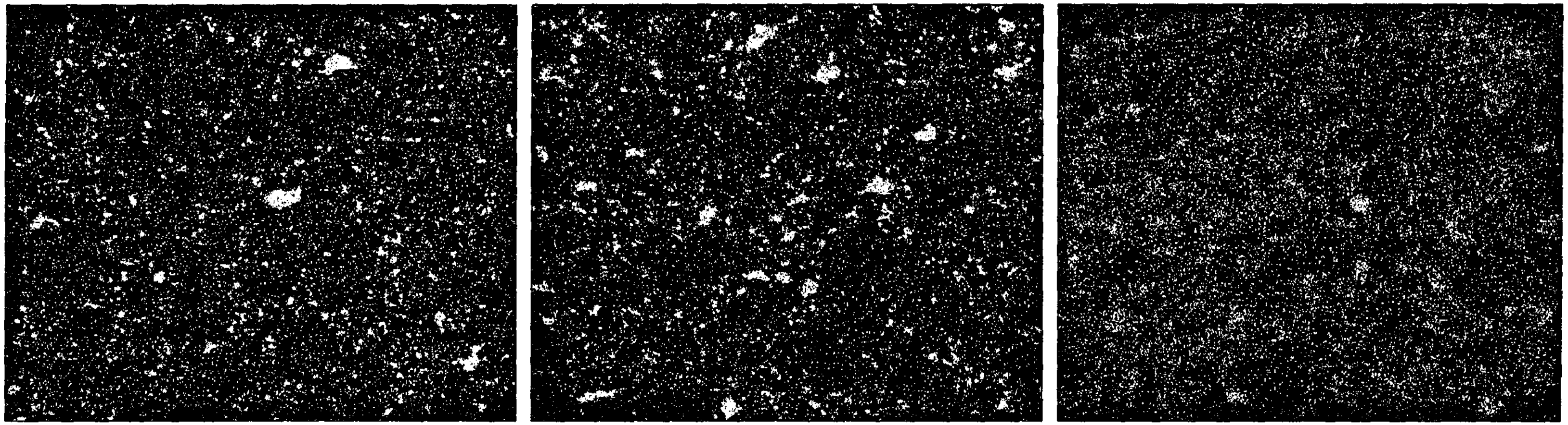

Fig. 3-37b. 100X X-ray maps - 2STD-Ni/2Cu/0.5C steel sintered @ (from left to right) 500°C, 800°C, and 1120°C.

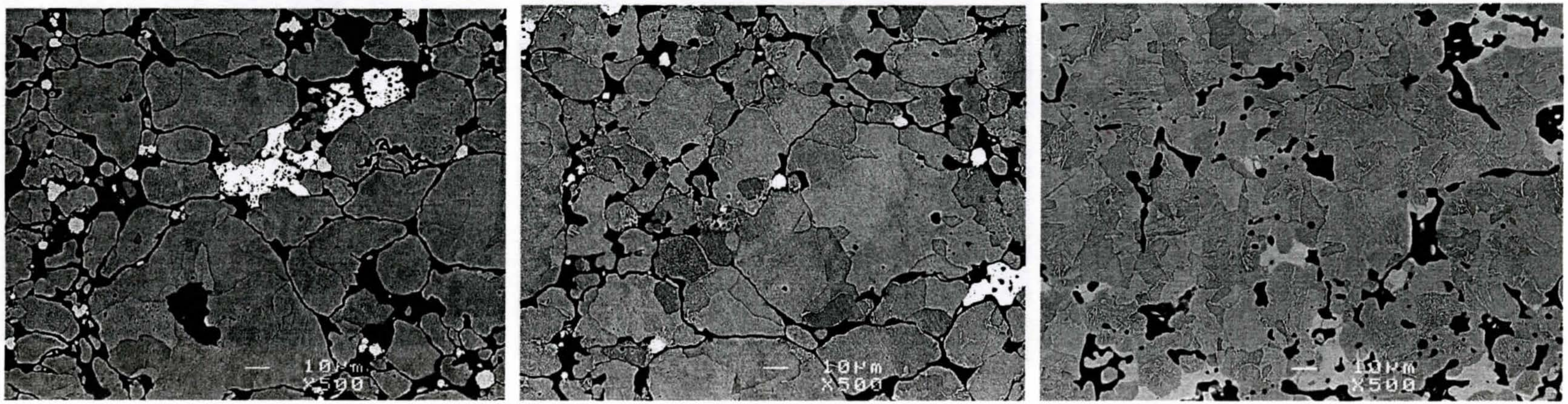

Fig. 3-37c. 500X SEM - 2STD-Ni/2Cu/0.5C steel sintered @ (from left to right) 500°C, 800°C, and 1120°C.

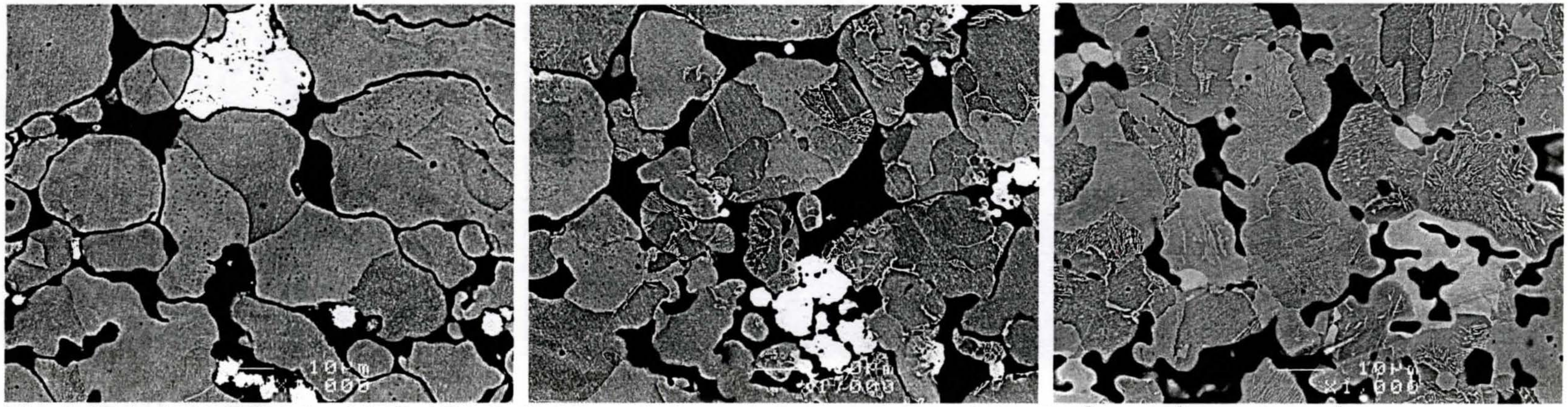

Fig. 3-37d. 1000X SEM - 2STD-Ni/2Cu/0.5C steel sintered @ (from left to right) 500°C, 800°C, and 1120°C.

2XF-Ni/Cu/0.5C steel

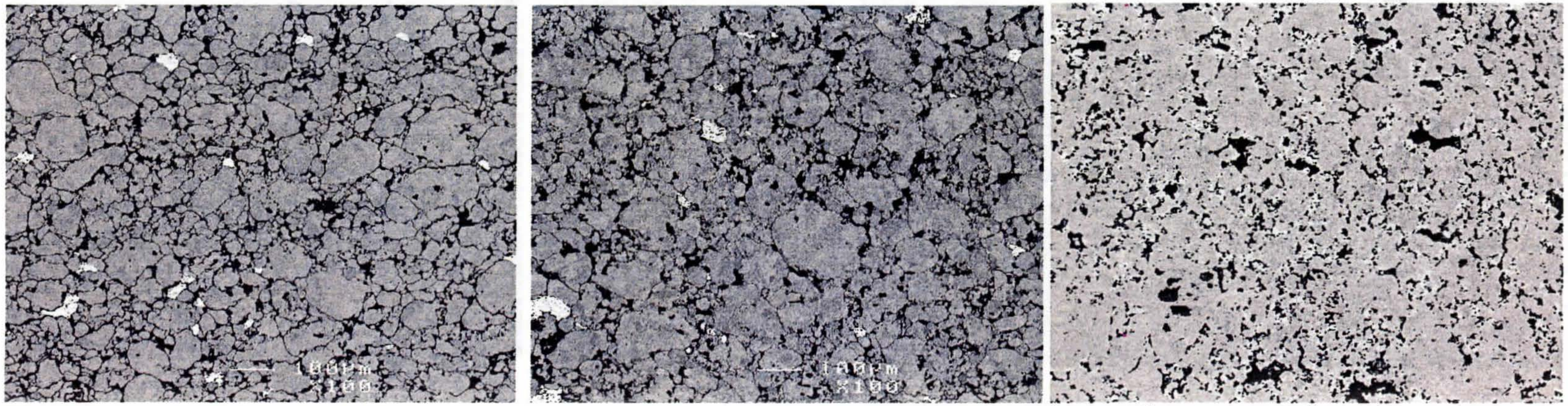

Fig. 3-38a. 100X SEM - 2XF-Ni/2Cu/0.5C steel sintered @ (from left to right) 500°C, 800°C, and 1120°C.

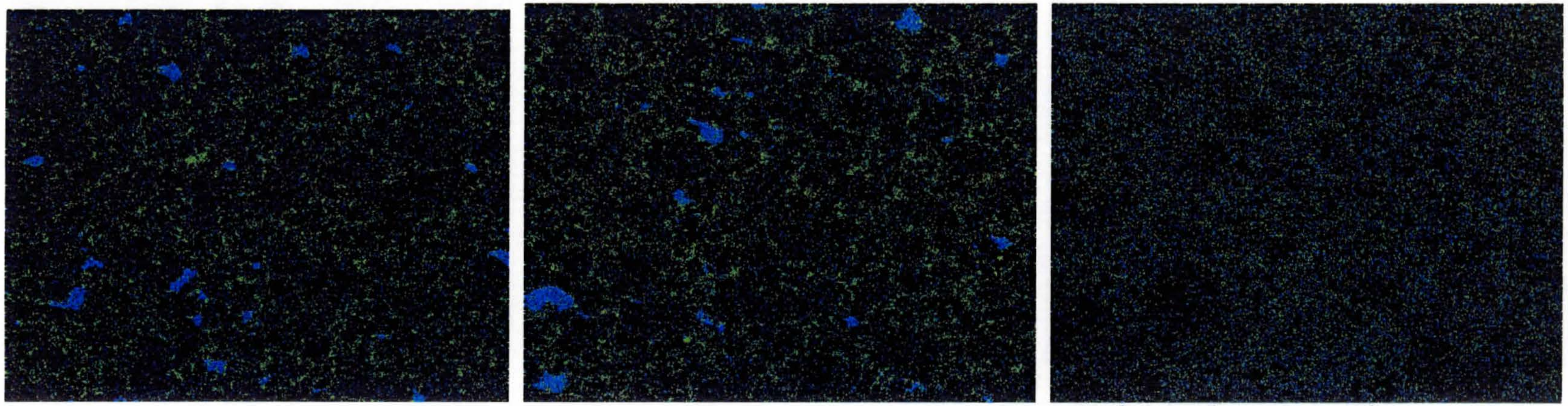

Fig. 3-38b. 100X X-ray maps - 2XF-Ni/2Cu/0.5C steel sintered @ (from left to right) 500°C, 800°C, and 1120°C.

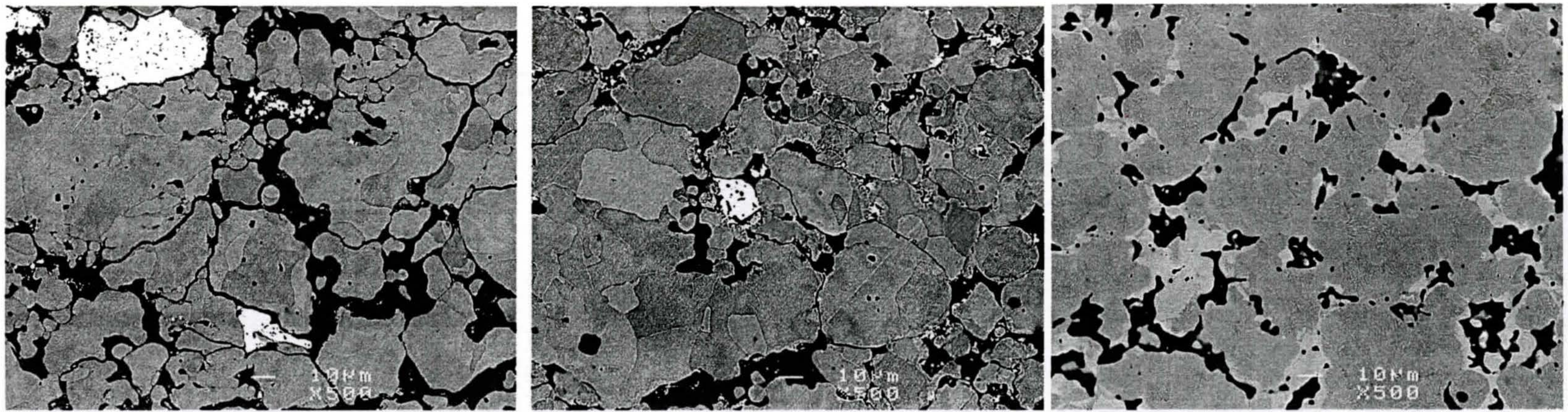

Fig. 3-38c. 500X SEM - 2XF-Ni/2Cu/0.5C steel sintered @ (from left to right) 500°C, 800°C, and 1120°C.

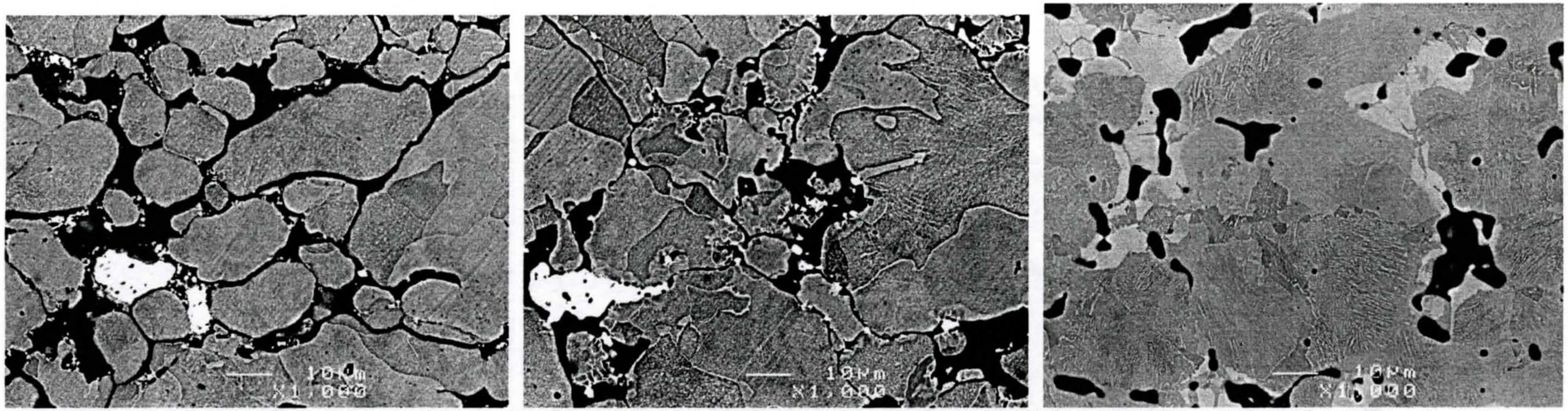

Fig. 3-38d. 1000X SEM - 2XF-Ni/2Cu/0.5C steel sintered @ (from left to right) 500°C, 800°C, and 1120°C.

4Cu/0.5C steel

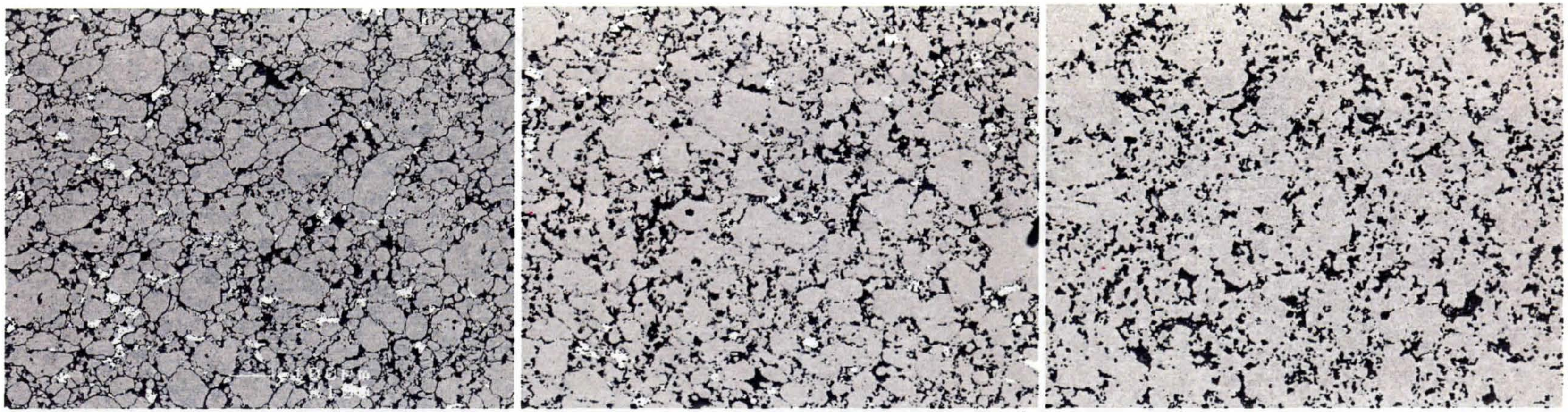

Fig. 3-39a. 100X SEM - 4Cu/0.5C steel sintered @ (from left to right) 500°C, 800°C, and 1120°C.

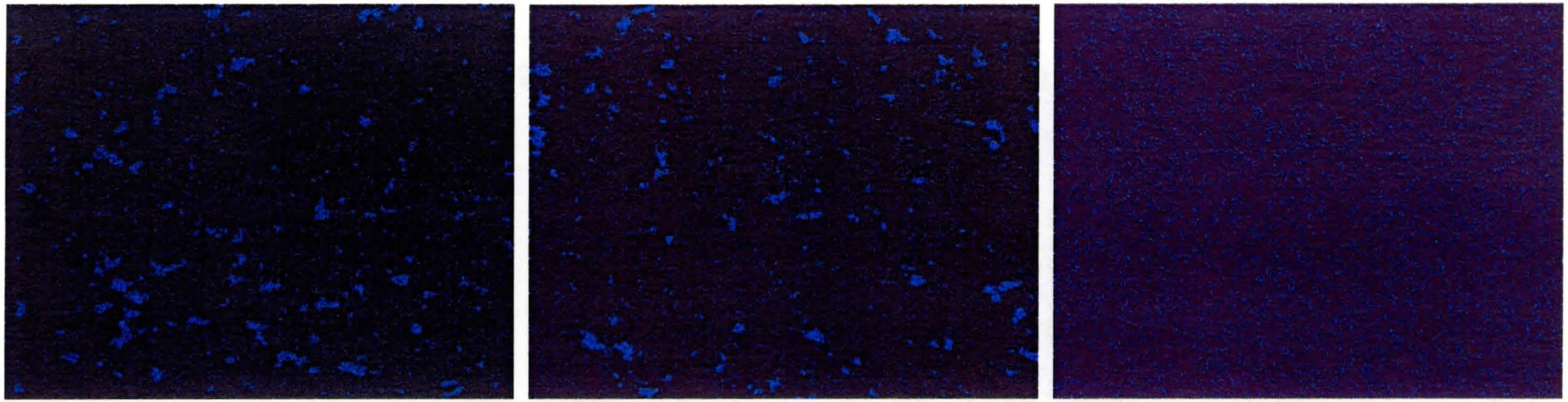

Fig. 3-39b. 100X X-ray maps - 4Cu/0.5C steel sintered @ (from left to right) 500°C, 800°C, and 1120°C.

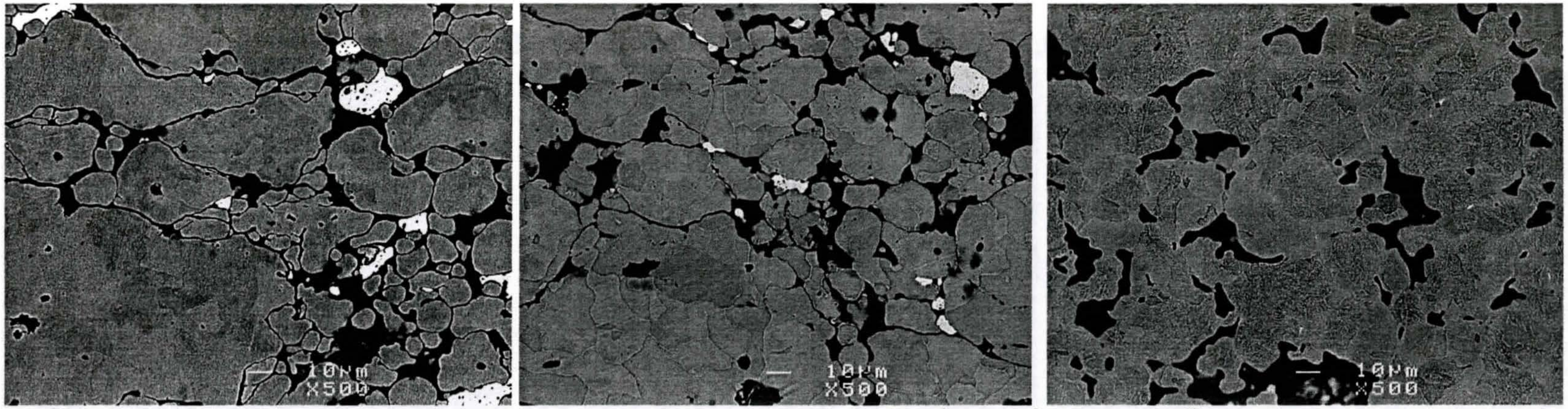

Fig. 3-39c. 500X SEM - 4Cu/0.5C steel sintered @ (from left to right) 500°C, 800°C, and 1120°C.

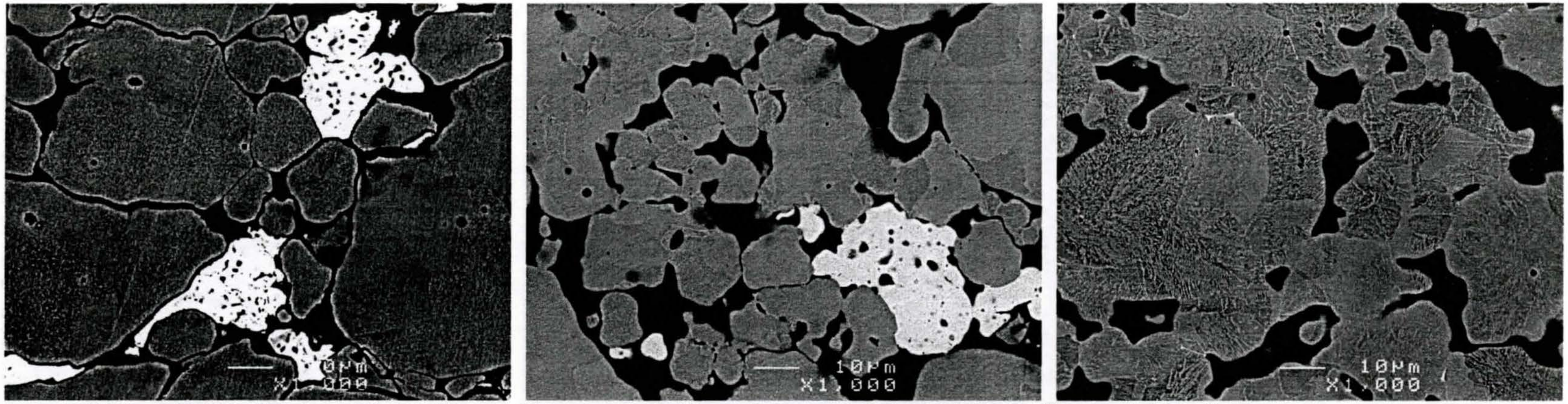

Fig. 3-39d. 1000X SEM - 4Cu/0.5C steel sintered @ (from left to right) 500°C, 800°C, and 1120°C.

2XF-Ni/2Cu/0.8C steel

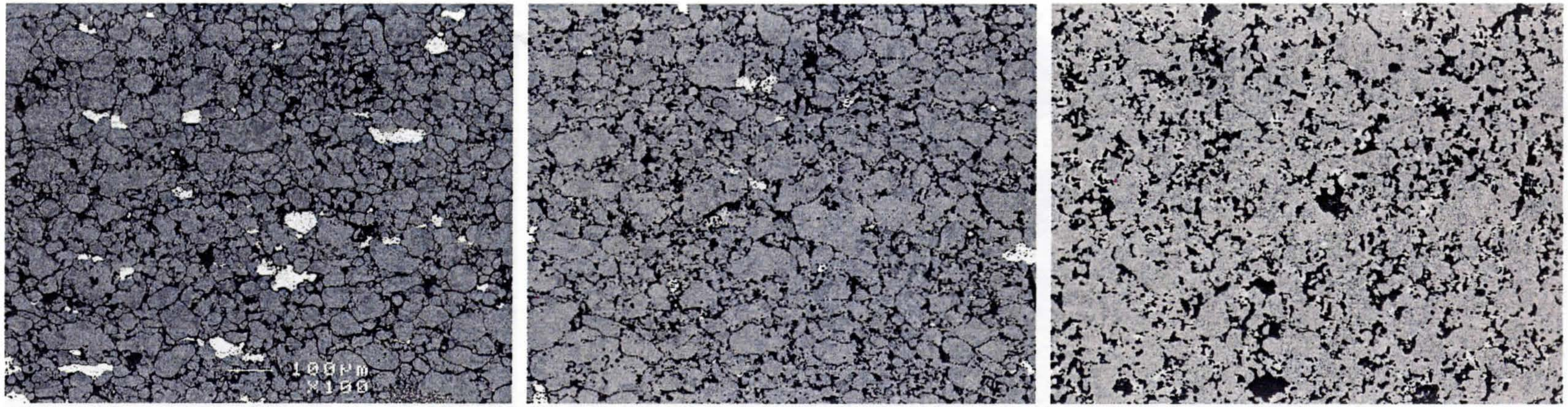

Fig. 3-40a. 100X SEM - 2XF-Ni/2Cu/0.8C steel sintered @ (from left to right) 500°C, 800°C, and 1120°C.

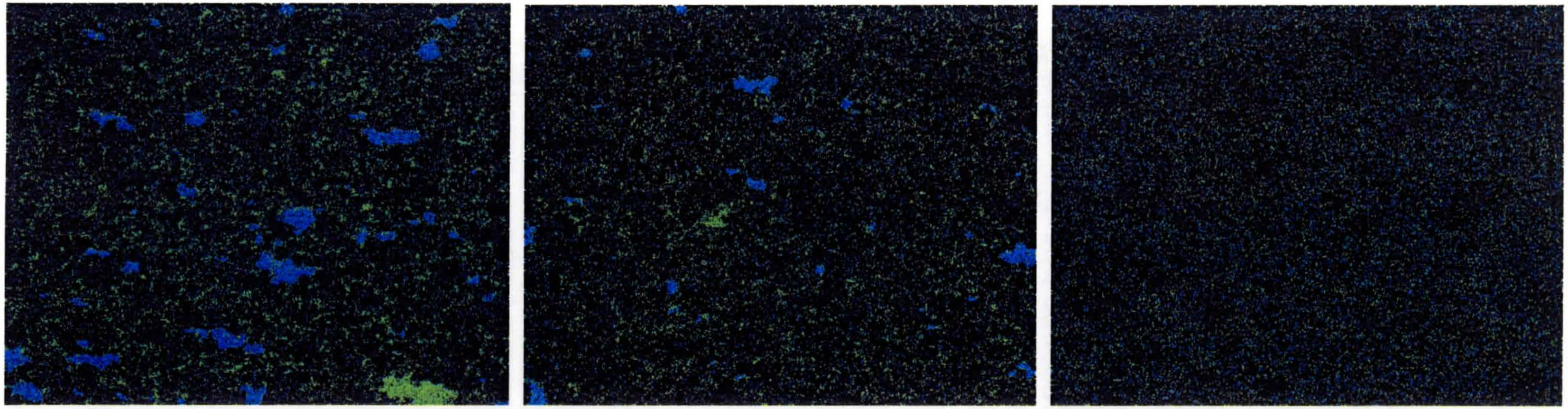

Fig. 3-40b. 100X X-ray maps - 2XF-Ni/2Cu/0.8C steel sintered @ (from left to right) 500°C, 800°C, and 1120°C.

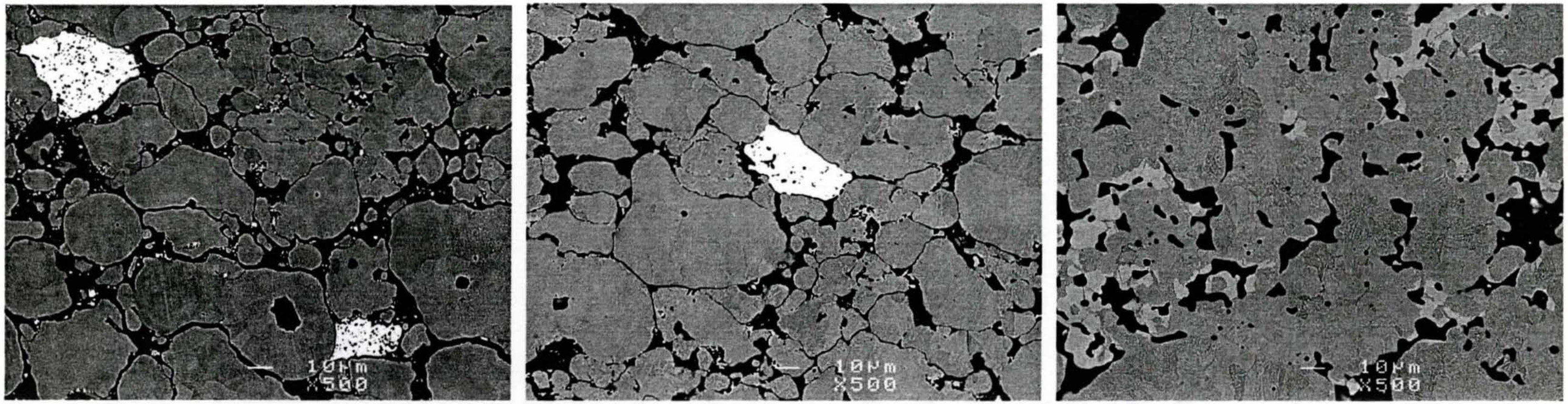

Fig. 3-40c. 500X SEM - 2XF-Ni/2Cu/0.8C steel sintered @ (from left to right) 500°C, 800°C, and 1120°C.

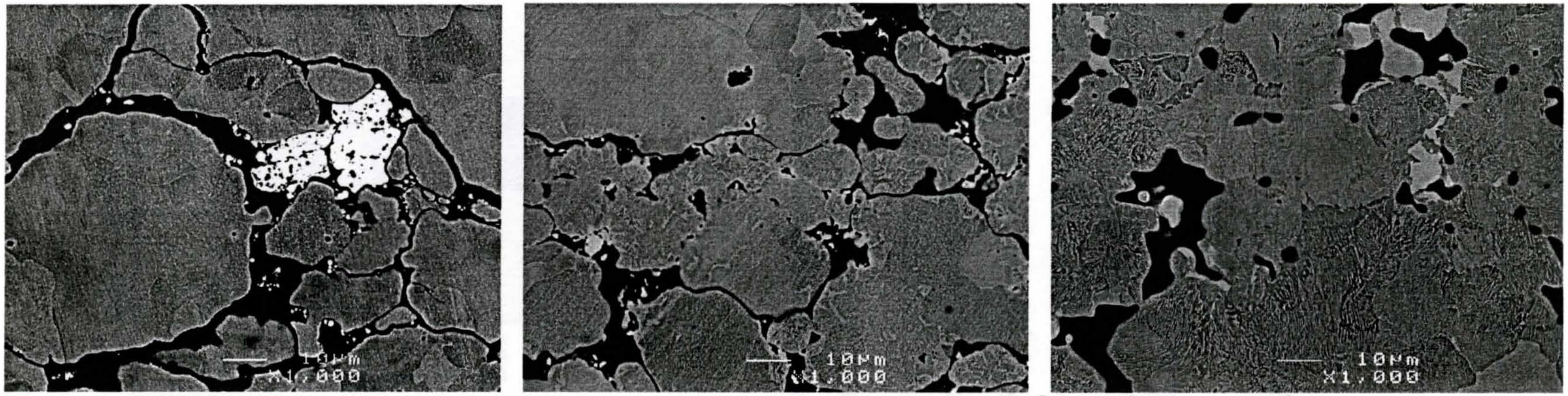

Fig. 3-40d. 1000X SEM - 2XF-Ni/2Cu/0.8C steel sintered @ (from left to right) 500°C, 800°C, and 1120°C.

3.2.2 Dimensional change properties

3.2.2.1 0.5C steels

At the 0.5C level, finer Ni powder additions reduce the dimensional swelling of the 2Ni-2Cu steels and improved the dimensional part-to-part consistency of the steels. Figure 3-44 shows the dimensional change results. The mean dimensional change of 2Ni/2Cu/0.5C steel was 0.77% with STD-Ni and was 0.56% for XF-Ni. In terms of dimensional consistency, the lot standard deviations of dimensional change of the STD-Ni and XF-Ni steels were 7.8 x 10^{-2} % and 2.5 x 10^{-2} % respectively. This translates into a reduction in swelling of approximately 30% and an improvement in consistency of approximately 70% through the use of XF-Ni powder.

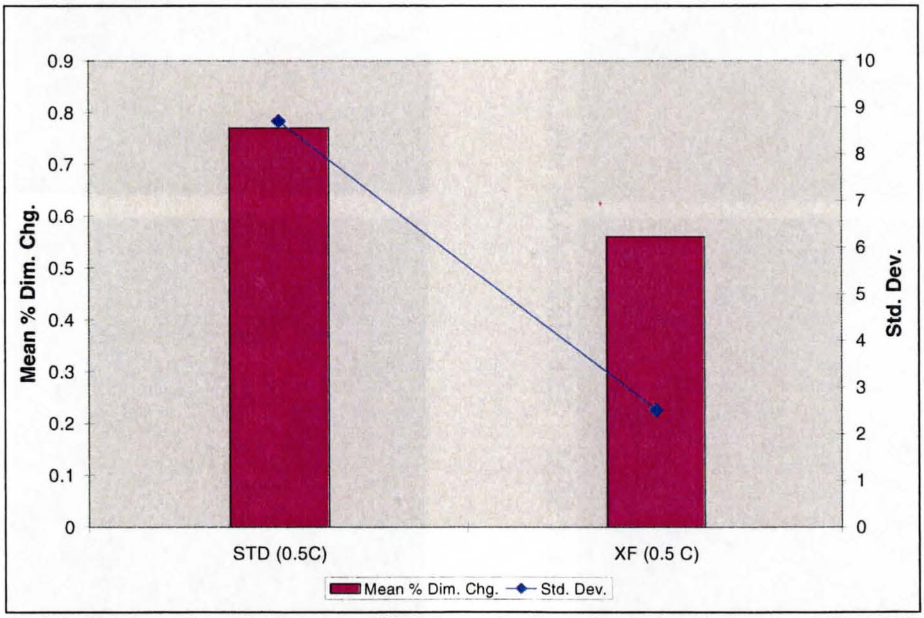

Figure 3-44. Dimensional Change (% Mean & Standard Deviation) of 2Ni/2Cu/0.5C steels.

3.2.2.2 0.8C steels

At the 0.8C level, finer Ni powder additions reduce the dimensional swelling of the 2Ni-2Cu steels and improve the dimensional part-to-part consistency. The mean dimensional change and standard deviation for 2Ni/2Cu/0.8C with STD Ni was 0.59 % and 2.5 x 10^{-2} % respectively. 2Ni-2Cu-0.8C with XF Ni had a dimensional change of 0.52 % and a standard deviation of 1.6 x 10^{-2} %, representing an improvement in these properties of approximately 10% and 40% respectively with a finer Ni addition.

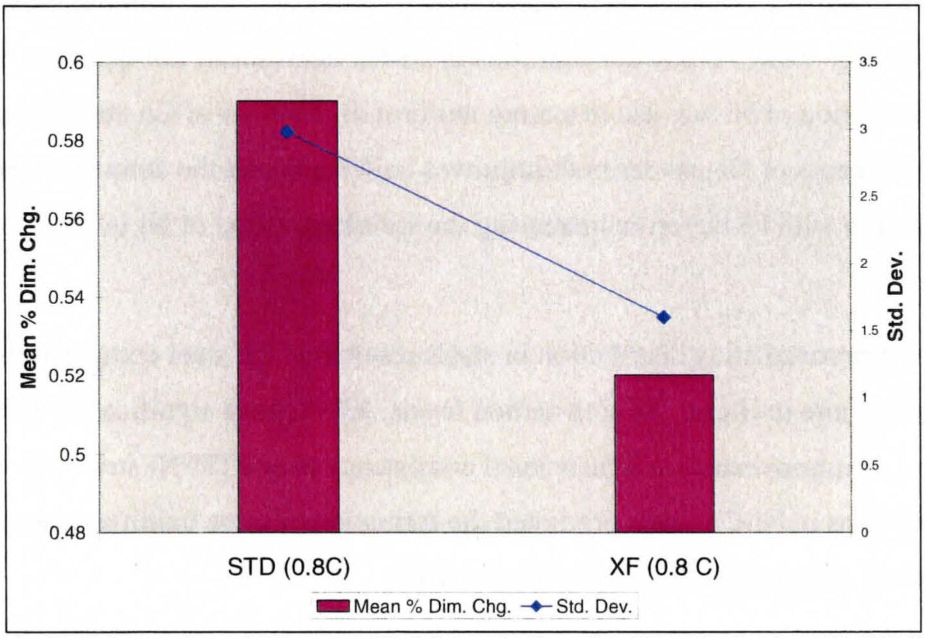

Figure 3-45. Dimensional Change (% Mean & Standard Deviation) of 2Ni/2Cu/0.8C steels.

3.2.2.3 Effect of Ni-Cu distribution on dimensional change properties

Extra-fine Ni (XF) powders have been shown to improve the Ni distribution in P/M Ni steels [15, 17]. With a particle volume approximately 1/200th the size of standard Ni powder, extra-fine Ni powder distributes (during mixing and compaction) and diffuses (during sintering) much more uniformly than standard Ni powder. For example, from Study 1 of the current work, for 4Ni steels sintered for one hour, steels with a STD-Ni powder addition have approximately 20% of the total Ni undiffused while the steels with an XF-Ni show complete Ni diffusion. The improved uniformity of XF-Ni in steels translates into in increased shrinkage (higher sintered densities) and less part-to-part dimensional scatter. Improved hardness and increased levels of bainite-martensite were also reported in steels with finer Ni powder additions [31].

In the current study, the microstructural analysis combined with EDX chemical profiling confirmed that Ni and Cu do indeed interact with each other significantly during sintering. Finer Ni powder additions in Ni-Cu steels result not only in a more uniform distribution of Ni but also in a more uniform distribution of Cu after sintering. Increasing the fineness of Ni powder both improves uniformity and the amount of Ni going into solution with Fe therefore increasing the shrinkage effect of Ni in Fe.

The improved alloy distribution in steels resulted in the steel composition and properties being more uniform. At both carbon levels, XF-Ni gave significantly reduced swelling and an improvement in dimensional consistency over STD-Ni steel. As well, finer Ni additions in Ni-Cu steels promoted the formation of more bainitic-martensitic regions giving a harder, stronger steel (higher TRS).

3.2.2.4 Effect of carbon level on dimensional change

In the present study, lower swelling (from die size) and standard deviation values were obtained in 0.8C vs. 0.5C Cu-containing steels. This is in agreement with other works which have found that increasing C reduces swelling of Cu-containing steels [32-34]. The main reason for the swelling effect caused by Cu in sintered steels is due to the separation of Fe interparticle boundaries (IPBs) caused by the solidification of molten Cu

[32]. Figure 3-46 shows the effect of C level on a 10Cu steel as reported by German [5]. Lawcock and Davies confirmed that increasing C increases the dihedral angle between solid Fe and liquid Cu and thus impedes Cu from penetrating and separating IPBs, restricting overall compact growth [34].

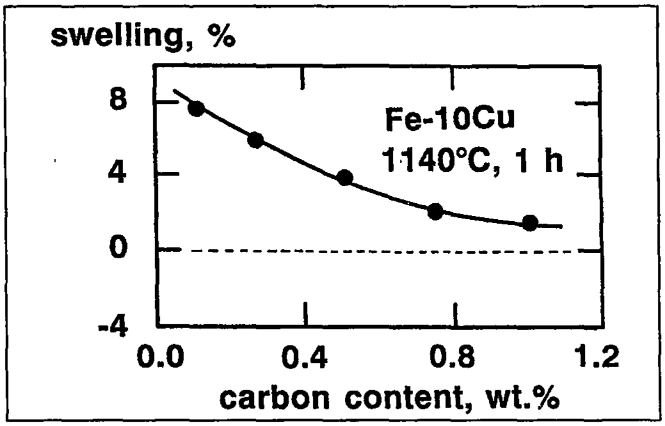

Figure 3-46. Effect of C level on dimensional change during sintering of a 10Cu steel [5].

At both 0.5C and 0.8C levels of 2Ni-2Cu steels, less swelling occurred in steels with finer Ni additions. Figure 3-47 and Figure 3-48 summarize the dimensional change results of the 0.5C steels and 0.8C steels respectively. 4Ni and 4Cu steels were also prepared and tested for comparison. At 0.5C, the dimensional swelling and lot standard deviation of 2Ni/2Cu steels was intermediate to 4Ni and 4Cu steels. At 0.8C, the dimensional swelling of 2Ni/2Cu steels was larger than that in 4Ni and 4Cu steels, while lot standard deviation was still intermediate. The dimensional change of 2Ni/2Cu was expected to be intermediate between 4Cu and 4Ni. The fact that the addition of Ni actually caused an increase in swelling relative to 4Cu suggests that the behaviour of Ni and/or Cu in Ni/Cu/0.8C steels is quite different than that in 0.5C steels.

Upon sintering, Cu melts and has three different routes to take: (1) migrate to the Fe IPBs; (2) form a solid solution with Fe and/or Ni; (3) form a Cu-Ni or Cu-Fe liquid. A mechanism involving the relative movement of liquid Cu and/or Cu-Ni to the IPBs and subsequent formation of a Cu-Ni-Fe solid phase is proposed below. The amount of Ni and Cu going into solution with Fe was assumed to be essentially constant based on mechanical properties.

At 0.5C, Cu moves into IPBs quickly and easily, followed by a slower Cu-Fe solid solution formation and a Cu-Ni-Fe solid solution formation. Here, the increased Ni-Cu interaction caused by XF Ni additions vs. STD Ni additions increases the amount of Cu forming the Cu-Ni-Fe phase, thereby decreasing the amount of Cu in the IPBs. The net result is that XF-2Ni/2Cu steel gives decreased swelling relative to STD-2Ni/2Cu and 4Cu.

At 0.8C, the formation of Cu-Ni(-Fe) competes with the movement of Cu to the IPBs and with the formation of a Cu-Fe solid solution. However, the Cu movement to the IPBs is impeded by higher C levels [33]. Therefore more Cu liquid is available to interact with Ni than in 0.5C case. This increased volume of Cu liquid that cannot enter the IPB regions can now dissolve more Ni than in 0.5C case. The surface tension of the Cu-Ni liquid is less than that of liquid Cu [32], therefore more of the Cu-Ni liquid can enter the IPBs [33]. The net result is more swelling in 2Ni/2Cu steels than in 4Cu steels. As in the 0.5C case, more Cu-Ni-Fe phase forms with XF Ni powder, therefore the swelling effect is reduced compared to STD-Ni powder. Even though 2Ni/2Cu steels swell more with higher C contents, the behaviour of dimensional change is still very predictable (i.e. low standard deviation).

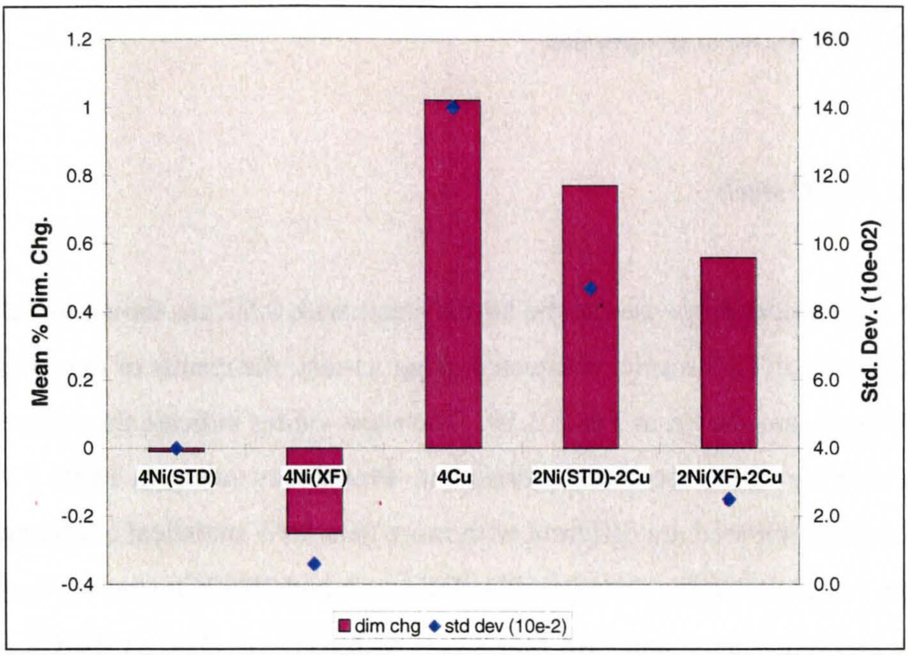

Figure 3-47. Summary of dimensional change results of 0.5C steels.

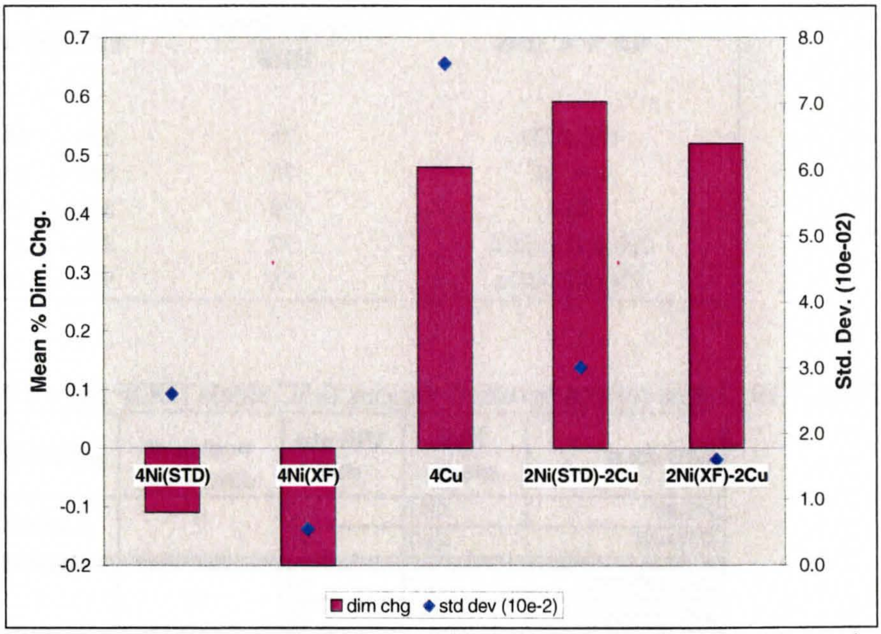

Figure 3-48. Summary of dimensional change results of 0.8C steels.

3.2.3 Mechanical properties

3.2.3.1 0.5C steels

The mechanical properties of the Ni-Cu steels with 0.5C are shown in Table 3.9. The confidence of TRS results was tested using a t-test; the results of the comparing several 0.5C steels are shown in Table 3.10. The t-test values indicate the degree of probability to which the values are actually different. Probability values in Table 3.10 indicate that the steels compared are different with more than 99% statistical confidence. 4Cu steel gives a slightly harder structure than 4Ni steels and 2Ni/2Cu steels. Steels with XF-Ni give higher hardness and TRS than steels with STD-Ni. The XF-Ni/Cu steel gave the highest TRS value.

Table 3.9. Mean Hardness & TRS values of 0.5C steels.

0.5 % C steel	**Hardness (HRB) +/- HRB**	**TRS (MPa)**
4Ni-STD	75	820 +/- 25
4Ni-XF	76	860 +/- 10
4Cu	79	890 +/- 15
2Ni(STD)-2Cu	77	830 +/- 25
2Ni(XF)-2Cu	78	920 +/- 10

Table 3.10. T-test results between various 0.5C steels (DOF (n) = 10 samples/steel).

0.8C steel	**TRS mean**	**TRS std dev**	**t-value of difference**	**probability**
XF-Ni	990	10	7	0.999989
STD-NI	920	30		
2Ni(XF)-2Cu	1020	10	10	1
2Ni(STD)-2Cu	920	30		
2Ni(XF)-2Cu	1020	10	1.414	0.91607
4Cu	1010	20		

3.2.3.2 0.8C steels

The mechanical properties of the Ni-Cu steels with 0.5C are shown in Table 3.11. The mechanical properties of the Ni-Cu steels with 0.8C are shown in Table 3.12. The confidence of TRS results was tested using a t-test; the results of the comparing several 0.8C steels are shown in Table 3.12. The t-test values indicate the degree of probability to which the results are different. Probability values in Table 3.12 indicate that 4Ni(XF) steel has a higher TRS than 4Ni(STD) steel and that 2Ni(XF)-2Cu steel has a higher TRS than 2Ni(STD)-2Cu steel with essentially 100% statistical confidence (~ or = 1). With ~ 91% statistical confidence, it can be concluded that the TRS value of 2Ni(XF)-2STD steel is greater than the TRS of the 4Cu steel.

Table 3.11. Mean Hardness & TRS values of 0.8C steels.

0.8 % C steel	**Hardness (HRA) +/- 2**	**TRS (MPa)**
4Ni-STD	47	920 +/- 30
4Ni-XF	48	990 +/- 10
4Cu	52	1010 +/- 20
2Ni(STD)-2Cu	48	920 +/- 30
2Ni(XF)-2Cu	49	1020 +/- 10

Table 3.12. T-test results between various 0.8C steels (DOF (n) = 10 samples/steel).

0.8C steel	**TRS mean**	**TRS std dev**	**t-value of difference**	**probability**
XF-Ni	990	10	7	0.999989
STD-NI	920	30		
2Ni(XF)-2Cu	1020	10	10	1
2Ni(STD)-2Cu	920	30		
2Ni(XF)-2Cu	1020	10	1.414	0.91607
4Cu	1010	20		

3.2.4 Dilatometry

The full dilatometry curves (dimensional change during a sintering cycle) of the four steels are shown in Figure 3-49. (Note: *The values of dimensional change in dilatometry testing are only relative.* The reasons for this are outline in section 2.4.3. Dilatometry curve appears to show shrinkage from original size but compacts have swelled from *die size*). The four steels are of STDNi/Cu/0.5C, XF-Ni/Cu/0.5C, STD-Ni/Cu/0.8C, XF-Ni/Cu/0.8C. At the 0.5C level, the steel with XF-Ni gives substantially less swelling during the sintering cycle. This corresponds well with standard dimensional change testing measurements. At the 0.8C level, the steel with XF-Ni gives more swelling than the steel with STD-Ni steel. This also is similar to the case seen with standard dimensional change testing measurements. At the 0.8C level, the dimensional change of STD-Ni and XF-Ni steels was similar and slightly was more than Cu steels (which is not the case at 0.5C). This was explained by the fact that hypereutectoid levels of C impede the movement of Cu into the steel matrix allowing more Cu liquid to form and, in the presence of Ni, more Ni-Cu liquid to form [33]. Ni-Cu liquid has a lower surface tension that plain Cu liquid and is able to enter IPBs more readily, causing more expansion [32].

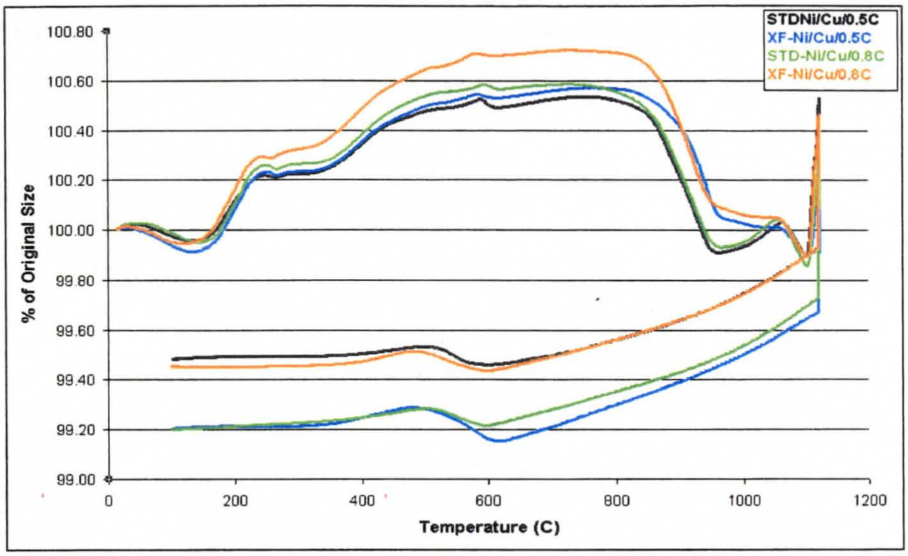

Figure 3-49. Full sintering cycle dilatometry curves of STD-Ni/Cu steel and XF-Ni/Cu steel at 0.5C and 0.8C.

3.2.4.1 Heating

Up to about 750°C, specimens expand similarly as the temperature increases. The expansion rate, 1.5×10^{-3} %/°C corresponds to the thermal expansion coefficient of ferrite [28]. The XF-Ni/Cu/0.8C steel is slightly more expanded by 750°C due to slightly increased expansion rates and before this temperature. At about 770°C, the expansion rate of the steels decreases and the specimens begin shrinking in the temperature range of 800-950°C. This is the temperature range of the ferrite-austenite transformation. At temperatures greater than 950°C, the diffusion of carbon is accelerated. The major difference in steels with STD-Ni vs. XF-Ni is that steels with STD-Ni begin to expand from 970-1070°C, as C diffuses into Fe, while steels with XF-Ni continue to slightly densify from 970-1020°C and then slightly expand from 1020-1070°C; The rate of expansion is notably less in steels with XF-Ni during this last expansion before reaching the sintering-soaking temperature. From 1070-1120°C, both steels begin to shrink due to liquid formation of Cu as it melts. The overall expansion of the steel with XF-Ni is 0.3% less even before soaking. During soaking, the samples densify and show a significant amount of shrinking. The amount of shrinking during sintering is 0.6% for steels with STD-Ni and 0.9% for steels with XF-Ni.

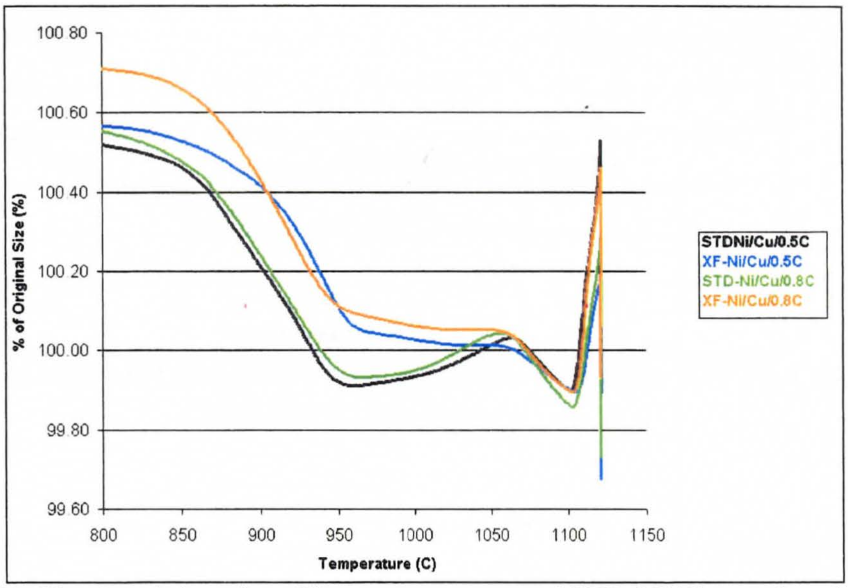

Figure 3-50. Heating / sintering dilatometry curves of STD-Ni/Cu steel and XF-Ni/Cu steel at 0.5C & 0.8C.

3.2.4.2 Cooling

The dilatometry curves for the steels for cooling from the sintering temperature is shown in Figure 3-51. Upon cooling from 1120°C to 950°C the slopes of all of the steels are similar. Below 950°C, the slope of steels with STD-Ni decrease and densification is less than that seen in steels with XF-Ni. At a temperature of ~ 630°C the samples with XF-Ni begin to undergo the austenite-ferrite transformation until ~ 490°C. The steels with STD-Ni begin this transformation slightly later at about 590°C and end slightly earlier at about 510°C. A wider austenite-ferrite transformation range observed in steels with XF-Ni results in more bainite and martensite being produced in the final microstructure.

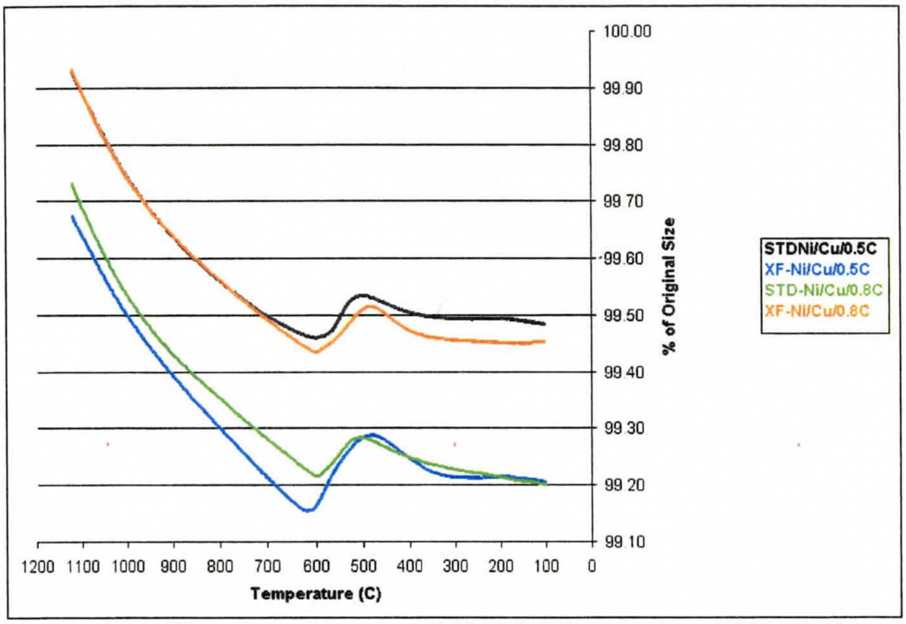

Figure 3-51. Cooling dilatometry curves of STD-Ni/Cu steel and XF-Ni/Cu steel at 0.5C and 0.8C.

3.2.5 Differential Thermal Analysis

The DTA plot in Figure 3-52 shows heat flow (released) vs. temperature during the sintering cycle of four steels (The four steels are of STDNi/Cu/0.5C, XF-Ni/Cu/0.5C, STD-Ni/Cu/0.8C, XF-Ni/Cu/0.8C). The wt%C does not appear to affect the DTA curves significantly. The type of Ni powder affects heatflow more than C level. The curves of all 4 steels appear very similar. Upon heating the XF-Ni/Cu/0.5C steel shows less heat release than the other steels. This could be related back to dilatometry and linescan results which show that the distribution of Ni and Cu in steels with XF-Ni to be significantly better than those with STD-Ni. The mass transport / reactions that take place during sintering seem to be more stable with finer Ni size. In addition, it is seen that as C level is increased the stability of heat released during sintering is decreased. This, in turn, is consistent with the dilatometric and dimensional change results of the current study.

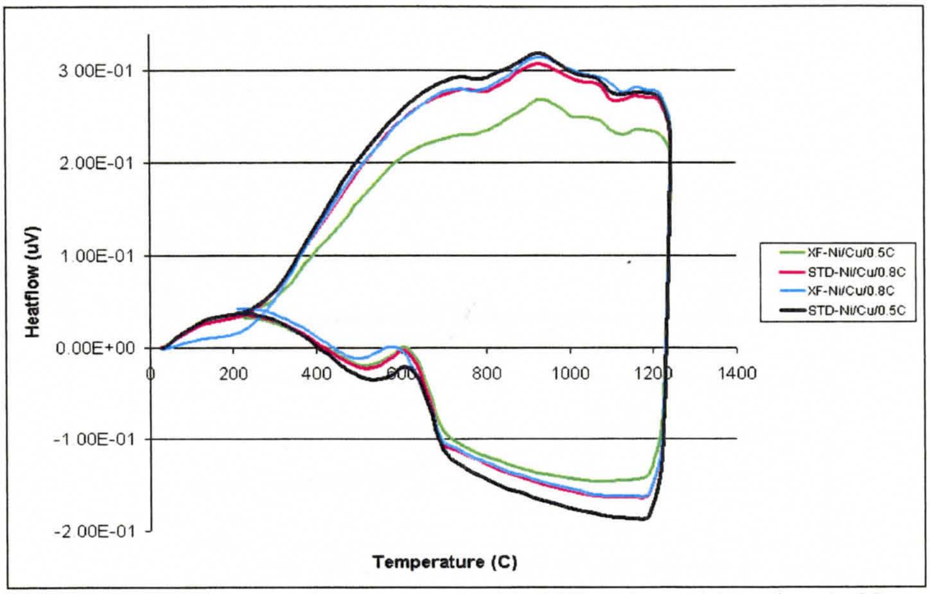

Figure 3-52. DTA curve of 2Ni/2Cu steels with STD-Ni and XF-Ni at 0.5C and 0.8C.

3.2.6 E-SEM analysis of sintering of P/M steels

An environmental SEM was employed to view microstructure development *during sintering*. The unit used was a JEOL 5600 with a hot-stage unit and a reducing 2%H_2-N_2 atmosphere . As a baseline, a 4Cu/0.5C steel was initially studied. A 0.5 mm thick compact was pressed to ~ 7.0 g/cm^3 (same as for bulk test pieces) and inserted as-pressed into the E-SEM unit. Figure 3-53 shows the microstructure that develops up to 320°C. Very little sintering has taken place up to this temperature; only the weak connections made through compaction hold the compact together. The light-coloured, small, spherical particles visible most likely are graphite particles; the very large ones most likely being Fe and the intermediate ones being Cu. Identification of the various elements within the steel was difficult since only particle size could be used to distinguish between elements.

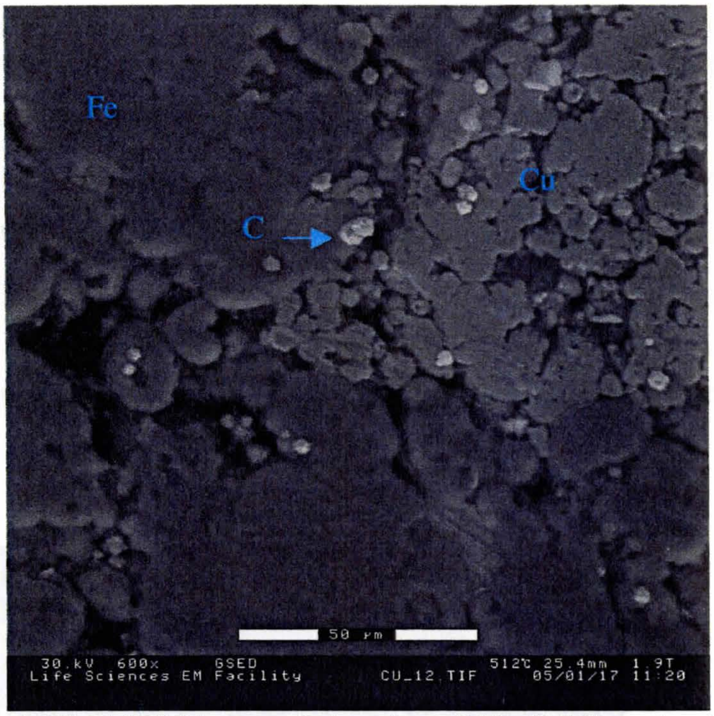

Figure 3-53. E-SEM image of sintering of 4Cu/0.5C steel at 320°C.

Figure 3-54. E-SEM image of sintering of 4Cu/0.5C steel at 710°C.

As seen in Figure 3-54, by 710°C, a significant amount of the pores have closed off but original particle boundaries are still visible, carbon has moved into solution and the grain texture of the steel is just appearing. At 710°C, it is unclear from the images whether the surface has become oxidized or whether surface in view is a relatively "clean" metal undergoing sintering. Figure 3-55 shows the steel at 830°C; it appears as if the steel structure is becoming visible in the matrix. At 960°C and 1010°C, in Fig. Figure 3-56 and Figure 3-57 respectively, further pores closure takes place and the liquefaction of Cu is initiated.

Figure 3-55. E-SEM image of sintering of 4Cu/0.5C steel at 830°C.

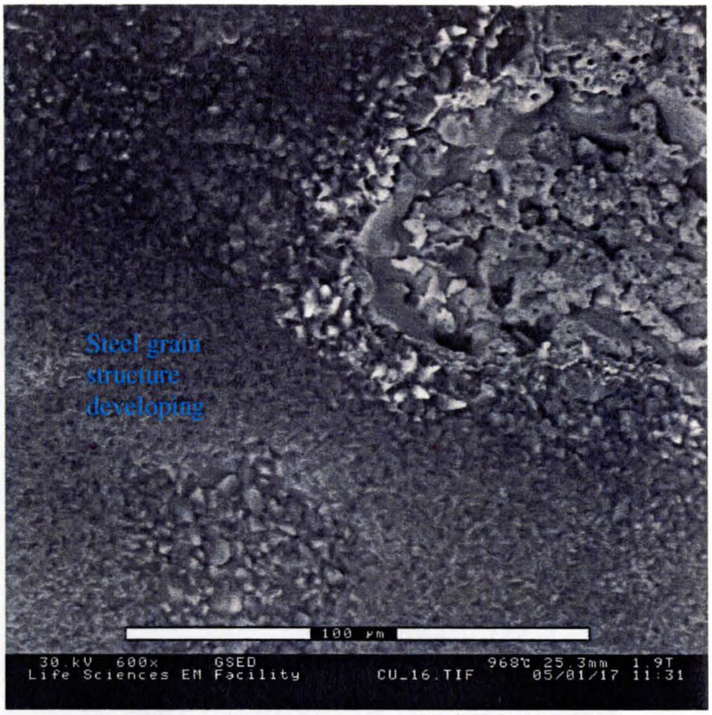

Figure 3-56. E-SEM image of sintering of 4Cu/0.5C steel at 960°C.

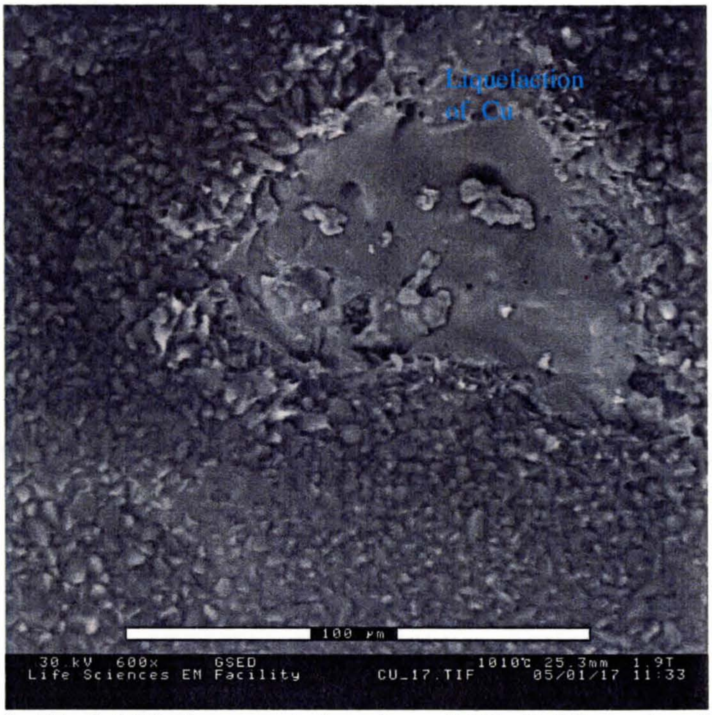

Figure 3-57. E-SEM image of sintering of 4Cu/0.5C steel at 1010°C.

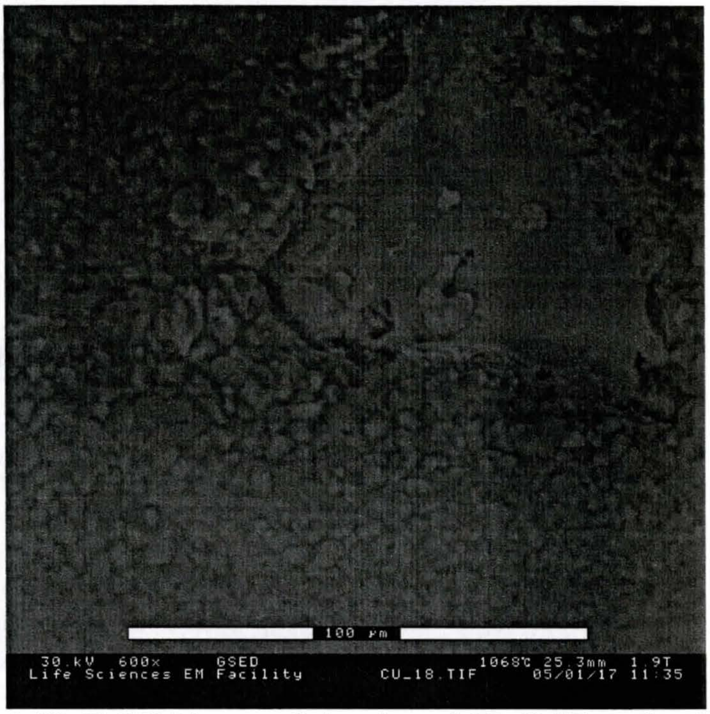

Figure 3-58. E-SEM image of sintering of 4Cu/0.5C steel at 1060°C.

At 1083°C, Figure 3-59, it appears as if phases of solid Fe and Fe-Cu as well as liquid phases of Cu and Cu-Fe. The drastic increase in the amount of liquid from 1060°C to 1083°C corresponds with the melting temperature of Cu, also 1083°C. Viewing at higher temperatures or cool down could not be carried out as the E-SEM unit became quite erratic at temperatures near 1100°C. This was most likely due to the interference of thermal electrons and / or the vapourization of an ultra-thin layer of metal from the sample. Further E-SEM work for the current project was thus abandoned.

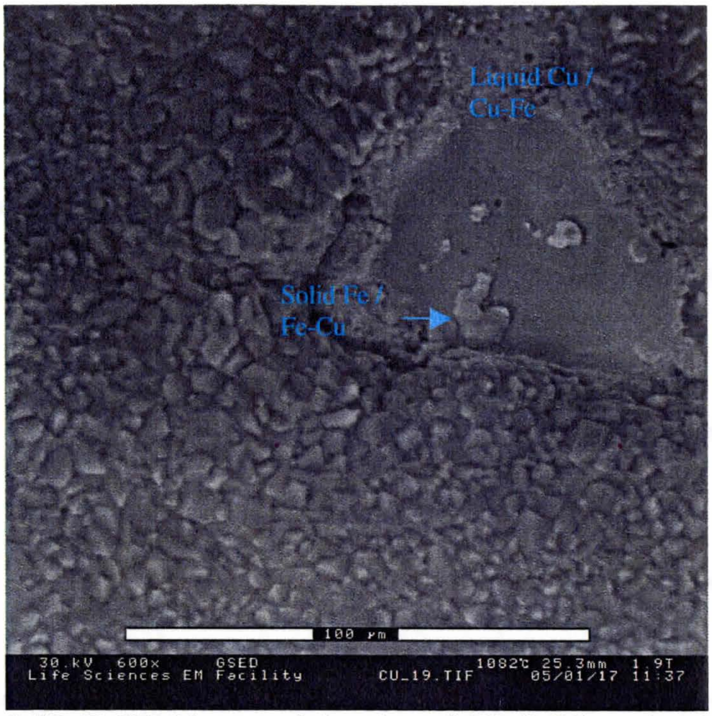

Figure 3-59. E-SEM image of sintering of 4Cu/0.5C steel at 1083°C.

3.3 Study 3 - Effect of Ni particle size & Cu particle size on properties of high-performance 2Ni/2Cu/0.8Mo/0.7C steel

3.3.1 Microstructure

3.3.1.1 Phase analysis

SEM micrographs of the steel microstructures are shown in Figure 3-60. In general, all of the steels possessed a pearlitic / bainitic matrix with colonies of martensite and austenite. A breakdown of the phases of the steels as calculated by analysis of optical micrographs in ProTools Imagegridder is shown in Table 3.13. The STD-Ni/STD-Cu steel had very little bainite and martensite compared to the other steels. The pores in this steel were isolated but fairly large. When using XF-Cu in the STD-Ni/XF-Cu steel, pearlite shifted to bainite and more martensite was present. Pores were expected to be smaller and more rounded [10], but this was not the case in this steel; the shape and size of pores did not change substantially when using XF-Cu powder.

The amount of bainite and martensite increased substantially with XF-Ni compared to STD-Ni. This was particularly noticeable when comparing the STD-Ni/STD-Cu vs. XF-Ni/STD-Cu steels. XF-Ni also resulted in finer, less interconnected porosity.

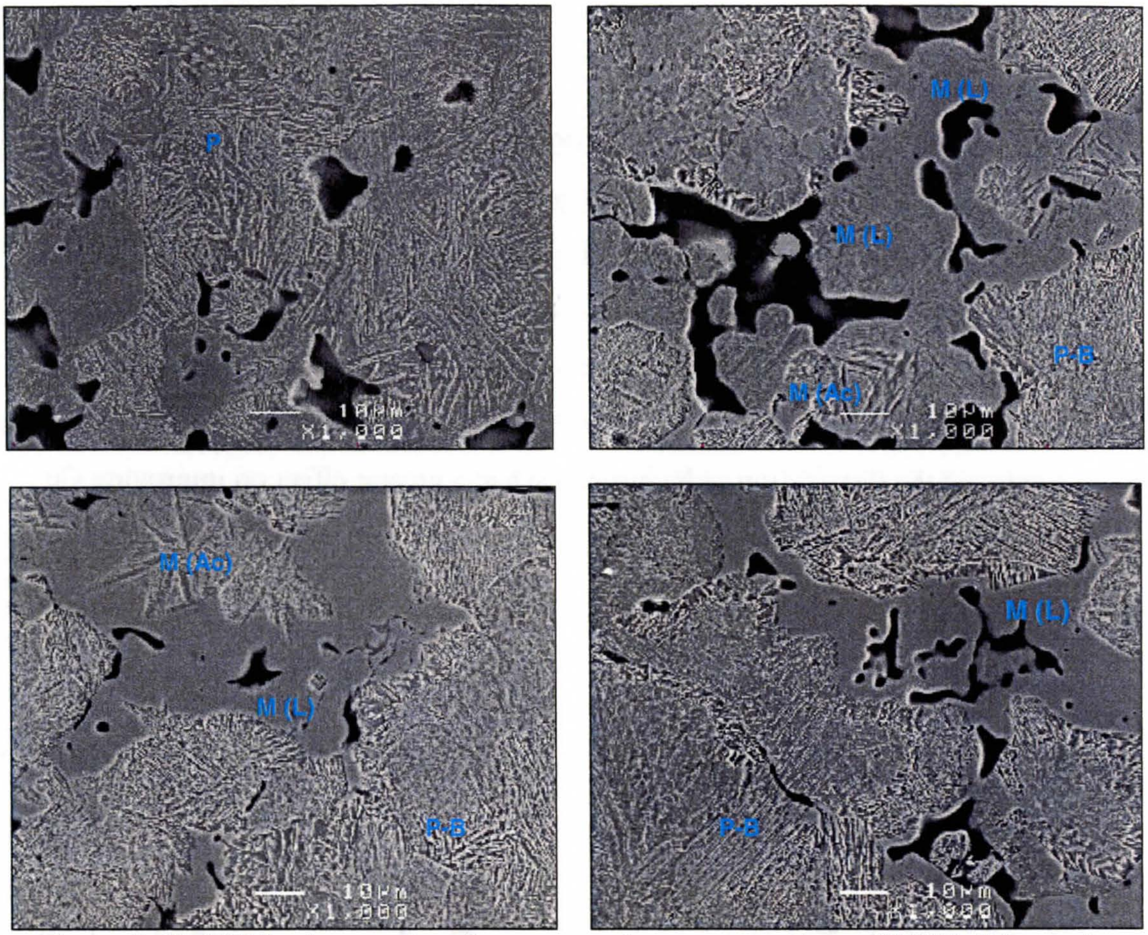

Figure 3-60. SEM micrographs of representative cross-sections of Ni/Cu/Mo steels. STD-Ni/STD-Cu steel (upper left), STD-Ni/XF-Cu steel (upper right), XF-Ni/STD-Cu steel (lower left), XF-Ni/XF-Cu steel (lower right). {M (Ac) = acicular martensite, M (L) = lathe martensite, P-B =pearlite-bainite, P= pearlite}.

Table 3.13. Quantitative phase analysis of 2Ni/2Cu/0.8Mo/0.7C steels

	Approximate area % phases +/- 5%			
	Martensite	*Bainite*	*Austenite*	*Pearlite*
STD-Ni/STD-Cu/Mo/0.7C steel	50	20	20	10
STD-Ni/XF-Cu/Mo/0.7C steel	55	15	20	10
XF-Ni/STD-Cu/Mo/0.7C steel	60	20	15	5
XF-Ni/XF-Cu/Mo/0.7C steel	60	20	15	5

3.3.1.2 SEM-EDX Analysis

Figures 3-58 – 3-61 show the EDX Ni/Cu/Mo wt% distribution linescan profiles across a representative field of each steel. The wt% Mo is very uniform whereas Ni and Cu can fluctuate considerably. The use of XF powders improves the distribution of Ni and Cu significantly. Table 3.14 compares the standard deviation of Ni/Cu/Mo profiles (50 points). The standard deviation of wt% values of the alloys is a good indication of the uniformity of alloy distribution in the steel. Interesting to note is that XF-Ni not only stabilized the distribution of Ni but it also had a greater effect on improving Cu distribution than XF-Cu.

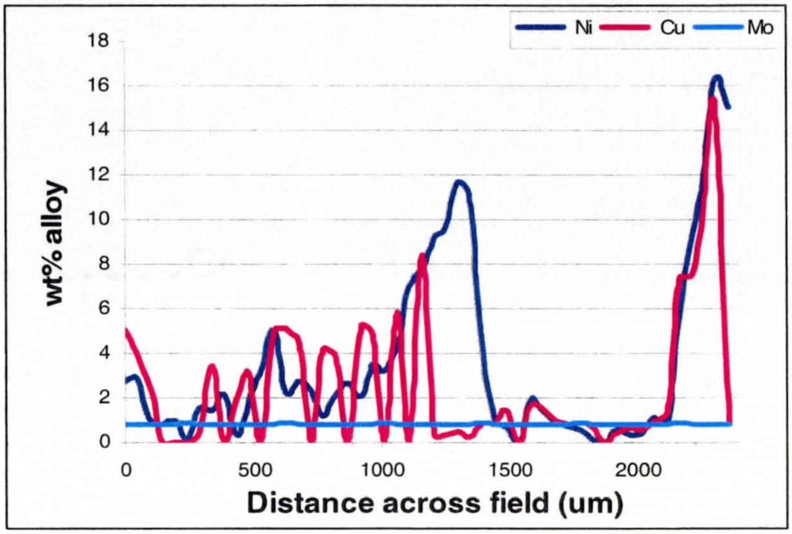

Figure 3-61. Linescan analysis of representative cross-section of 2STD-Ni/2STD-Cu/0.8Mo/0.7C steel.

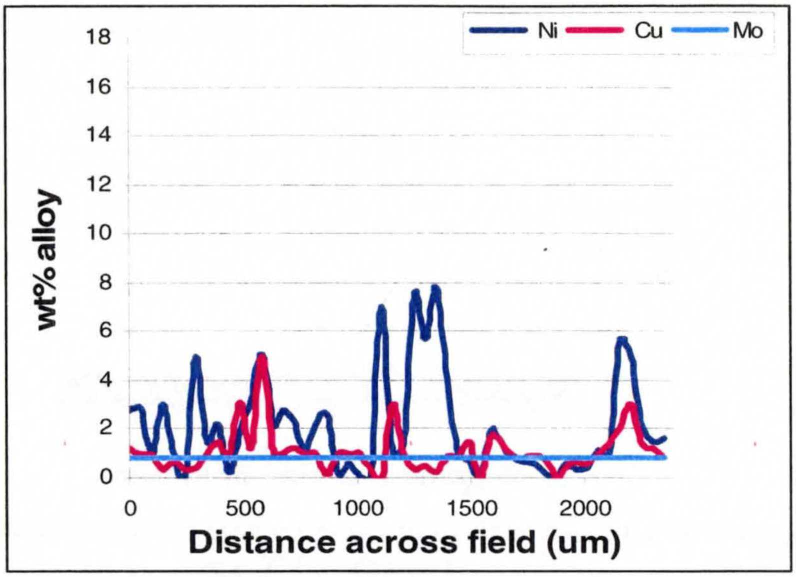

Figure 3-62. Linescan analysis of representative cross-section of 2STD-Ni/2XF-Cu/0.8Mo/0.7C steel.

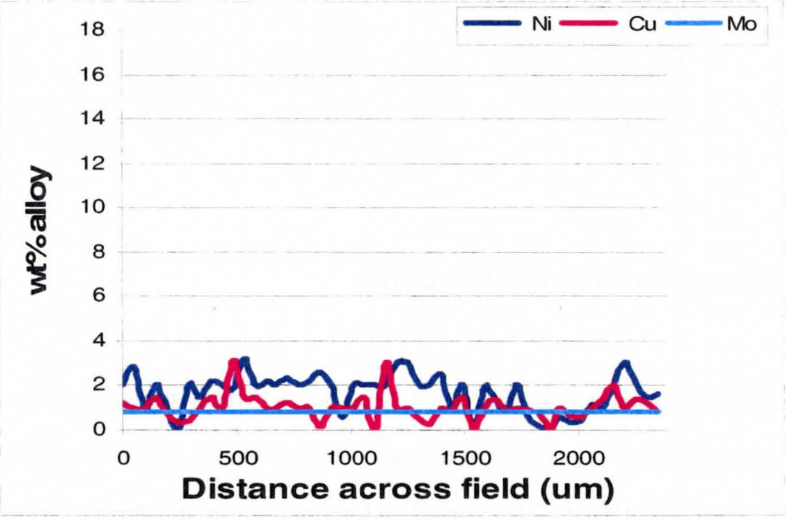

Figure 3-63. Linescan analysis of representative cross-section of 2XF-Ni/2STD-Cu/0.8Mo/0.7C steel.

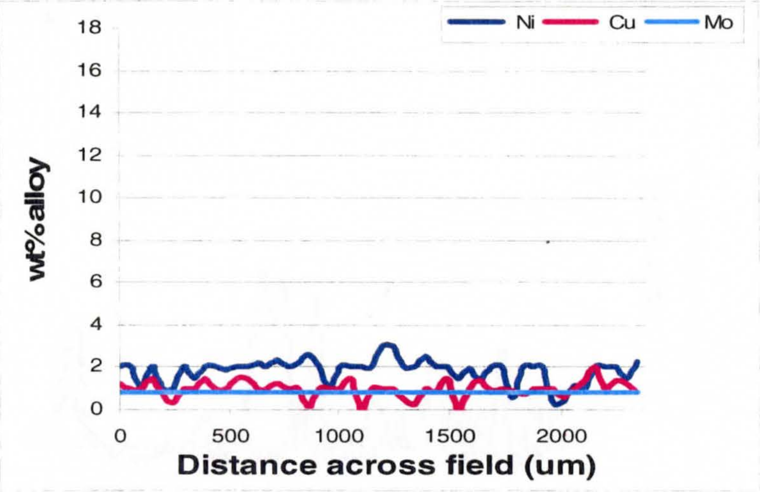

Figure 3-64.Linescan analysis of representative cross-section of 2XF-Ni/2XF-Cu/0.8Mo/0.7C steel.

Table 3.14. Std. Deviation of Ni/Cu/Mo wt% profiles.

Steel	Standard Deviation of wt%		
	2Ni +/-	2Cu +/-	0.8Mo +/-
STD-Ni/STD-Cu	4.1	3.2	<0.1
STD-Ni/XF-Cu	2.0	0.7	<0.1
XF-Ni/STD-Cu	0.3	0.3	<0.1
XF-Ni/XF-Cu	0.2	0.2	<0.1

3.3.2 Dimensional change properties

Finer Cu and Ni powder additions both reduced the dimensional swelling and improved the dimensional part-to-part consistency of the steels. The dimensional change was therefore strongly affected by both the Cu and Ni powder size. Figure 3-65 shows that the substitution of XF-Ni powder for STD-Ni powder and the substitution of XF-Cu powder for STD-Cu powder had gave similar improvements in reducing dimensional change and lowering part-to-part standard deviation.

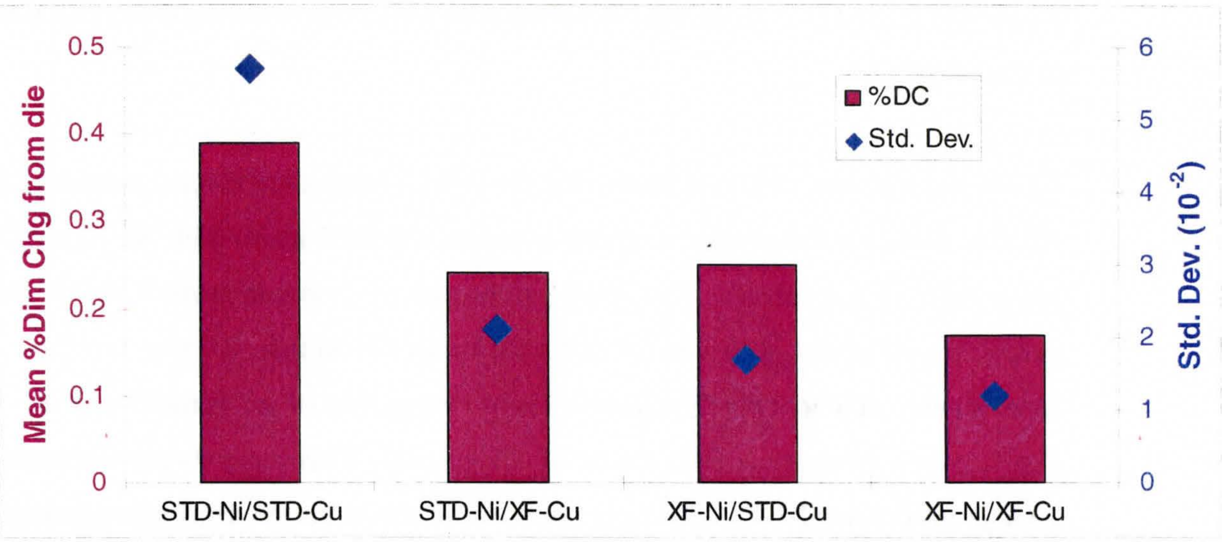

Figure 3-65. Dimensional Change (% Mean & Standard Deviation) of Ni/Cu/Mo steels with STD- and XF-Ni & Cu powder additions.

The substitution of XF-Ni or XF-Cu with STD powders reduced overall part growth and improved the part-to-part consistency of size change. The effect of XF powders on reducing growth is similar: a replacement of XF-Ni or XF-Cu with either STD-Ni or STD-Cu respectively gave 35-40% less swelling.

In a study by Chagnon and Gagne [35], a 2Ni/1Cu/0.6Mo/0.6C steel at 6.9 g/cm^3, with Ni and Mo prealloyed to Fe (QMP ATOMET 4601), gave a mean % dimensional change from die size of 0.34%. This result is similar to the STD-Ni/STD-Cu steel in this study which showed a mean dimensional change of 0.38%. The slightly larger size change of the latter is most likely due to the higher wt% Cu of the steels in the current study. Upon substituting XF-Ni for STD-Ni, dimensional change was reduced to 0.25%, while substituting XF-Cu for STD-Cu reduced dimensional change to 0.24%. The magnitude of the effect of XF-Ni and XF-Cu on dimensional change was therefore similar. As Chagnon reported higher dimensional change in an alloy of similar composition with prealloyed Ni, admixed XF-Ni appears to affect the distribution of Cu more than prealloyed Ni and as a result has the potential to reduce the swelling effect of Cu to a greater extent.

XF-Ni had a greater effect on improving the overall batch dimensional consistency than XF-Cu. Dimensional change standard deviation was 80% lower with XF-Ni and 50% lower with XF-Cu powder. This result agrees with the linescan profiles which show a greater improvement in Ni and Cu uniformity with XF-Ni than XF-Cu. It is also interesting to note that the dimensional change properties of steels made with XF-Ni were similar when using either STD-Cu or XF-Cu powder. This suggests that dimensional change in admixed Ni-Cu-Mo steels relies most heavily on the distribution (particle size) of Ni.

3.3.3 Mechanical Properties

Mechanical properties of the four steels are shown in Table 3.15. XF-Ni and XF-Cu additions increased the mechanical properties of the steels and improved the consistency of the mechanical properties. XF-Ni additions increased the mechanical properties values and consistency more than XF-Cu.

Table 3.15. Mean Hardness, TRS, UTS values of 2Ni/2Cu/0.8Mo/0.7C steels.

Steel	Green Density (g/cc)	Sintered Density (g/cc)	TRS (MPa)	TRS Std. Dev.	HRC	UTS (MPa)	UTS Std. Dev.	% El (in 25.4 mm)
STD-Ni/STD-Cu	7.00	7.01	1030	100	20	520	60	1.0
STD-Ni/XF-Cu	6.99	7.02	1140	30	24	600	20	1.0
XF-Ni/STD-Cu	6.99	7.03	1380	20	26	670	10	1.0
XF-Ni/XF-Cu	6.98	7.04	1400	15	28	710	10	1.0

XF-Ni and XF-Cu both increased the mechanical properties of the steels and improved the batch consistency of the mechanical properties. With STD-Ni powder, the use of XF-Cu vs. STD-Cu powder improved hardness by 4 HRC, TRS by 110 MPa and UTS by 80

MPa. The standard deviation of TRS and UTS values was approximately 60% lower when using XF-Cu vs. STD-Cu. With STD-Cu powder, the use of XF-Ni vs. STD-Ni powder improved hardness by 6 HRC, TRS by 350 MPa, and UTS by 150 MPa. The UTS and TRS standard deviation was approximately 80% lower when using XF-Ni vs. STD-Ni powder. XF-Ni improved the level and consistency of mechanical properties more than XF-Cu.

Standard MPIF properties of common sinter-hardened (cooled under accelerated conditions after sintering to produce effect similar to heat treatment) steels (FLC-4608, FLNC-4408) and a diffusion-alloyed steel (FD-0208) with compositions similar to that of the steel in the current study are shown in Table 3.16 [14]. Mechanical property values of the current study compared favourably to MPIF Standard 35 sinter-hardened steels, considering the latter had a higher carbon content and were cooled under accelerated conditions. The steels made with XF-Ni had mechanical properties superior to the standard diffusion-alloyed (see section 1.1.4) steel of similar composition.

In a study by St. Laurent et al [36], a 4Ni/1.5Cu/0.8Mo/0.6C steel at 7.0 g/cm^3, with Mo prealloyed and STD-Ni and Cu diffusion-bonded, had a hardness of 30 HRC and a tensile strength of 750 MPa. These values are similar to steels with XF powders in this study which is significant since the steels of the current study were conventionally admixed and the nickel content was half of that in St. Laurent's study. Chagnon and Trudel [37] obtained values of 25 HRC hardness and 750 MPa tensile strength in sinter-hardened 2Ni/1Cu/0.6Mo/0.6C steel at 6.9 g/cm^3. Although the steel in Chagnon's study was cooled under accelerating conditions (1.5°C/s) and had Ni prealloyed, it had similar hardness values and only slightly higher tensile strength than the conventional admixed steels made with XF-Ni in the current study.

Table 3.16. Composition & properties of steels from MPIF Std. 35 [14] & selected steel from current study.

MPIF Material Designation	Chemical composition				Properties				
	C	Ni	Mo	Cu	Density (g/cc)	UTS (MPa)	% El	TRS (MPa)	Hardness
FLC-4608	0.8	1.75	0.55	2.00	7.00	690	< 1.0	1310	31 HRC
FLNC-4408	0.8	2.00	0.85	2.00	7.00	790	< 1.0	1520	25 HRC
FD-0208	0.8	1.75	0.50	1.50	6.90	540	< 1.0	1070	83 HRB
XF-Ni/STD-Cu - current study	*0.7*	*1.75*	*0.80*	*1.50*	*7.03*	*670*	*1.0*	*1380*	*26 HRC*

3.3.3.1 Sintering of Ni-Cu-Mo steels

The results of the present study suggest that Ni particle size is a more important factor in controlling dimensional precision than Cu particle size during the sintering of steels containing admixed Ni and Cu powder. Linescan profiles and dimensional change show that the interaction of Ni and Cu is more strongly dependent on the size of Ni and that XF-Ni powder additions improve Cu distribution even more than an XF-Cu powder. Part size control was slightly more with a XF-Ni substitution than with an XF-Cu substitution. Mechanical properties were affected much more with an XF-Ni substitution.

Although Ni particle size affected the overall properties of steel more than Cu particle size, changing the particle size of Cu did have some effect on steel properties. Steels with XF-Cu had more martensite in the microstructure as well as improved alloy distribution, dimensional control and mechanical properties over those with STD-Cu. The fact that Cu particle size does have some effect on properties indicates that Cu does not *completely* wet the Fe particles as it liquefies. In theory, if Cu particles wetted Fe particles completely, Cu particle size would have no effect on the properties of the steel [5].

In agreement with results from Study 2 of the current work, Ni appears to stabilize the movement of Cu within the steel matrix during sintering. With coarser Ni and Cu particles, there is little Ni-Cu interaction. Liquid Cu is free to migrate between the Fe particles. The diffusion of Cu into Fe is relatively slow compared to carbon into Fe for example and creates an opportunity for non-uniform distribution of Cu. Increasing the Ni-Cu interaction with XF-Ni or XF-Cu powders restricts the movement of Cu by pinning it to well dispersed XF-Ni powder through the formation of Ni-Cu-Fe phases or Cu-rich Cu-Ni liquid.

3.3.4 Dilatometry analysis

3.3.4.1 Heating

The dilatometry curves for the steels for heating up to sintering temperature and soaking are shown in Figure 3-66. Up to about 650°C, specimens expand similarly as the temperature increases. The expansion rate, 1.5 x 10^{-3} %/°C, corresponds to the thermal expansion coefficient of ferrite [28]. At about 750°C, the expansion rate decreases and the specimens begin shrinking in the temperature range of 800-950°C. This is the temperature range of the ferrite-austenite transformation. At temperatures greater than 950°C, the diffusion of carbon is accelerated. The major difference in steels with STD-Ni vs. XF-Ni is that steels with STD-Ni begin to expand from 950-1075°C, as C diffuses into Fe, while steels with XF-Ni continue to densify. At a temperature of about 1100°C the steels with STD-Ni expand; the steels with XF-Ni start expanding slightly later, at about 1110-1115°C. This expansion at 1100-1120°C corresponds to the melting of Cu (T_m = 1083°C), as liquid Cu flows in between the Fe particles and causes them to separate. The rate of expansion is notably less in steels with XF-Ni and the overall expansion just before the sintering temperature is reached is much less. This indicates that XF-Ni is able to control the movement (and consequently the distribution) of Cu to a greater extent than STD-Ni. During sintering the samples densify and show a significant amount of shrinking.

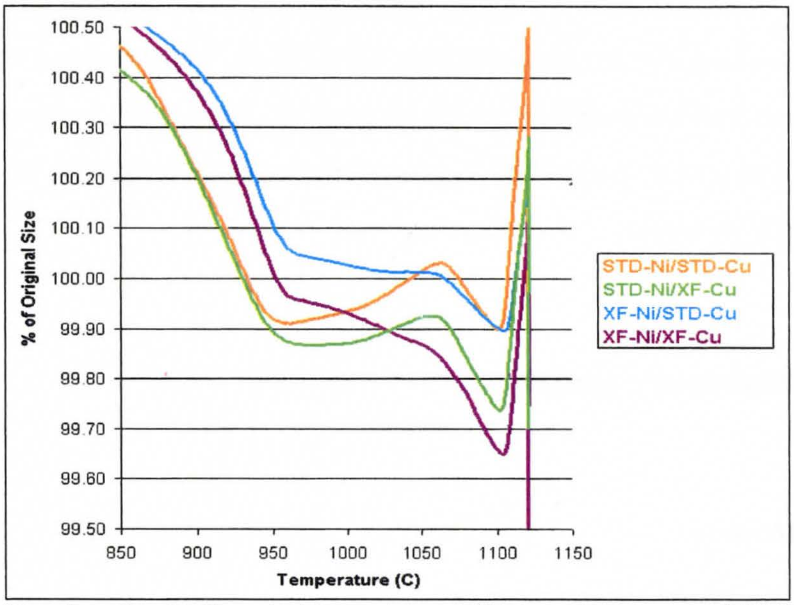

Figure 3-66. Heating (including soak) portion of dilatometry curve of Ni/Cu/Mo steels.

3.3.4.2 Cooling

The dilatometry curves for the steels for cooling from the sintering temperature is shown Figure 3-67. Upon cooling from 1120°C to 950°C the slopes of all of the steels are similar. Below 950°C, the slope of steels with STD-Ni decreases and densification is less than that seen in steels with XF-Ni. At a temperature of ~ 630°C the samples with XF-Ni begin to undergo the austenite-ferrite transformation until ~ 490°C. The steels with STD-Ni begin this transformation slightly later at about 590°C and end slightly earlier at about 510°C. A wider austenite-ferrite transformation range observed in steels with XF-Ni results in more bainite and martensite being produced in the final microstructure.

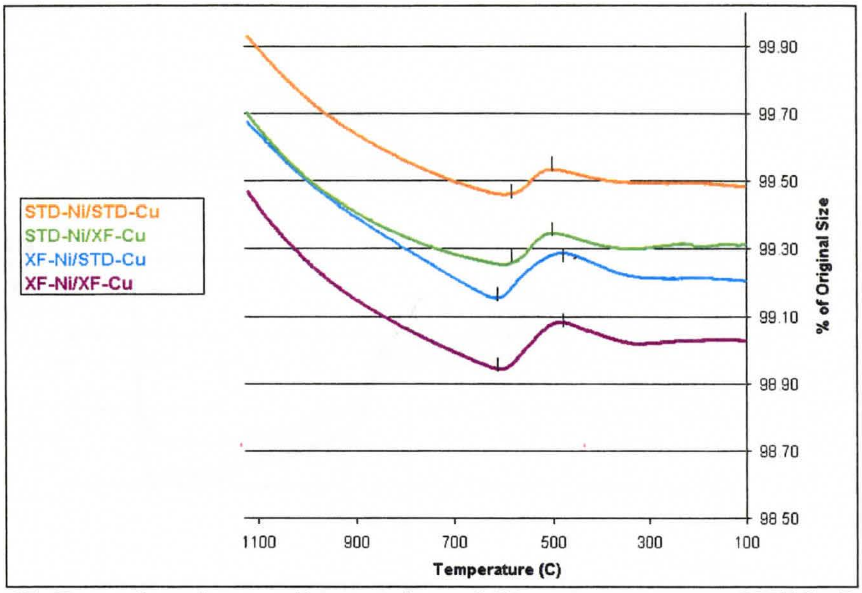

Figure 3-67. Post-sintering cooling portion of dilatometry curve of Ni/Cu/Mo steels.

3.3.5 Differential Thermal Analysis

The DTA plot in Figure 3-68 shows heat flow (released) vs. temperature during the sintering cycle of the four steels. The particle size of Cu does not affect the DTA curves as significantly as the particle size of Ni. Upon heating, steels with XF-Ni show less heat release than the other steels. This could be related to dilatometry and linescan results which show that the distribution of Ni and Cu in steels relies much more on Ni particle size than Cu particle size. The mass transport / reactions that take place during sintering seem to be more stable with finer Ni size. Finer powders appear to release less heat during sintering. This may indicate that less liquid forms when finer powders are used and thus less swelling is induced. If more Ni and Cu interact, the higher the concentration of Ni available to form a solid solution with Ni and the higher the melting temperature of the binary Ni-Cu alloy (Cu-Ni phase diagram shown in Fig. 3-66). Thus less liquid will form and less dimensional swelling will result.

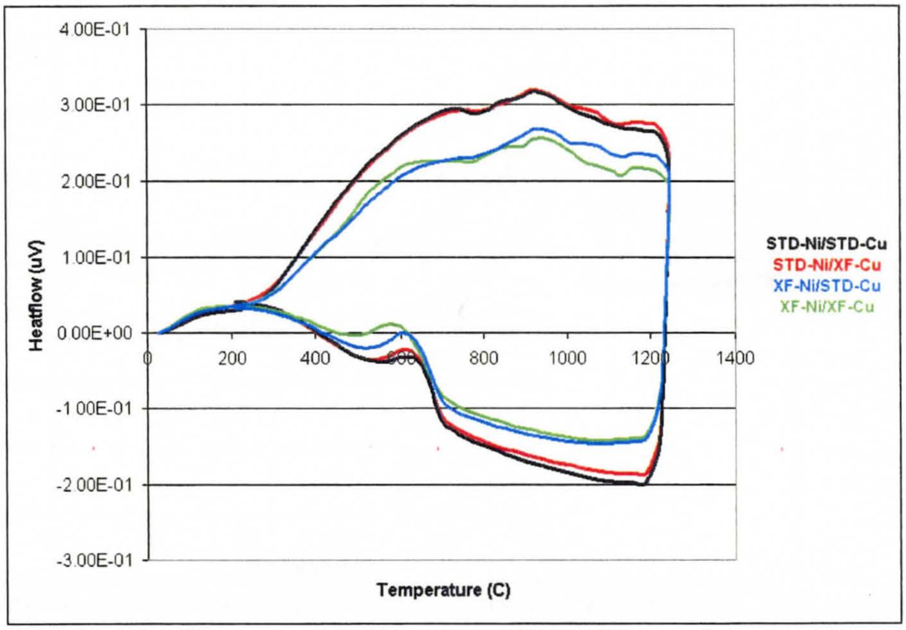

Figure 3-68. DTA plot of Ni/Cu/Mo steels.

3.3.6 Modeling Diffusion Analysis of Ni & Cu during sintering

3.3.6.1 Nominal Diffusion distance of Ni and Cu particles into Fe during sintering

A very simple model can be applied that approximates the relative distance which Ni and Cu move into the Fe particle. The classical equation for diffusion which relates the rate of diffusion of one species (solute) into another (solvent) is given by the Arhenius equation:

$$D = D_0 \exp\left(\frac{-Q}{RT}\right) \quad \text{.... Eqn. 3.3}$$

Where D is the diffusivity, D_0 is the diffusion coefficient for the specific solvent-solute system, Q is the activation energy specific to the system, T is the temperature in question (1120°C) and R is a constant,8.314 kJ/mol-K. For the systems in question:

- Ni diffusing into γ-Fe, $D_0 = 7.70 \times 10^{-5}$, $Q = 280$ kJ/mol, $D = 2.44 \times 10^{-15}$ m^2/s
- Cu diffusing into γ-Fe, $D_0 = 3.00 \times 10^{-4}$, $Q = 255$ k J/mol, $D = 8.22 \times 10^{-14}$ m^2/s

The nominal diffusion distance, $\underline{L}$, is considered a good approximation to the average penetration depth that the diffusing species will diffuse into the solvent [30]. The equation for $\underline{L}$ is:

$$\underline{L} = \sqrt{Dt} \quad \text{.... Eqn. 3.4}$$

Where D is the diffusivity and t is the time at temperature, in this case 30 mins. Solving for $\underline{L}$ for both Ni and Cu:

- Ni @ t = 30 mins, L = 2.1 μm
- Cu @ t = 30 mins, L = 12.2 μm

Therefore, in 30 mins, on *average*, Ni particles would only have moved ~ 2 μm into the Fe particles. The average Cu particle movement would be ~ 12 μm into the Fe particle. This result suggests that, *assuming solid state diffusion*, a particle size up to 2 μm of Ni could "completely dissolve" into Fe during sintering for 30 min. at 1120°C, and a Cu particle size of ~ 12 μm could "completely dissolve" into Fe in the same sintering cycle. This supports microstructural analyses which show that XF-Ni completely diffuses into Fe after 30 mins during sintering while STD-Ni leaves behind distinct Ni-rich areas. In the case of Cu, XF-Cu completely diffused into Fe; STD-Cu did leave behind some very subtle Cu-rich rings surrounding pores but it more or less fully dissolved. The author acknowledges the fact that this model does not account for the fact that Cu liquefies during sintering. These calculations are simply done as an exercise to get an idea of the effect of particle size of Cu on its diffusion into an Fe matrix during P/M sintering and can provide a good guideline to understanding the diffusion behaviour of the two elements.

3.3.6.2 Path of Cu – Diffusion into Ni vs. Diffusion into Fe

Eqn 3.3 can be used to show that Cu preferentially reacts with and diffuses faster into Ni rather than Fe:

- For Cu diffusing into γ-Fe: $D_0 = 3.00 \times 10^{-4}$, $Q = 255$ k J/mol, $D = 8.22 \times 10^{-14}$ m^2/s
- For Cu diffusing into Ni: $D_0 = 1.93 \times 10^{-4}$, $Q = 232$ kJ/mol, $D = 3.98 \times 10^{-13}$ m^2/s

Thus diffusion of Cu into Ni is 5 times higher than the diffusion of Cu into Fe, so Cu and Ni interactions will dominate. Also, the fact that Ni is so much finer than Fe is important. Even though there is only a few wt% Ni, the actual surface area of Ni with XF-Ni may be comparable to that for Fe.

3.4 General Discussion

In sintered Ni steels, the particle size of Ni powder strongly affects the diffusion and resulting distribution of Ni in the Fe matrix. A finer, more uniform distribution achieved via finer powders may alter the phase transformations which ultimately dictates the steel properties. Dilatometry suggests that the martensite-forming zone is enlarged when XF-Ni is used. Increased martensite levels result in better overall part properties – including a harder, stronger, more uniform microstructure, improved dimensional precision, increased densification and improved mechanical properties. Diffusion calculations also show that XF-Ni will more or less fully diffuse into Fe while STD-Ni cannot.

In steels with Ni and Cu, there is a strong affinity for Ni and Cu during sintering. Improving the Ni distribution, via finer Ni powders (similar to that of the Ni steel case), will lead to improved Cu distribution. Detailed SEM-EDX calculations during sintering showed that finer Ni improves the diffusion of Cu into the matrix. The interaction between Ni and Cu during sintering is three-fold:

(1) *Increased Ni-Cu interactions decrease the amount of liquid that forms during sintering.* In Cu steels, all of the Cu melts and causes significant swelling due to separation of Fe interparticle boundaries. With Ni in its presence, Cu is less likely to form a liquid but rather forms solution with Ni that remains semi-solid (see Ni-Cu phase diagram, Figure 3-69). The liquid that does form, forms in a stable manner (because of improved uniformity) and spreads evenly throughout the Fe matrix.

(2) *Increased Ni-Cu interaction increases the diffusion of Cu into the Fe matrix.* In wrought steels Cu is known to cause a detrimental effect called “hot shortness”,

which is essentially precipitation of Cu near grain boundaries and subsequent embrittlement at these sites. Work by Salter [38] has shown that, in wrought steels, nickel can offset the detrimental effects of copper. By a point-counting method, Salter showed that nickel progressively increased the solubility of copper in austenite at 1250°C, from 8.9% to 14.8% with a 13 wt% Ni addition; this is illustrated in Figure 3-70. In wrought steels, the tendency to "hot shortness" will be much lower with increasing levels of nickel additions.

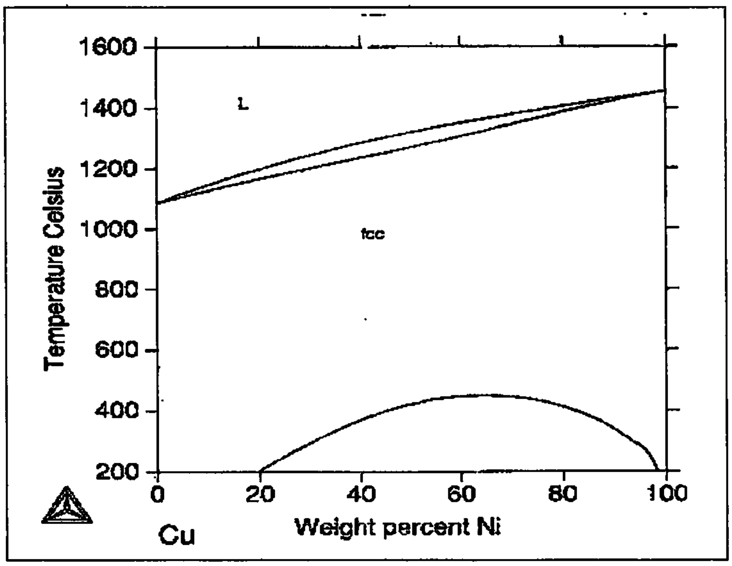

Figure 3-69. Cu-Ni phase diagram [27].

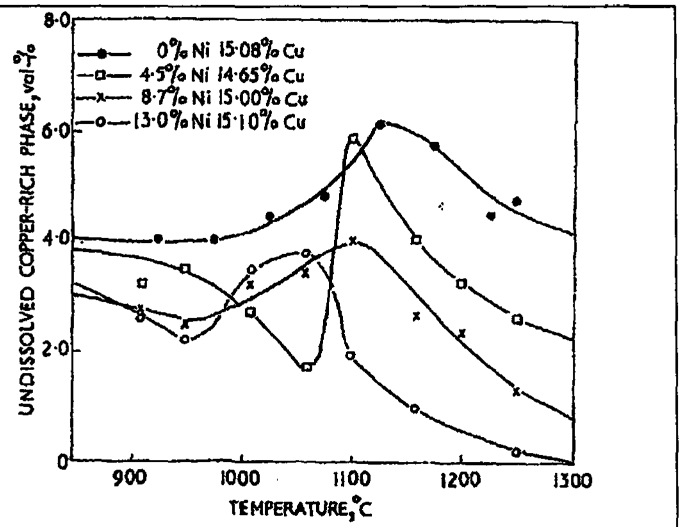

Effect of nickel on the undissolved copper-rich phase in alloys containing about 15%Cu

Figure 3-70. Effect of Ni on the undissolved Cu-rich phase in alloys containing ~ 15% Cu [38].

(3) *Increased Ni-Cu interactions decrease the dihedral angle of liquid Cu* (in between Fe particles). The inference of this fact is that Ni-Cu liquid is able to enter Fe interparticle boundaries more readily than pure Cu liquid, increasing the risk of part swelling. This corresponds with effects seen in 0.8C steels in the current work – Ni-Cu steels swelled slightly more than a Cu steel. At conventional sintering temperatures, however, this effect is not so serious as might be expected; the dihedral angle is only decreased by about 2° by nickel additions to pure Cu – and this is within experimental error [38]. At temperatures significantly higher than 1100°C, however, Ni-Cu will have an increased susceptibility to penetrate grain boundaries vs. pure Cu.

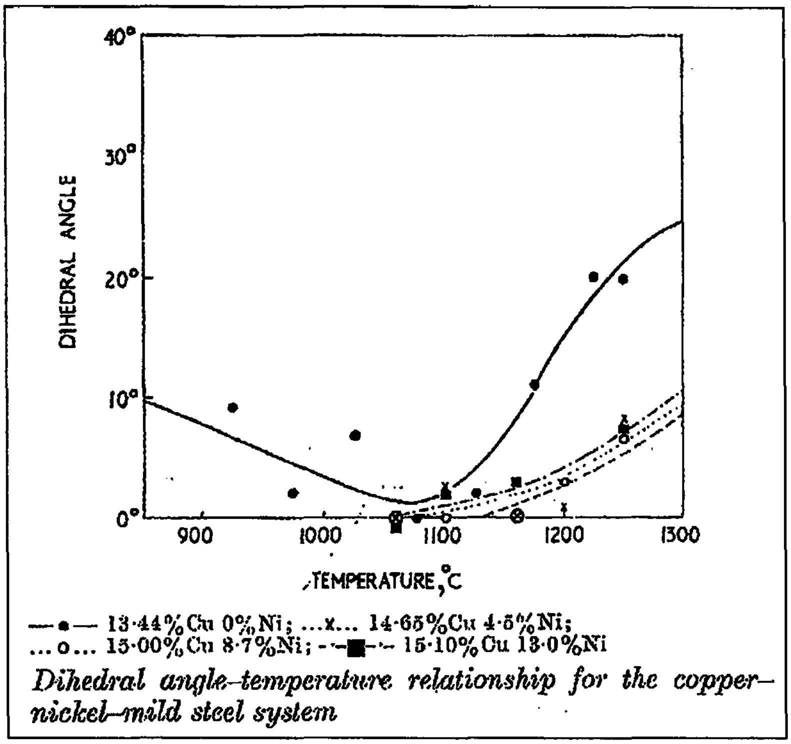

Figure 3-71. Dihedral angle-temperature relationship for the copper-nickel-mild steel system[38].

In steels containing Ni, Cu and Mo (a frequently used alloying combination), the interaction between Mo and the other alloying elements is negligible from the results of the current study. Since Mo is prealloyed to Fe it essentially remains stationary during the sintering process. Ni-Cu-Mo-Fe solid solutions will form as Ni and Cu diffuse through the steel matrix [11].

4 CONCLUSIONS

1. In powder metal Ni steels and Cu steels, alloying elements (Ni and Cu respectively) of finer particle size give improved alloy distribution. This results in improved microstructural uniformity and an increase in the amount of alloy diffusing into Fe matrix during sintering.
2. Increased uniformity and diffusion of Ni and Cu into Fe alters phase transformations, promoting a more uniform, and stronger / harder microstructure.
3. Improved alloy uniformity in the microstructure subsequently leads to improved dimensional precision, which is important for higher tolerance parts and difficult-to-hold tolerances in larger parts. This can reduces scrap rates and need for costly secondary processing such as coining and sizing. In addition, improved alloy uniformity results in reduced variability in mechanical properties, improving consistency in part performance.
4. In powder metal mixed Ni-Cu steels, Cu melts during sintering and associates with Ni. Ni-Cu interactions are increased with finer Ni powder additions. Since increasing the fineness of Ni powder both improves uniformity and the amount of Ni going into solution with Fe, Cu distribution in sintered steels can be improved with finer Ni powder additions. Finer Ni powder additions have more of an effect on improving the Cu distribution than Cu particle size itself. Ni stabilizes the movement of Cu, increasing its diffusion into the Fe matrix and decreasing the formation of pure liquid Cu phase which causes swelling problems in P/M steels. Improved alloy distribution in turn positively affects microstructure and mechanical properties.

REFERENCES

1. Engstrom, U., "Challenges of High Density," *Metal Powder Report*, Vol. 55, No. 11, 2000, p. 8, 9.
2. German, R.M.. Powder Metallurgy of Iron and Steel. 1st edition, Wiley, 1998, p. 20-45.
3. Pease, L., "Consultants' Corner," *The International Journal of Powder Metallurgy*, Vol. 37, No. 5, 2001, p. 28.
4. Gosselin, F., Gangne, M., Trudel, Y., "Double Press-Double Sintering of a Low Alloy Steel Powder for High Performance Applications," *Advances in Powder Metallurgy and Particulate Materials,* Vol. 5, 1992, pp. 127-141.
5. German, R.M. Sintering Theory & Practice. 1st edition, Wiley, 1996, p. 225-230
6. Yano, K., Furukimi, O., Takajo, S., "New Composite Type Alloyed 2%Ni-1%Mo Steel Powder of Utrahigh-Strength Sintered Components," *Advances in Powder Metallurgy and Particulate Materials,* Vol. 5, 1991, pp. 59-67.
7. James, W., "Ferrous Powder Metallurgy Materials," ASM Handbook: Powder Metallurgy Technologies and Applications, Vol. 7, ASM International, Materials Park, OH, 1998, pp.751-768.
8. Motooka, N., Hanada, Honda, T., "Development of Ultra-High Strength Sintered Steel," *Advances in Powder Metallurgy and Particulate Materials, Vol. 5, 1992, pp. 215-226.*

9. Tengzelius, J., Narasimhan, K., "P/M Low Alloy Steels- Alloying Methods and Continuous Improvements," *Advances in Powder Metallurgy and Particulate Materials, Vol. 5, 1992, pp. 153-176.*

10. Morioka, Y., "Recent Advances in Production of Steel Powders for High Strength P/M Parts," *Metal Powder Report*, Vol. 45, No. 3, 1990, pp. 181-183.

11. Furukimi, O., Maruta, K., Abe, T., Takajo, S., Habu, Y., "Partially Prealloyed Steel Powder Containing Nickel and Molybdenum for Ultrahigh Strength Sintered Materials," *Powder Metallurgy*, Vol. 34, No. 3, 1991, pp. 212-214.

12. Tracey, V.A., "Nickel Sintered Steels: Developments, Status and Prospects," *Proceedings from the 1992 International Conference on Powder Metallurgy and Particulate Materials, 1992.*

13. Chagnon, F., Trudel, Y., "Effect of Compaction Temperature on Sintered Properties of High Density P/M Materials," *Advances in Powder Metallurgy and Particulate Materials, Vol. 2, 1995, pp. 3-21.*

14. Metal Powder Industries Federation, Princeton, NJ, Standard 35, 2003 edition, p.16-25.

15. Singh, T.; Stephenson, T.F.; Campbell, S. "Nickel-Copper Interactions in P/M Steels." Advances in Powder Metallurgy & Particulate Materials - 2004, MPIF (Metal Powder Industries Federation), p 7/93-7/104.

16. Engström, U, "Copper in P/M Steels", Int. J. of Powder Met., 2003, vol. 39, no. 4, p.29.

17. Stephenson, T.F.; T. Singh; S. Sun; Z. Wang, "Effect of Ni Powder Morphology on the Fatigue Properties of P/M Ni Steels" in Advances in powder metallurgy & particulate materials - 2002: proceedings of the 2002 International Conference on Powder Metallurgy & Particulate Materials - PM2TEC 2002 World Congress, June

16-21, Orlando, compiled by Volker Arnhold, Metal Powder Industries Federation, Princeton, NJ, 2002, p. 5-153 to 5-164.

18. Causton, R., Fulmer, J., "Sinter Hardening Low-Alloy Steels," *Advances in Powder Metallurgy and Particulate Materials, Vol. 5, 1992, pp. 17-52.*
19. Quebec Metal Powders® ATOMET 1001 data sheet.
20. Hoeganes® 85HP data sheet.
21. Southwestern® 1651 graphite data sheet.
22. INCO® T123 PM powder data sheet.
23. INCO® T110 PM Powder data sheet.
24. ACuPowder website – http://www.acupowder.com/cu_powders.
25. ASM Handbook: Metallography and Microstructures, "Powder Metallurgy Materials," Vol. 9, ASM International, Materials Park, OH, 1998, pp.509-527.
26. Standard Test Methods for Metal Powders and Powder Metallurgy Products, ed. MPIF, Princeton, NJ, 1985.
27. SGTE phase diagram collection website – www.met.kth.se/dct/pd/element/Cu-Ni.html
28. Chagnon, F., Gagne, M., "Dimensional control of sinter hardened P/M components." Advances in Powder Metallugry & Particulate Materials (2004), Metal Powder Industries Federation, Princeton, NJ, 2004, p. 87-101.
29. Shrager, A.M., Elementary Metallurgy and Metallography, 3rd edition, Wiley, 1969, p.85.

30. Wilkinson, D.S., Mass Transport in Solids and Fluids., Cambridge Univeristy Press, 2000, p. 72-76.

31. Stephenson, T.F.; T. Singh; S.T. Campbell, "Influence of Extra-fine Ni Powder on P/M Steel Properties" in Advances in powder metallurgy & particulate materials - 2003: proceedings of the 2002 International Conference on Powder Metallurgy & Particulate Materials - PM2TEC 2003, p. 340-348, June 2003, Las Vegas, compiled by Roger Lawcock, Metal Powder Industries Federation, Princeton, NJ, 2002

32. Durdaller, C., "The Effect of Additions of Copper, Nickel and Graphite on the Sintered Properties of Iron-Base Sintered P/M Parts", Progress in Powder Met., Metal Powder Ind. Fed., New York, NY, 1969, vol. 25, p. 73.

33. Berner, D; H.E. Exner; G. Petzow, "Swelling of Iron-Copper Mixtures During Sintering and Infiltration", Modern Developments in Powder Metallurgy, edited by H.H. Hausner and W.E. Smith, Metal Powder Ind. Fed., Princeton, NJ, 1973, p.237.

34. Lawcock, R.L.; T.J. Davies, "Effect of Carbon on Dimensional and Microstructural Characteristics of Fe-Cu Compacts During Sintering", Powder Metall., 1990, vol. 33, no. 2, p. 147.

35. Chagnon, F.; M. Gagné, "Dimensional Control of Sinter Hardened P/M Components" Advances in Powder Metallurgy & Particulate Materials (2001), Metal Powder Industries Federation, p. 5/31-5/42.

36. St-Laurent, S.; Chagnon, F.; Poirier, J., "Selecting low alloy Mo steel powders for high performance applications." Advances in Powder Metallurgy & Particulate Materials (2003), Metal Powder Industries Federation, p. 1078-1091

37. Chagnon, F.; Trudel, Y., "Optimizing properties of P/M parts through selection of proper sinter hardening powder grades." Advances in Powder Metallurgy &

Particulate Materials (2002), Metal Powder Industries Federation, Princeton, NJ, p. 785-792.

38. Salter, W.J.M., “Effects of alloying elements on solubility and surface energy of copper,” *The Journal of the Iron & Steel Institute, pp. 473-83, 1966.*